Windowed multipole representation of R -matrix cross sections

Windowed multipole representation of *R*-matrix cross sections

Pablo Ducru,[*] Abdulla Alhajri,[†] Isaac Meyer,[‡] and Benoit Forget[§]
Massachusetts Institute of Technology, Department of Nuclear Science and Engineering 77 Massachusetts Avenue, Cambridge, Massachusetts 02139, USA

Vladimir Sobes[‖]
University of Tennessee, Department of Nuclear Engineering 1412 Circle Drive, Knoxville, Tennessee 37996, USA

Colin Josey[¶]
Los Alamos National Laboratory, P.O. Box 1663 MS A143, Los Alamos, New Mexico 87545, USA

Jingang Liang[**]
Tsinghua University, Institute of Nuclear and New Energy Technology, Beijing 100084, China

(Received 22 October 2020; accepted 4 December 2020; published 14 June 2021)

Nuclear cross sections are basic inputs to any nuclear computation. Campaigns of experiments are fitted with the parametric *R*-matrix model of quantum nuclear interactions, and the resulting cross sections are documented—both pointwise and as resonance parameters (with uncertainties)—in standard evaluated nuclear data libraries (ENDF, JEFF, BROND, JENDL, CENDL, TENDL): these constitute our common knowledge of fundamental low-energy nuclear cross sections. In the past decade, a collaborative effort has been deployed to establish a new nuclear cross-section library format—the *Windowed Multipole Library*—with the goal of considerably reducing the computational cost of cross-section calculations in nuclear transport simulations. This paper lays the theoretical foundations underpinning these efforts. From general *R*-matrix scattering theory, we derive the *windowed multipole representation* of nuclear cross sections. Though physically and mathematically equivalent to *R*-matrix cross sections, the windowed multipole representation is particularly well suited for subsequent temperature treatment of angle-integrated cross sections, in particular Doppler broadening, which is the averaging of cross sections over the thermal motion of the target atoms. Doppler broadening is of critical importance in neutron transport applications, as it ensures the stability of many nuclear reactors (negative thermal reactivity). Yet, Doppler broadening of nuclear cross sections has been a considerable bottleneck for nuclear transport computations, often requiring memory-costly pretabulations. We show that the windowed multipole representation can perform accurate Doppler broadening analytically (up to the first reaction threshold), from which we derive cross-section temperature derivatives to any order—all computable on the fly (without precalculations stored in memory). Furthermore, we here establish a way of converting the *R*-matrix resonance parameters uncertainty (covariance matrices) into windowed multipole parameters uncertainty. We show that generating stochastic nuclear cross sections by sampling from the resulting windowed multipole covariance matrix can reproduce the cross-section uncertainty in the original nuclear data file. The windowed multipole representation is therefore a novel nuclear physics formalism able to generate Doppler broadened stochastic nuclear cross sections on the fly, unlocking breakthrough computational gains for nuclear computations. Through this foundational paper, we hope to make the windowed multipole representation accessible, reproducible, and usable for the nuclear physics community, as well as provide the theoretical basis for future research on expanding its capabilities.

DOI: 10.1103/PhysRevC.103.064610

I. INTRODUCTION

Our knowledge of nuclear reactions is progressively built up by undertaking experiments and analyzing their outcomes

[*]Also at École Polytechnique, France and Schwarzman Scholars, Tsinghua University, China.; p_ducru@mit.edu, pablo.ducru@polytechnique.org
[†]alhajri@mit.edu
[‡]icmeyer@mit.edu
[§]bforget@mit.edu
[‖]sobesv@utk.edu
[¶]cjosey@lanl.gov
[**]jingang@mit.edu

through the prism of a quantum model of nuclear collisions called R-matrix theory [1–4]. This is known as the nuclear data evaluation process. Evaluators conduct campaigns to measure nuclear cross sections and fit them with R-matrix parameters. To account for the epistemic uncertainty introduced, evaluators generate nuclear resonance parameters covariance matrices to reproduce the variance observed in the measurements.

Other parametrizations of nuclear cross sections exist– -such as the Humblet-Rosenfeld pole expansions in wavenumber space [5–13]—but none have proven as practical to document or use as R-matrix theory, which is why our standard evaluated nuclear data libraries (ENDF [14], JEFF [15], BROND [16], JENDL [17], CENDL [18], TENDL [19,20]) are constituted of R-matrix parameters (and their covariance uncertainties).

At the end of the 20$^{\text{th}}$ century, Hwang from Argonne National Laboratory found a way to calculate from R-matrix parameters the Humblet-Rosenfeld pole expansion of neutron cross sections without thresholds, where the wave number is proportional to the square root of energy $k_c(E) \propto \sqrt{E}$. He also showed that this *pole representation* in $z \triangleq \sqrt{E}$ space presents a major advantage for subsequent temperature treatment: integral Doppler broadening can be accurately computed with analytic expressions [21–25]. This formalism was further developed into the *windowed multipole representation* in order to perform efficient on-the-fly computations of no-threshold neutron cross sections with a lesser computational memory footprint [26–30]. In this article, which follows [31] and [32], we extend the windowed multipole representation to all cross sections in the context of R-matrix theory—be they Coulomb, photon, or neutrons, with or without thresholds—thereby closing our trilogy on pole parametrizations of R-matrix theory (as described in the Supplemental Material of Ref. [31]). We also provide means of converting resonance parameters uncertainties into windowed multipole uncertainties. We thus lay the foundations to constitute a full *Windowed Multipole Library*, encompassing all present nuclear data [33].

In Sec. II, we derive the windowed multipole representation from general R-matrix theory, showing it is the meromorphic continuation of cross sections to complex energies, and discuss numerical ways of computing the multipoles, either from resonance parameters or pointwise cross-section data. In Sec. III, we expand the windowed multipole representation to account for the epistemic uncertainty of the nuclear cross sections [34,35]. We establish the analytic sensitivities of the windowed multipole parameters to the Wigner-Eisenbud R-matrix resonance parameters. This enables us to convert to first order the standard resonance parameters covariance matrix into a windowed multipoles covariance matrix, and show the latter reproduces the statistical properties of nuclear cross-section uncertainties. Having done so, we consider temperature effects in Sec. IV, showing how to analytically Doppler broaden windowed multipole angle-integrated cross sections, and how to compute arbitrary-order temperature derivatives that can prove useful in multiphysics simulations [36,37].

By deriving conversion methods of R-matrix resonance parameters and their uncertainties (covariance matrices) to windowed multipoles, and showing how to account for temperature effects, we thus establish the windowed multipole representation as a general, physically equivalent parametrization of R-matrix cross sections. By its efficient on-the-fly treatment of uncertainty and Doppler broadening, the windowed multipole representation can achieve considerable computational gains, and has already found several new nuclear reactor physics applications, from the establishment of a new analytic benchmark for neutron slowing down that resolves nuclear resonances overlap [38,39], or explicit resonance treatment for thermal up-scattering of angular cross sections [40], to differential temperature tallies for higher-order neutronics-thermohydraulics coupling schemes in nuclear transport solvers [36,37], or enabling new uncertainty inference and propagation methods across intractable nuclear systems [34].

II. FROM R-MATRIX TO WINDOWED MULTIPOLE

We here establish the *windowed multipole representation*, deriving it from general R-matrix scattering theory. In doing so, we show that R-matrix cross sections are the sum of two phenomena: thresholds and resonances. Thresholds have a behavior in the wave number k_c space of the channel c, so that in the vicinity of a threshold the cross section admits a Laurent expansion in powers of k_c (starting at k_c^{-2}). Resonances have a behavior in the energy space E, and can thus be locally expressed as a sum of single-level Breit-Wigner (SLBW) resonances, with both symmetric and antisymmetric Lorentzian functions. In Ref. [31], we linked the R-matrix parametrization of the scattering matrix $\boldsymbol{U}(E)$ to its wave number k_c expansion, established by Humblet and Rosenfeld in their *Theory of Nuclear Reactions* [5–13]. In this paper, we use this connection to establish the windowed multipole representation, which is the meromorphic continuation of R-matrix cross sections in $z \triangleq \sqrt{E}$ space, locally expressing open channels as pole expansions. We build upon our previous work on such expansions [31,32], using the same consistent notation as reference. As such, this article closes our trilogy on pole parametrizations of R-matrix theory (see Supplemental Material of Ref. [31]).

A. R-matrix cross-section parametrization

R-matrix theory models two-body-in/two-body-out scattering events interacting with a "black-box" Hamiltonian [1–4]. Each pair of possible two-body-inputs/two-body-outputs, along with all the corresponding quantum numbers that describe them, constitutes a channel c. It is assumed that for each channel, the Hamiltonian can be partitioned into two regions: within an "inner region" sphere of channel radius a_c, the many bodies interacting through the strong nuclear forces are considered an intractable black-box Hamiltonian; past the channel radius a_c, the "outer region" Hamiltonian is well known (say Coulomb potential or free-wave). For each channel c, R-matrix theory studies the many-body scattering event into the reduced one-body system, where the solution of the Schrödinger equation is a superposition of an incoming wave function I_c and an outgoing wave function O_c, both

functions of the wave number k_c. The latter can be multiplied by the arbitrary (but fixed) channel radius a_c to yield the *dimensionless wave number*

$$\rho_c \triangleq k_c a_c \tag{1}$$

and we define the corresponding diagonal matrix over all the channels $\boldsymbol{\rho} = \mathrm{diag}(\rho_c)$.

1. Wave-number–energy mapping

Each wave number is related to the total energy E of the system, which is an eigenvalue of the Hamiltonian in the reduced center-of-mass frame. In the semiclassical limit, a two massive particles channel (i.e., not photons) of respective masses $m_{c,1}$ and $m_{c,2}$ will have a wave number k_c of

$$k_c(E) = \sqrt{\frac{2m_{c,1}m_{c,2}}{(m_{c,1}+m_{c,2})\hbar^2}\left(E - E_{T_c}\right)} \tag{2}$$

where E_{T_c} denotes a threshold energy below which the channel c is closed, as energy conservation cannot be respected ($E_{T_c} = 0$ for reactions without threshold). In the same semiclassical limit, a photon particle interacting with a massive body of mass $m_{c,1}$, the center-of-mass wave number k_c is linked to the total center-of-mass energy E according to

$$k_c(E) = \frac{\left(E - E_{T_c}\right)}{2\hbar c}\left[1 + \frac{m_{c,1}c^2}{\left(E - E_{T_c}\right) + m_{c,1}c^2}\right]. \tag{3}$$

These two semiclassical limits can be encompassed within a single relativistic framework as discussed in Eqs. (4) and (5), Sec. II.A of [32]. Because one must choose the sign of the square root $\pm\sqrt{\cdot}$ in Eq. (2), these $k_c(E)$ relations engender a wave-number–energy mapping

$$\rho_c(E) \longleftrightarrow E \tag{4}$$

which forms a complex multisheeted Riemann surface with branch points at (or close to) the threshold energies E_{T_c}, as discussed in Sec. II.A p. 2 of [32].

2. Transmission matrix and cross-section expressions

General scattering theory expresses the incoming channel c and outgoing channel c' angle-integrated partial cross section $\sigma_{c,c'}(E)$ at energy E as a function of the probability *transmission matrix* $T_{cc'}(E)$, according to Eq. (3.2d) VIII.3 p. 293 of [4]:

$$\sigma_{cc'}(E) = 4\pi g_{J_c^\pi}\left|\frac{T_{cc'}(E)}{k_c(E)}\right|^2 \tag{5}$$

where the *spin statistical factor* is defined in Eq. (3.2c) VIII.3 p. 293. of [4] as

$$g_{J_c^\pi} \triangleq \frac{2J+1}{(2I_1+1)(2I_2+1)}. \tag{6}$$

The transmission matrix is itself derived from the *scattering matrix* $\boldsymbol{U}$ of the interaction:

$$\boldsymbol{T} \triangleq \frac{\mathbb{I} - \boldsymbol{e}^{-i\boldsymbol{\omega}}\boldsymbol{U}\boldsymbol{e}^{-i\boldsymbol{\omega}}}{2} \tag{7}$$

where $\boldsymbol{\omega} \triangleq \mathrm{diag}(\omega_c)$ is the diagonal matrix composed of $\omega_c \triangleq \sigma_{\ell_c}(\eta_c) - \sigma_0(\eta_c)$, that is the difference in *Coulomb phase shift*, $\sigma_{\ell_c}(\eta_c)$, which are linked to the phases (argument) of the Gamma function as defined by Thompson in Eq. (33.2.10) of [41] for angular momentum ℓ_c,

$$\sigma_{\ell_c}(\eta_c) \triangleq \arg[\Gamma(1 + \ell_c + i\eta_c)], \tag{8}$$

and *dimensionless Coulomb field parameter*:

$$\eta_c \triangleq \frac{Z_1 Z_2 e^2 M_\alpha a_c}{\hbar^2 \rho_c}. \tag{9}$$

Note that this transmission matrix (7) definition $T_{cc'} \triangleq \frac{\delta_{cc'} - e^{-i\omega_c}U_{cc'}e^{-i\omega_{c'}}}{2}$ is a scaled rotation of the one defined by Lane and Thomas, $T^{\mathrm{L\&T}}_{cc'} \triangleq \delta_{cc'}e^{2i\omega_c} - U_{cc'}$ [see Eq. (2.3) VIII.2 p. 292 and Eq. (3.2d) VIII.3 p. 293 of [4]]. We introduce definition (7) for better physical interpretability, algebraic simplicity, and numerical stability.

Unitarity of the scattering matrix entails that $\sum_{c'}|\delta_{cc'} - e^{-i\omega_c}U_{cc'}e^{-i\omega_{c'}}|^2 = 2(1 - \mathrm{Re}[e^{-2i\omega_c}U_{cc}])$, which in turn leads to the following expression for the total cross section of a given channel:

$$\sigma_c(E) \triangleq \sum_{c'}\sigma_{cc'}(E) = 4\pi g_{J_c^\pi}\frac{\mathrm{Re}[T_{cc}(E)]}{|k_c(E)|^2}. \tag{10}$$

In both cross-section expressions (5) and (10), the $1/|k_c|^2$ term links the cross section to the probability of interaction, and expresses the channel reversibility equivalence:

$$\frac{k_c^2\sigma_{cc'}}{g_{J_c^\pi}} = \frac{k_{c'}^2\sigma_{c'c}}{g_{J_{c'}^\pi}}. \tag{11}$$

The incoming I_c and outgoing O_c waves are functions of the dimensionless wave number $\rho_c \triangleq a_c k_c$ and are linked to the regular and irregular Coulomb wave functions (or Bessel functions in the case of neutral particle channels), defined in Eqs. (2.13a) and (2.13b) III.2.b p. 269 [4]:

$$\begin{aligned} O_c &= H_{+c}e^{-i\omega_c} = (G_c + iF_c)e^{-i\omega_c}, \\ I_c &= H_{-c}e^{i\omega_c} = (G_c - iF_c)e^{i\omega_c} \end{aligned} \tag{12}$$

and for properties of which we refer to Thompson's Chap. 33, Eq. (33.2.11) in Ref. [41], or Abramowitz and Stegun Chap. 14, p. 537 [42]. In polar notation,

$$\begin{aligned} H_{+c} &= |H_{+c}|e^{i\phi_c}, \\ |H_{+c}| &= |\sqrt{|G_c|^2 + |F_c|^2}| \\ \phi_c &\triangleq \arg(H_{+c}) = 2\arctan\left(\frac{|F_c|}{|H_{+c}| + |F_c|}\right). \end{aligned} \tag{13}$$

3. R-matrix scattering matrix parametrization

R-matrix theory parametrizes the energy dependence of the scattering matrix $\boldsymbol{U}(E)$ as

$$\boldsymbol{U} = \boldsymbol{O}^{-1}\boldsymbol{I} + 2i\boldsymbol{\rho}^{1/2}\boldsymbol{O}^{-1}\boldsymbol{R}_L\boldsymbol{O}^{-1}\boldsymbol{\rho}^{1/2} \tag{14}$$

where the incoming and outgoing wave functions, $\boldsymbol{I} = \mathrm{diag}(I_c)$ and $\boldsymbol{O} = \mathrm{diag}(O_c)$, are subject to the following Wronksian condition for all channel c, $w_c \triangleq O_c^{(1)}I_c -$

$I_c^{(1)} O_c = 2i$, and where $\boldsymbol{R}_L$ is the *Kapur-Peierls operator*, defined as [see Eq. (17) Sec. II.D of [32]]

$$\boldsymbol{R}_L \triangleq [\mathbb{I} - \boldsymbol{R}\boldsymbol{L}^{\boldsymbol{0}}]^{-1}\boldsymbol{R} = \boldsymbol{\gamma}^{\mathsf{T}}\boldsymbol{A}\boldsymbol{\gamma} \tag{15}$$

where $\boldsymbol{R}$ is the Wigner-Eisenbud *R matrix* [2]

$$R_{cc'}(E) \triangleq \sum_{\lambda=1}^{N_\lambda} \frac{\gamma_{\lambda,c}\gamma_{\lambda,c'}}{E_\lambda - E} \tag{16}$$

parametrized by the real *resonance energies* $E_\lambda \in \mathbb{R}$ and the real *resonance widths* $\gamma_{\lambda,c} \in \mathbb{R}$—of which we, respectively, build the diagonal matrix $\boldsymbol{e} = \mathrm{diag}(E_\lambda)$ of size equal to the number of levels (resonances) N_λ, and the rectangular matrix $\boldsymbol{\gamma} = \mathbf{mat}(\gamma_{\lambda,c})$ of size $N_\lambda \times N_c$ where N_c is the number of channels. The Kapur-Peierls operator (15) is thus a function of $\boldsymbol{R}$ and $\boldsymbol{L}^{\boldsymbol{0}} \triangleq \boldsymbol{L} - \boldsymbol{B}$, where $\boldsymbol{B} = \mathrm{diag}(B_c)$ is the diagonal matrix of real arbitrary boundary conditions B_c, and $\boldsymbol{L} = \mathrm{diag}(L_c)$ where $L_c(\rho_c)$ is the dimensionless reduced logarithmic derivative of the outgoing-wave function at the channel surface:

$$L_c(\rho_c) \triangleq \frac{\rho_c}{O_c}\frac{\partial O_c}{\partial \rho_c}. \tag{17}$$

An equivalent definition (15) of the Kapur-Peierls operator $\boldsymbol{R}_L$ can be expressed with the *level matrix* $\boldsymbol{A}$ [see Eqs. (14) and (15) of Sec. II.C of [32]]:

$$\boldsymbol{A}^{-\mathbf{1}} \triangleq \boldsymbol{e} - E\mathbb{I} - \boldsymbol{\gamma}(\boldsymbol{L} - \boldsymbol{B})\boldsymbol{\gamma}^{\mathsf{T}} \tag{18}$$

As such, provided with the threshold energies, the channel radius, boundary conditions, and Wigner-Eisenbud resonance energies and widths, which we can collectively call the set of R-matrix parameters $\{E_{T_c}, a_c, B_c, E_\lambda, \gamma_{\lambda,c}\}$, one can entirely determine the energy behavior of the scattering matrix $\boldsymbol{U}$ through (14), and therefore the cross sections through (5) and (10).

4. Reich-Moore and Breit-Wigner approximations to R-matrix theory

In practice, many evaluations in standard nuclear data libraries are carried out with approximations of R-matrix theory. The most important and common is the *Reich-Moore* approximation. It reduces the R matrix to only the channels of interest, and accounts for the effect of all the other channels not explicitly treated by means of the Teichmann and Wigner channel elimination method (see [43] or Sec. X, p. 299 of [4]). This approximation is most useful when many channels are eliminated, such that the effect on the off-diagonal elements of the level matrix is small, a scenario often encountered in heavy nuclei. Usually, photon channels (γ "gamma capture") are eliminated, so that in practice the Reich-Moore approximation of R-matrix theory [44] consists of adding a partial eliminated capture width $\Gamma_{\lambda,\gamma}$ to every resonance energy E_λ, shifting the latter into the complex plane (see Sec. IV.A of [32]):

$$\boldsymbol{e}_{\mathrm{RM}} \triangleq \mathrm{diag}\left(E_\lambda - i\frac{\Gamma_{\lambda,\gamma}}{2}\right). \tag{19}$$

The R matrix (16) without the eliminated photon channels becomes

$$R_{c,c'\notin\gamma_{\mathrm{elim.}}} \triangleq \sum_{\lambda=1}^{N_\lambda} \frac{\gamma_{\lambda,c}\gamma_{\lambda,c'}}{E_\lambda - i\frac{\Gamma_{\lambda,\gamma}}{2} - E},$$

$$\text{i.e.,} \quad \boldsymbol{R}_{\mathrm{RM}} = \boldsymbol{\gamma}^{\mathsf{T}}(\boldsymbol{e}_{\mathrm{RM}} - E\mathbb{I})^{-1}\boldsymbol{\gamma}, \tag{20}$$

and the Reich-Moore inverse level matrix (18) becomes

$$\boldsymbol{A}^{-\mathbf{1}}_{\mathbf{RM}} \triangleq \boldsymbol{e}_{\mathrm{RM}} - E\,\mathbb{I} - \boldsymbol{\gamma}(\boldsymbol{L} - \boldsymbol{B})\boldsymbol{\gamma}^{\mathsf{T}}. \tag{21}$$

All the other R-matrix expressions linking these operators to the scattering matrix (14), and therefore the cross sections, remain unchanged. Practically, the only consequence of the Reich-Moore formalism is to introduce complex resonance energies (19). In this sense, one can consider the Reich-Moore formalism as a generalization of R-matrix theory, even though it finds its source in the elimination of intractable channels. It can thus also be seen as a compression algorithm. Indeed, it is possible to convert Reich-Moore parameters into standard R-matrix ones (not complex resonance energies) by means of the *generalized Reich-Moore* formalism, as established in Ref. [45]. Yet this comes at the cost of introducing many more parameters, thereby considerably increasing memory requirements. This is because generalized Reich-Moore converts the eliminated channels R matrix ($N_c \times N_c$ with $c \notin \gamma_{\mathrm{elim.}}$) into a square R matrix of the size of the levels ($N_\lambda \times N_\lambda$), and we often have $N_\lambda \gg N_c$, especially for large nuclides (see [45]).

Also, note that some older evaluations are made in the *multi-level Breit-Wigner* approximation, which simply consists of assuming the level matrix (18) is diagonal. This can be expressed using the Hadamard product "$\circ$" with the identity matrix as

$$\boldsymbol{A}^{-\mathbf{1}}_{\mathbf{MLBW}} \triangleq \boldsymbol{A}^{-\mathbf{1}} \circ \mathbb{I}. \tag{22}$$

Apart from these modified expressions of the level matrix, neither the Reich-Moore nor the multilevel Breit-Wigner approximations have any further incidence on how to convert R-matrix cross sections to windowed multipole representation: it suffices to take the corresponding level matrix and proceed as follows.

5. Parametrizing R-matrix cross sections

By substituting the R-matrix parametrization (14) of the scattering matrix $\boldsymbol{U}$ into the transmission matrix $\boldsymbol{T}$ definition (7), and noticing that wave-function relations (12) entail $\frac{\boldsymbol{H}_+ - \boldsymbol{H}_-}{2i} = \boldsymbol{F}$, one finds the transmission matrix can be decomposed into the rotated (by a factor of imaginary i) difference between a diagonal *potential matrix* $\boldsymbol{D}$ and a full *resonance matrix* $\boldsymbol{Z}$:

$$\begin{aligned}
\boldsymbol{T} &= i(\boldsymbol{D} - \boldsymbol{Z}),\\
\boldsymbol{Z} &\triangleq \boldsymbol{H}_+^{-1}\boldsymbol{\rho}^{1/2}\boldsymbol{R}_L\boldsymbol{\rho}^{1/2}\boldsymbol{H}_+^{-1},\\
\boldsymbol{D} &\triangleq \boldsymbol{H}_+^{-1}\boldsymbol{F} = \frac{\mathbb{I} - \boldsymbol{Y}}{2i},\\
\boldsymbol{Y} &\triangleq \boldsymbol{H}_+^{-1}\boldsymbol{H}_-.
\end{aligned} \tag{23}$$

From cross-section expression (5), the transmission probabilities from channel c to channel c' are then the square modulus

$|T_{cc'}|^2$. Decomposition (23) expresses this as

$$|T_{cc'}|^2 = |Z_{cc'}|^2 + |D_c|^2\delta_{cc'} - 2\mathrm{Re}[Z_{cc'}D_c^*]\delta_{cc'} \tag{24}$$

where $[\,\cdot\,]^*$ designates the complex conjugate. For the total cross section (10), it is the real part of the transmission matrix that appears: $\mathrm{Re}[T_{cc}] = \mathrm{Re}[iD_c] - \mathrm{Re}[iZ_{cc}]$. Note that $\boldsymbol{D}$ definition (23) entails $2\boldsymbol{D}^* = i(\mathbb{I} - \boldsymbol{Y}^*)$ and $|\boldsymbol{D}|^2 = \mathrm{Re}[i\boldsymbol{D}]$, since definition (13) yields

$$\mathrm{Re}[iD_c] = \frac{|F_c|^2}{|G_c|^2 + |F_c|^2} = |D_c|^2 = \sin^2(\phi_c). \tag{25}$$

We can thus decompose the cross sections into the following components, all expressed as the real part of some matrix elements calculable from R-matrix theory.

(1) Potential cross section (of channel c):

$$\sigma_c^{\mathrm{pot}}(E) \triangleq 4\pi g_{J_c^\pi}\left|\frac{D_c}{k_c}\right|^2 = 4\pi g_{J_c^\pi}\frac{\mathrm{Re}[iD_c]}{|k_c|^2}. \tag{26}$$

(2) Total cross section (of channel c):

$$\sigma_c(E) \triangleq \sigma_c^{\mathrm{pot}}(E) + 4\pi g_{J_c^\pi}\frac{\mathrm{Re}[-iZ_{cc}]}{|k_c|^2}. \tag{27}$$

(3) Self-scattering cross section (of channel c):

$$\sigma_c^{\mathrm{scat}}(E) \triangleq 4\pi g_{J_c^\pi}\frac{\mathrm{Re}[-2Z_{cc}D_c^*]}{|k_c|^2}. \tag{28}$$

(4) Interference cross section (of channel c):

$$\sigma_c^{\mathrm{int}}(E) \triangleq 4\pi g_{J_c^\pi}\frac{\mathrm{Re}[-iZ_{cc}Y_c^*]}{|k_c|^2}. \tag{29}$$

(5) Reaction cross section (from channel c to c'):

$$\sigma_{cc'}^{\mathrm{react}}(E) \triangleq 4\pi g_{J_c^\pi}\left|\frac{Z_{cc'}}{k_c}\right|^2. \tag{30}$$

(6) Partial (angle-integrated) cross section (from channel c to c'):

$$\begin{aligned}\sigma_{cc'}(E) &\triangleq \left[\sigma_c^{\mathrm{pot}}(E) + \sigma_c^{\mathrm{scat}}(E)\right]\delta_{cc'} + \sigma_{cc'}^{\mathrm{react}}(E)\\ &= \left[\sigma_c^{\mathrm{tot}}(E) - \sigma_c^{\mathrm{int}}(E)\right]\delta_{cc'} + \sigma_{cc'}^{\mathrm{react}}(E).\end{aligned} \tag{31}$$

Writing these expressions as functions of the dimensionless wave numbers of each channel, $\rho_c \triangleq k_c a_c$, cross sections appear as proportional to the area of the channel radius disk $\sigma_c(E) \propto 4\pi a_c^2$, and the modulation of this area is linked to both the transmission matrix amplitudes $|T_{cc'}(E)|^2$—which exhibit the resonance behavior—and the $1/k_c^2$ wave-number effect that dominates the total cross section close to the zero energy threshold.

B. Kapur-Peierls operator pole expansion in Siegert-Humblet radioactive states

The first step towards the windowed multipole representation consists of performing the pole expansion of the Kapur-Peierls operator $\boldsymbol{R}_L$ into what are called the Siegert-Humblet radioactive states [46–50]. We here summarize this process for the usual case of nondegenerate solutions, and we refer to Secs. II and IV of [31] for a detailed study.

The *radioactive states problem* consists of finding the poles $\{\mathcal{E}_j\}$ and residue widths vectors $\{\boldsymbol{r_j}\}$ of the Kapur-Peierls operator $\boldsymbol{R}_L$, that is solving the following generalized eigenvalue problem [46–50]:

$$\boldsymbol{R}_L^{-1}(E)\big|_{E=\mathcal{E}_j}\boldsymbol{r_j} = \boldsymbol{0} \tag{32}$$

where the residue widths vectors $\{\boldsymbol{r_j}\}$ are subject to the following normalization:

$$\boldsymbol{r}_j^{\mathsf{T}}\left(\frac{\partial \boldsymbol{R}_L^{-1}}{\partial E}\bigg|_{E=\mathcal{E}_j}\right)\boldsymbol{r}_j = 1 \tag{33}$$

which can be calculated using

$$\frac{\partial \boldsymbol{R}_L^{-1}}{\partial E}\bigg|_{E=\mathcal{E}_j} = \frac{\partial \boldsymbol{R}^{-1}}{\partial E}(\mathcal{E}_j) - \frac{\partial \boldsymbol{L}}{\partial E}(\mathcal{E}_j) \tag{34}$$

if the R matrix $\boldsymbol{R}$ is invertible at $\mathcal{E}_j$, whence

$$\frac{\partial \boldsymbol{R}^{-1}}{\partial E}(E) = -\boldsymbol{R}^{-1}\boldsymbol{\gamma}^{\mathsf{T}}(\boldsymbol{e} - E\mathbb{I})^{-2}\boldsymbol{\gamma}\boldsymbol{R}^{-1}. \tag{35}$$

If the R matrix $\boldsymbol{R}$ is not invertible at $\mathcal{E}_j$, these *radioactive poles* $\{\mathcal{E}_j\}$ and *radioactive widths* $\{\boldsymbol{r_j} = [r_{j,c_1}, \ldots, r_{j,c}, \ldots, r_{j,c_{N_c}}]^{\mathsf{T}}\}$, jointly called the Siegert-Humblet parameters, can be obtained by solving the level matrix $\boldsymbol{A}$ radioactive eigenproblem:

$$\boldsymbol{A}^{-1}(E)|_{E=\mathcal{E}_j}\boldsymbol{a_j} = \boldsymbol{0} \tag{36}$$

where the eigenvectors $\boldsymbol{a_j}$ are subject to normalization:

$$\boldsymbol{a}_j^{\mathsf{T}}\left(\frac{\partial \boldsymbol{A}^{-1}}{\partial E}\bigg|_{E=\mathcal{E}_j}\right)\boldsymbol{a}_j = 1 \tag{37}$$

which is readily calculable from

$$\frac{\partial \boldsymbol{A}^{-1}}{\partial E}(\mathcal{E}_j) = -\mathbb{I} - \boldsymbol{\gamma}\frac{\partial \boldsymbol{L}}{\partial E}(\mathcal{E}_j)\boldsymbol{\gamma}^{\mathsf{T}}. \tag{38}$$

The level-matrix residues widths vectors are then linked to the radioactive widths by the following relation:

$$\boldsymbol{r_j} = \boldsymbol{\gamma}^{\mathsf{T}}\boldsymbol{a_j}. \tag{39}$$

The radioactive energy poles are complex and usually decomposed as

$$\mathcal{E}_j \triangleq E_j - i\frac{\Gamma_j}{2}. \tag{40}$$

It can be shown (see discussion section IX.2.d pp. 297–298 in Ref. [4], or section 9.2 Eq. (9.11) in Ref. [5]) that fundamental physical properties (conservation of probability, causality, and time reversal) ensure either that the poles reside on the positive semiaxis of purely imaginary $k_c \in i\mathbb{R}_+$—corresponding to bound states for real subthreshold energies, i.e., $E_j < E_{T_c}$ and $\Gamma_j = 0$—or that all the other poles are on the lower-half k_c plane, with $\Gamma_j > 0$, corresponding to "resonance" or "radioactively decaying" states. All poles enjoy the specular symmetry property: if $k_c \in \mathbb{C}$ is a pole of the Kapur-Peierls operator, then $-k_c^*$ is too. Additional discussion on these radioactive poles and residues can be found in Ref. [4], Secs. IX.2.c–IX.2.e pp. 297–298, or in Refs. [46–50].

For our purpose of constructing the windowed multipole representation for R-matrix cross sections, the key property of the radioactive states is that they allow one, by virtue of the Mittag-Leffler theorem [51,52], to locally decompose the Kapur-Peierls operator into a sum of poles and residues and a holomorphic entire part $\mathbf{Hol}_{\boldsymbol{R}_L}(E)$, in the neighborhood $\mathcal{W}(E)$ (vicinity) of any complex energy $E \in \mathbb{C}$ away from the branch points (threshold energies E_{T_c}) of mapping (4):

$$\boldsymbol{R}_L(E) \underset{\mathcal{W}(E)}{=} \sum_{j\geqslant 1} \frac{\boldsymbol{r}_j \boldsymbol{r}_j^{\mathsf{T}}}{E-\mathcal{E}_j} + \mathbf{Hol}_{\boldsymbol{R}_L}(E) \tag{41}$$

Theorem 1 of [31] presents the branch structure of the radioactive poles $\mathcal{E}_j$ on the Riemann surface of the energy–wave-number mapping (4). We also show that when solving in dimensionless wave-number space ρ_c, there are N_L number of solutions to the radioactive problem (32). In the case of massive neutral particles (neutrons and neutrinos) we have

$$N_L = \left(2N_\lambda + \sum_{c=1}^{N_c} \ell_c\right) \times 2^{(N_{E_{T_c}\neq E_{T_{c'}}}-1)} \tag{42}$$

where $N_{E_{T_c}\neq E_{T_{c'}}}$ denotes the number of channels with different thresholds. For charged particles, there is an infinite number (countable) of radioactive poles: $N_L = \infty$. In essence, this is because for each different sheet of the energy–wave-number mapping (4), of which there are $2^{(N_{E_{T_c}\neq E_{T_{c'}}}-1)}$, the R matrix contributes $2N_\lambda$ poles in wave-number space [each resonance energy E_λ yielding two $\rho_c(E)$ space poles], and in addition each pole of the reduced logarithmic derivative $L_c(\rho_c)$ yields another radioactive pole in ρ_c space (see Theorem 1 of [31] for more detailed discussion).

Be that as it may, radioactive poles usually have the following characteristics (as can be observed in Table I of [31] for the case of xenon ^{134}Xe): for each resonance energy E_λ there are two radioactive poles nearby, usually on opposite sheets, close to but not exactly the specular symmetric of one another across the imaginary axis in wave number ρ_c space (i.e., near opposite complex conjugates); moreover, for each root ω_n of the outgoing function $O_c(\rho_c)$, there is a radioactive pole nearby. Often, only one of the two radioactive poles $\mathcal{E}_j$ close to the E_λ is responsible for most of the cross-section resonance behavior, while all the other radioactive poles are more akin to nonresonant "background levels," though they are still necessary to fully describe the cross section.

A critical property of the radioactive poles $\mathcal{E}_j$ is that these are exactly all the poles of the scattering matrix $\boldsymbol{U}(E)$ (proof in Theorem 3 of [31]). From decomposition (23), this entails that the transmission matrix readily admits the following Mittag-Leffler expansion:

$$\boldsymbol{T}(E) \underset{\mathcal{W}(E)}{=} -i \sum_{j\geqslant 1} \frac{\boldsymbol{\tau}_j \boldsymbol{\tau}_j^{\mathsf{T}}}{E-\mathcal{E}_j} + \mathbf{Hol}_{\boldsymbol{T}}(E) \tag{43}$$

where the residue width vectors are obtained by evaluating the functions in Eq. (23) at the pole values:

$$\boldsymbol{\tau}_j = \boldsymbol{H}_+^{-1}(\mathcal{E}_j)\boldsymbol{\rho}^{1/2}(\mathcal{E}_j)\,\boldsymbol{r}_j. \tag{44}$$

C. Transmission matrix T and resonance matrix Z expansions in the square root of energy z space

Though energy E-space expansion (43) is correct, we will nonetheless also introduce expansions in the square root of energy z space:

$$z \triangleq \sqrt{E}. \tag{45}$$

We do this to better express the behavior of massive particles (not massless photons) near the zero energy threshold, and in order to perform analytic Doppler broadening of massive particles. Indeed, for the zero threshold $E_{T_c} = 0$, the wave number of massive particles is simply proportional to the square root of energy: $k \propto z$. Hwang noticed this entails a remarkable property: for neutral particles without threshold, the Kapur-Peierls operator $R_L(z)$ is a rational function of z (see [21]), and therefore the radioactive problem (32) can be completely solved using polynomial root finders (see Sec. II F).

The general Mittag-Leffler expansion (41) of the Kapur-Peierls operator in z space is

$$\boldsymbol{R}_L(z) \underset{\mathcal{W}(z)}{=} \sum_{j\geqslant 1} \frac{\boldsymbol{\kappa}_j \boldsymbol{\kappa}_j^{\mathsf{T}}}{z-p_j} + \mathbf{Hol}_{\boldsymbol{R}_L}(z) \tag{46}$$

where square root of energy z space poles are

$$p_j \triangleq \sqrt{\mathcal{E}_j} \tag{47}$$

and the residue widths are connected to the poles as

$$\boldsymbol{\kappa_j} \triangleq \frac{\boldsymbol{r_j}}{\sqrt{2p_j}}. \tag{48}$$

This is readily obtained from previous E-space expressions using partial fraction decomposition of simple poles:

$$\frac{\boldsymbol{r}_j \boldsymbol{r}_j^{\mathsf{T}}}{E-\mathcal{E}_j} = \frac{\frac{\boldsymbol{r}_j \boldsymbol{r}_j^{\mathsf{T}}}{2\sqrt{\mathcal{E}_j}}}{\sqrt{E}-\sqrt{\mathcal{E}_j}} + \frac{-\frac{\boldsymbol{r}_j \boldsymbol{r}_j^{\mathsf{T}}}{2\sqrt{\mathcal{E}_j}}}{\sqrt{E}+\sqrt{\mathcal{E}_j}}.$$

The poles p_j come in opposite pairs ($p_j^+ = +\sqrt{\mathcal{E}_j}$ and $p_j^- = -\sqrt{\mathcal{E}_j}$), and the corresponding residue widths are thus rotated by $\pm\pi/2$ (multiplication by $\pm i$): $\boldsymbol{\kappa}_j^- \triangleq \boldsymbol{r}_j/\sqrt{2p_j^-} = -i\boldsymbol{r}_j/\sqrt{2p_j^+}$. The same $\boldsymbol{r}_j$ is shared by both poles p_j^+ and p_j^-, so that $\boldsymbol{\kappa}_j{}^- \boldsymbol{\kappa}_j{}^{-\mathsf{T}} = -\boldsymbol{\kappa}_j{}^+ \boldsymbol{\kappa}_j{}^{+\mathsf{T}}$.

Alternatively, Mittag Leffler expansion (46) can also be directly obtained by solving the radioactive problem in the square root of energy z space:

$$\boldsymbol{R}_L^{-1}(z)\big|_{z=p_j}\boldsymbol{\kappa_j} = \boldsymbol{0} \tag{49}$$

where the residue widths vectors $\{\boldsymbol{\kappa_j}\}$ are subject to the following normalization:

$$\boldsymbol{\kappa}_j^{\mathsf{T}}\left(\frac{\partial \boldsymbol{R}_L^{-1}}{\partial z}\bigg|_{z=p_j}\right)\boldsymbol{\kappa}_j = 1 \tag{50}$$

which yields relationship (48) (from $z = \sqrt{E}$), and can be calculated directly using

$$\frac{\partial \boldsymbol{R}_L^{-1}}{\partial z}\bigg|_{z=p_j} = \frac{\partial \boldsymbol{R}^{-1}}{\partial z}(p_j) - \frac{\partial \boldsymbol{L}}{\partial z}(p_j) \tag{51}$$

where $\boldsymbol{R}$ is invertible at z-space radioactive poles $\{p_j\}$ as

$$\frac{\partial \boldsymbol{R}^{-1}}{\partial z}(z) = -2z\boldsymbol{R}^{-1}\boldsymbol{\gamma}^{\mathsf{T}}(\boldsymbol{e} - z^2\mathbb{I})^{-2}\boldsymbol{\gamma}\boldsymbol{R}^{-1} \tag{52}$$

and where the partial derivatives $\frac{\partial \boldsymbol{L}}{\partial z}(p_j)$ can be derived from the Mittag-Leffler expansion of $\boldsymbol{L}(\rho)$ established in Theorem 1 of [32]:

$$\frac{\partial \boldsymbol{L}}{\partial z} = \left[i + \sum_{n\geqslant 1} \frac{1}{\rho - \omega_n} + \frac{\rho}{(\rho-\omega_n)^2} \right] \frac{\partial \rho}{\partial z} \tag{53}$$

where $\{\omega_n\}$ are the roots of the $O_c(\rho)$ outgoing wave functions, and also roots of $H_{+c}(\rho)$ from (12): $\forall n,\ H_{+c}(\omega_n) = 0$. For neutral particles, there are a finite number of such roots, reported in Table I of [32].

Equivalently, we can solve for the level matrix $\boldsymbol{A}$ radioactive problem in z space:

$$\boldsymbol{A}^{-1}(z)|_{z=p_j}\boldsymbol{\alpha_j} = \boldsymbol{0} \tag{54}$$

with eigenvectors $\boldsymbol{\alpha_j} \triangleq \frac{\boldsymbol{a_j}}{\sqrt{2p_j}}$ subject to normalization:

$$\boldsymbol{\alpha}_j^{\mathsf{T}} \left(\frac{\partial \boldsymbol{A}^{-1}}{\partial z}\bigg|_{z=p_j} \right) \boldsymbol{\alpha_j} = 1 \tag{55}$$

which is readily calculable from

$$\frac{\partial \boldsymbol{A}^{-1}}{\partial z}(p_j) = -2z\mathbb{I} - \boldsymbol{\gamma}\frac{\partial \boldsymbol{L}}{\partial z}(p_j)\boldsymbol{\gamma}^{\mathsf{T}}. \tag{56}$$

The level-matrix residues widths vectors are then linked to the radioactive widths by the following relation:

$$\boldsymbol{\kappa_j} = \boldsymbol{\gamma}^{\mathsf{T}}\boldsymbol{\alpha_j}. \tag{57}$$

Regardless of the method deployed to obtain Eq. (46), the latter entails the following Mittag Leffler expansion for resonance matrix $\boldsymbol{Z}$:

$$\boldsymbol{Z}(z) \underset{\mathcal{W}(z)}{=} \sum_{j\geqslant 1} \frac{\boldsymbol{\zeta_j}\boldsymbol{\zeta_j}^{\mathsf{T}}}{z - p_j} + \mathbf{Hol}_{\boldsymbol{Z}}(z) \tag{58}$$

where the residue widths are connected to the poles as

$$\begin{aligned} \boldsymbol{\zeta_j} &= \frac{\boldsymbol{\tau_j}}{\sqrt{2p_j}} \\ &= \boldsymbol{H_+^{-1}}(p_j)\boldsymbol{\rho}^{1/2}(p_j)\ \boldsymbol{\kappa_j} \\ &= \boldsymbol{H_+^{-1}}(p_j)\boldsymbol{\rho}^{1/2}(p_j)\ \frac{\boldsymbol{r_j}}{\sqrt{2p_j}}. \end{aligned} \tag{59}$$

This links back to the transmission matrix Mittag-Leffler expansion (43), which in z space entails

$$\boldsymbol{T}(z) \underset{\mathcal{W}(z)}{=} -i \sum_{j\geqslant 1} \frac{\boldsymbol{\zeta_j}\boldsymbol{\zeta_j}^{\mathsf{T}}}{z - p_j} + \mathbf{Hol}_{\boldsymbol{T}}(z). \tag{60}$$

This transmission matrix Mittag-Leffler expansion (60) corresponds to the Humblet-Rosenfeld scattering matrix expansion in Eq. (1.54) Sec. I.1.4, p. 538, of [5], where they denote the holomorphic (entire) part $\mathbf{Hol}_{\boldsymbol{T}}(z)$ as $Q_\ell(k)$. As they discuss, the natural variable for this nonresonant part is indeed the wave number k_c. Equations (60) and (59) thus explicitly link the residues of the Humblet-Rosenfeld expansions to the Wigner-Eisenbud R-matrix parameters. Unfortunately, there exists no simple general method to express the expansion coefficients of this entire part directly from R-matrix parameters.

D. Hwang's conjugate continuation

The windowed multipole representation is essentially an analytic continuation of R-matrix cross sections into the complex plane, in z space. R-matrix cross sections (5) and (10) are the square moduli and real parts of the transmission matrix $T_{cc'}(E)$ and the wave number $k_c(E)$, yielding real cross sections. Yet one can analytically continue these cross sections by performing the *conjugate continuation* of all R-matrix operators, which consists of taking the value of the modulus and real parts on the real axis $z \in \mathbb{R}$, and continuing them to the complex plane. This was the key insight introduced by Hwang in Ref. [21].

For any meromorphic function $f(z)$, we define its *continued conjugate* $f^*(z)$ as

$$f^*(z) \triangleq f(z^*)^*. \tag{61}$$

As such, the continued conjugate real part is defined as

$$\mathrm{Re}_{\mathrm{cont}}[f(z)] \triangleq \frac{f(z) + f^*(z)}{2} \tag{62}$$

and the continued conjugate square modulus is defined as

$$|f|^2_{\mathrm{cont}}(z) \triangleq f(z) \times f^*(z). \tag{63}$$

These are meromorphic complex functions: $\mathrm{Re}_{\mathrm{cont}}[f(z)] \in \mathbb{C}$ and $|f|^2_{\mathrm{cont}}(z) \in \mathbb{C}$. They are the analytic continuation to complex $z \in \mathbb{C}$ of the real part and the square modulus, which they match on the real axis $z \in \mathbb{R}$. Consider a meromorphic function $f(z)$ with simple poles and Mittag-Leffler expansion:

$$f(z) \underset{\mathcal{W}(z)}{=} \sum_{j\geqslant 1} \frac{r_j}{z - p_j} + \sum_{n\geqslant 0} a_n z^n. \tag{64}$$

Its continued conjugate square modulus is thus

$$\begin{aligned} |f|^2_{\mathrm{cont}}(z) \underset{\mathcal{W}(z)}{=} &\left(\sum_{j\geqslant 1} \frac{r_j}{z - p_j} + \sum_{n\geqslant 0} a_n z^n \right) \\ &\times \left(\sum_{j\geqslant 1} \frac{r_j^*}{z - p_j^*} + \sum_{n\geqslant 0} a_n^* z^n \right). \end{aligned} \tag{65}$$

The unicity of poles and residues entails all the poles of $|f|^2_{\mathrm{cont}}(z)$ are the poles p_j of $f(z)$ and their complex conjugate p_j^*. By evaluating the corresponding residues, one finds the following Mittag-Leffler expansion for the conjugate continuation:

$$|f|^2_{\mathrm{cont}}(z) \underset{\mathcal{W}(z)}{=} \sum_{j\geqslant 1} \frac{r_j\ f(p_j^*)^*}{z - p_j} + \frac{r_j^*\ f(p_j^*)}{z - p_j^*} + \sum_{n\geqslant 0} c_n z^n \tag{66}$$

where

$$c_n \triangleq \mathrm{Re}\left[\sum_{k=0}^{n} a_{n-k}a_k^* + 2\sum_{j\geqslant 1} \frac{r_j\ [f(p_j^*)^* - a_n^*]}{p_j} \right] \tag{67}$$

which can be obtained by developing (65) and applying Cauchy's residues theorem to (66) with contour integrations of $\frac{|f|^2(z)}{z^{n+1}}$. In Eq. (66), one recognizes the remarkable property that the continued square modulus can be expressed as a continued conjugate real part

$$|f|^2_{\text{cont}}(z) \underset{\mathcal{W}(z)}{=} \text{Re}_{\text{cont}}\left[\sum_{j\geqslant 1}\frac{\widetilde{r}_j}{z-p_j}+\sum_{n\geqslant 0}c_n z^n\right] \tag{68}$$

with

$$\widetilde{r}_j \triangleq 2\, r_j\, f(p_j^*)^*. \tag{69}$$

Therefore, by using Hwang's conjugate continuation, one can express all R-matrix cross sections as the continued conjugate real part of conjugate continued R-matrix operators: this is the key to converting R-matrix cross sections to windowed multipole representation.

E. Windowed multipole representation

The windowed multipole representation is the analytic continuation of the pole expansion of R-matrix cross sections. For open channels (energies above thresholds $E > E_{T_c}$), the energy dependence of R-matrix cross sections—described by Eqs. (5) and (10)—is expanded along the real energy axis $E \in \mathbb{R}$, and the corresponding expressions are analytically continued to all complex energies $E \in \mathbb{C}$. The windowed multipole representation can thus be seen as a generalization of R-matrix cross sections to the complex plane, for open channels, as shown in Fig. 1. As such, windowed multipole cross sections only match R-matrix cross sections for real energies above the channel threshold: $E > E_{T_c}$.

1. *Windowed pole representation: Transmission matrix approach*

The most straightforward approach is to consider the transmission matrix $\boldsymbol{T}(E)$ Mittag-Leffler expansion (43), and apply Hwang's conjugate continuation in energy space, which yields

$$|\boldsymbol{T}|^2_{\text{cont}}(E) \underset{\mathcal{W}(E)}{=} \text{Re}_{\text{cont}}\left[\sum_{j\geqslant 1}\frac{-i\widetilde{\boldsymbol{\tau}}_j}{E-\mathcal{E}_j}+\mathbf{Hol}_{|\boldsymbol{T}|^2}(E)\right] \tag{70}$$

where we use the Hadamard product "$\circ$" to express the residues as

$$\widetilde{\boldsymbol{\tau}}_j \triangleq 2\,\boldsymbol{\tau}_j\boldsymbol{\tau}_j^{\intercal}\circ\boldsymbol{T}(\mathcal{E}_j^*)^*. \tag{71}$$

Thus, for real energies with open channels, the partial and total cross sections can be expressed, respectively, as

$$\sigma_{cc'}(E) \underset{\mathcal{W}(E)}{=} \frac{4\pi g_{J_c^\pi}}{|k_c(E)|^2}\text{Re}_{\text{cont}}\left[\sum_{j\geqslant 1}\frac{-i[\widetilde{\boldsymbol{\tau}}_j]_{cc'}}{E-\mathcal{E}_j}+\text{Hol}_{|\boldsymbol{T}|^2}(E)\right] \tag{72}$$

and

$$\sigma_c(E) \underset{\mathcal{W}(E)}{=} \frac{4\pi g_{J_c^\pi}}{|k_c(E)|^2}\text{Re}_{\text{cont}}\left[\sum_{j\geqslant 1}\frac{-i[\boldsymbol{\tau}_j\boldsymbol{\tau}_j^{\intercal}]_{cc}}{E-\mathcal{E}_j}+\text{Hol}_{\boldsymbol{T}}(E)\right]. \tag{73}$$

Expressions (72) and (73) are general; they apply to any cross section described by R-matrix theory (be it massless photons or massive charged or neutral particle channels). They are

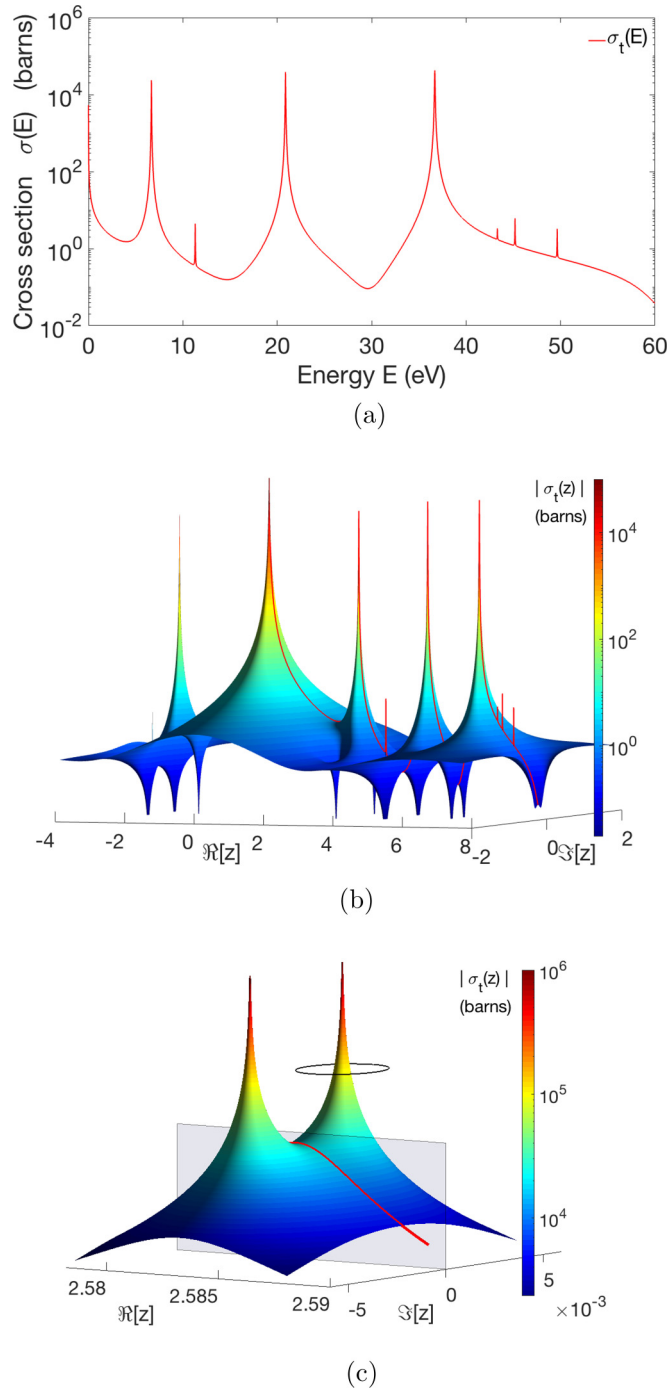

FIG. 1. Windowed multipole representation of R-matrix cross sections: ^{238}U total cross-section (minus potential scattering) meromorphic continuation into the complex z plane, for $z = \pm\sqrt{E}$ in eV. This surface's crest and thalweg line along the real axis is the R-matrix cross section above the zero threshold. (a) ^{238}U first resonances (three s waves and four p waves). (b) ^{238}U windowed multipole cross-section surface. (c) ^{238}U first s-wave resonance peak. Negative z in (b) are on the shadow branch $\{E, -\}$ of mapping (2). (c) shows the resonance peaks are the saddle points between the complex conjugate poles. The black circle in (c) represents the contour integrals around the poles of the complex cross section which enable both conversion to windowed multipole covariances (Theorem 2) and analytic Doppler broadening (Theorem 3).

local expressions, only valid on the neighborhood $\mathcal{W}(E)$ of any given energy E away from the thresholds [branch points E_{T_c} of (4) mapping], though this neighborhood can be as large as the distance between thresholds (for more discussion on this point, we refer to the penultimate paragraph of Sec. II.D in Ref. [31]). They reflect the fact that two physical phenomena dictate the behavior of R-matrix cross sections: resonances and thresholds.

Away from threshold energies E_{T_c}—the branch points of wave-number–energy mapping (4)—each resonance can be accurately represented by a SLBW profile in energy space E, that is the combination of symmetric and antisymmetric Lorentzian functions. These are made evident by recalling definition (40), which splits the radioactive poles into real and imaginary components $\mathcal{E}_j \triangleq E_j - i\frac{\Gamma_j}{2}$, and noticing that each resonance of the windowed multipole representation (72) can be expressed as

$$\mathrm{Re}\left[\frac{a+ib}{E-\mathcal{E}_j}\right] = a\frac{(E-E_j)}{(E-E_j)^2+\frac{\Gamma_j^2}{4}} + b\frac{\frac{\Gamma_j}{2}}{(E-E_j)^2+\frac{\Gamma_j^2}{4}}. \tag{74}$$

The sum of resonances is complemented by the holomorphic background term $\mathbf{Hol}_{\boldsymbol{T}}$, and modulated by the $\frac{1}{|k_c(E)|^2}$ term. This illustrates the fact that the wave number k_c dominates the behavior of R-matrix cross sections near thresholds E_{T_c}, where $k_c \to 0$. Moreover, the holomorphic (entire) part is itself more naturally described as a function of the wave number k_c rather then the energy: $\mathbf{Hol}_{\boldsymbol{T}}(\boldsymbol{k})$, as explained by Humblet and Rosenfeld through Eqs. (1.64) and (1.67) Sec. I.1.4, pp. 539–540, of [5]. The threshold behavior of R-matrix cross sections was detailed by Wigner in Ref. [53]. Depending on the angular momenta ℓ and ℓ' and the charges of the particles, reaction and scattering cross sections either (a) have threshold behaviors in powers of $k_c^{N(\ell,\ell')}$, where $N(\ell,\ell') \in \mathbb{Z}$ is some integer depending on the different angular momenta, but never smaller than -2 [$N(\ell,\ell') \geqslant -2$]; or (b) in some cases of Coulomb repulsion, modulate this with an exponential decay $\propto \exp(-a/k_c)$ with some real positive $a > 0$ (see Sec. III of [53] for more details). This means we can represent in all generality the threshold behavior as a Laurent expansion around the threshold: $\sigma_{cc'} \underset{k_c\to 0}{\sim} \sum_{n\geqslant -2} a_n k_c^n$.

By thus expressing the threshold behavior explicitly, we can constitute the *windowed multipole representation* of R-matrix cross sections:

$$\sigma_{cc'}(E) \underset{\mathcal{W}(E)}{\triangleq} \sum_{n\geqslant -2} \widetilde{a}_n^{cc'} k_c^n(E) + \frac{1}{E}\mathrm{Re}_{\mathrm{cont}}\left[\sum_{j\geqslant 1}\frac{\widetilde{R}_j^{cc'}}{E-\mathcal{E}_j}\right] \tag{75}$$

and

$$\sigma_c(E) \underset{\mathcal{W}(E)}{\triangleq} \sum_{n\geqslant -2} a_n^c k_c^n(E) + \frac{1}{E}\mathrm{Re}_{\mathrm{cont}}\left[\sum_{j\geqslant 1}\frac{R_j^c}{E-\mathcal{E}_j}\right] \tag{76}$$

where the residues are obtained by evaluating at the pole values as

$$\widetilde{R}_j^{cc'} \triangleq -i\frac{4\pi g_{J_c^\pi}\mathcal{E}_j}{|k_c(\mathcal{E}_j)|^2}[\widetilde{\boldsymbol{\tau}}_{\boldsymbol{j}}]_{cc'} \tag{77}$$

and

$$R_j^c \triangleq -i\frac{4\pi g_{J_c^\pi}\mathcal{E}_j}{|k_c(\mathcal{E}_j)|^2}\left[\boldsymbol{\tau_j}\boldsymbol{\tau_j}^{\mathsf{T}}\right]_{cc}. \tag{78}$$

Equivalently, the windowed multipole representation can be carried out in the square root of energy z space, in what constitutes Theorem 1.

Theorem 1. WINDOWED MULTIPOLE REPRESENTATION

Let $\mathcal{E}_j$ be the energy-space poles of the Kapur-Peierls operator $\boldsymbol{R}_L$, defined in Eq. (15), and let $z \triangleq \sqrt{E}$ be the square root of energy. The energy dependence of R-matrix cross sections can be exactly expressed as a Laurent expansion in wave number k_c, of order no less than k_c^{-2}, plus the conjugate continuation real part (62) of a sum of energy-space resonances with poles $\mathcal{E}_j$, which in z space yield pairs of opposite poles $p_j = \pm\sqrt{\mathcal{E}_j}$, so that partial cross sections (5) take the windowed multipole representation

$$\sigma_{cc'}(z) \underset{\mathcal{W}(z)}{\triangleq} \sum_{n\geqslant -2} \widetilde{a}_n^{cc'} k_c^n(z) + \frac{1}{z^2}\mathrm{Re}_{\mathrm{cont}}\left[\sum_{j\geqslant 1}\frac{\widetilde{r}_j^{cc'}}{z-p_j}\right] \tag{79}$$

and the total cross section (10) takes the form

$$\sigma_c(z) \underset{\mathcal{W}(z)}{\triangleq} \sum_{n\geqslant -2} a_n^c k_c^n(z) + \frac{1}{z^2}\mathrm{Re}_{\mathrm{cont}}\left[\sum_{j\geqslant 1}\frac{r_j^c}{z-p_j}\right] \tag{80}$$

where the partial residues can be constructed from R-matrix parameters as

$$\widetilde{r}_j^{cc'} \triangleq -i\frac{4\pi g_{J_c^\pi} p_j^2}{|k_c(p_j)|^2}\left[2\ \boldsymbol{\zeta_j}\boldsymbol{\zeta_j}^{\mathsf{T}} \circ \boldsymbol{T}(p_j^*)^*\right]_{cc'} \tag{81}$$

and the total residues can be constructed as

$$r_j^c \triangleq -i\frac{4\pi g_{J_c^\pi} p_j^2}{|k_c(p_j)|^2}\left[\boldsymbol{\zeta_j}\boldsymbol{\zeta_j}^{\mathsf{T}}\right]_{cc} \tag{82}$$

where the $\boldsymbol{\zeta_j}$ residue widths vectors are linked to the Kapur-Peierls operator $\boldsymbol{R}_L$ poles and residues through relations (59).

Alternatively, the residues can be numerically obtained through Cauchy's residues theorem contour integrals

$$\widetilde{r}_j^{cc'} = \frac{1}{i\pi}\oint_{\mathfrak{C}_{p_j}} z^2\sigma_{cc'}(z)dz \tag{83}$$

where $\mathfrak{C}_{p_j}$ designates a positively oriented simple closed contour containing only pole p_j. For instance, if $\mathfrak{C}_{p_j}$ is a circle of small radius $\epsilon > 0$ around pole p_j, this yields

$$r_j^c = \frac{\epsilon}{\pi}\int_{\theta=0}^{2\pi}(p_j+\epsilon e^{i\theta})^2\sigma_c(p_j+\epsilon e^{i\theta})e^{i\theta}d\theta. \tag{84}$$

In order to perform these contour integrals, R-matrix cross sections (5) and (10) must have been meromorphically continued to complex energies by means of conjugate continuations (63) and (62), respectively.

Therefore, by solving the radioactive problem (32)—or level-matrix one (36)—to find the poles $\mathcal{E}_j$ and residues $\boldsymbol{r_j}$ of the Kapur-Peierls operator [respectively, p_j and $\boldsymbol{\kappa_j}$ from (50) or level-matrix equivalent (54) in z space], we can compute the transmission matrix residues $\boldsymbol{\tau_j}$ from (44) and the conjugate

continuation ones $\widetilde{\boldsymbol{\tau}}_j$ from (71) [respectively, $\boldsymbol{\zeta}_j$ from (59) in z space], to find the poles and residues of the windowed multipole representation of R-matrix cross sections, through Eqs. (75)–(78) or, respectively, Eqs. (79)–(82) for z space.

2. *Windowed multipole representation: Potential and resonance matrices approach*

The transmission matrix approach is exact, but it has three drawbacks: (1) it is not simple to interpret physically; (2) it does not give us information on the "background" behavior (nonresonant Laurent expansion $\sum_{n\geqslant -2} a_n k_c^n$); (3) it can be numerically unstable. Decomposition (23) of the transmission matrix helps us separate the cross sections into parts we can interpret physically: the potential cross section σ_c^{pot} has no resonances (26); the reaction cross section $\sigma_{cc'}^{\text{react}}$ has all the resonances (30); and both the partial cross section $\sigma_{cc'}$ from (31) and the total cross section σ_c from (86) also have interference resonances from the real part of the resonance matrix $\boldsymbol{Z}$. This means all the resonances of R-matrix cross sections can be recovered from the resonance matrix $\boldsymbol{Z}$ Mittag-Leffler expansion (58). Applying Hwang's conjugate continuation method to construct the windowed multipole representation then yields the following.

(1) Potential scattering cross section (of channel c):

$$\sigma_c^{\text{pot}}(E) \underset{\mathcal{W}(z)}{=} 4\pi g_{J_c^\pi} \frac{\text{Re}[iD_c]}{|k_c|^2}. \tag{85}$$

(2) Total cross section (of channel c):

$$\sigma_c(z) \underset{\mathcal{W}(z)}{\triangleq} \sigma_c^{\text{pot}}(z) + \frac{1}{z^2}\text{Re}_{\text{cont}}\left[\sum_{j\geqslant 1}\frac{r_j^c}{z-p_j}\right] + \sum_{n\geqslant -2} b_n^c k_c^n(z) \tag{86}$$

where the total residues r_j^c are defined in Eq. (82).

(3) Self-scattering cross section (of channel c):

$$\sigma_c^{\text{scat}}(E) \underset{\mathcal{W}(z)}{=} \frac{1}{z^2}\text{Re}_{\text{cont}}\left[\sum_{j\geqslant 1}\frac{{}^{\text{scat}}r_j^c}{z-p_j}\right] + \sum_{n\geqslant -2} c_n^c k_c^n(z)\delta_{cc'} \tag{87}$$

with scattering residues

$${}^{\text{scat}}r_j^c \triangleq -\frac{4\pi g_{J_c^\pi} p_j^2}{|k_c(p_j)|^2}\left[2\,\boldsymbol{\zeta}_j\boldsymbol{\zeta}_j^{\mathsf{T}} \circ \boldsymbol{D}(p_j^*)^*\right]_{cc'}\delta_{cc'}. \tag{88}$$

(4) Interference cross section (of channel c):

$$\sigma_c^{\text{int}}(E) \underset{\mathcal{W}(z)}{=} \frac{1}{z^2}\text{Re}_{\text{cont}}\left[\sum_{j\geqslant 1}\frac{{}^{\text{int}}r_j^c}{z-p_j}\right] + \sum_{n\geqslant -2} d_n^c k_c^n(z)\delta_{cc'} \tag{89}$$

with interference residues

$${}^{\text{int}}r_j^c \triangleq -i\frac{4\pi g_{J_c^\pi} p_j^2}{|k_c(p_j)|^2}\left[\boldsymbol{\zeta}_j\boldsymbol{\zeta}_j^{\mathsf{T}} \circ \boldsymbol{Y}(p_j^*)^*\right]_{cc'}\delta_{cc'}. \tag{90}$$

(5) Reaction cross section (from channel c to c'):

$$\sigma_{cc'}^{\text{react}}(z) \underset{\mathcal{W}(z)}{=} \frac{1}{z^2}\text{Re}_{\text{cont}}\left[\sum_{j\geqslant 1}\frac{{}^{\text{react}}r_j^{cc'}}{z-p_j}\right] + \sum_{n\geqslant -2}\widetilde{b}_n^{cc'} k_c^n(z) \tag{91}$$

with reaction residues

$${}^{\text{react}}r_j^{cc'} \triangleq \frac{4\pi g_{J_c^\pi} p_j^2}{|k_c(p_j)|^2}\left[2\,\boldsymbol{\zeta}_j\boldsymbol{\zeta}_j^{\mathsf{T}} \circ \boldsymbol{Z}(p_j^*)^*\right]_{cc'}. \tag{92}$$

(6) Partial (angle-integrated) cross section (31) (from channel c to c'):

$$\begin{aligned}\sigma_{cc'}(E) &= \left[\sigma_c^{\text{pot}}(E) + \sigma_c^{\text{scat}}(E)\right]\delta_{cc'} + \sigma_{cc'}^{\text{react}}(E)\\ &= \left[\sigma_c^{\text{tot}}(E) - \sigma_c^{\text{int}}(E)\right]\delta_{cc'} + \sigma_{cc'}^{\text{react}}(E).\end{aligned}$$

Noticing that $-i\boldsymbol{T}^* = \boldsymbol{Z}^* - \boldsymbol{D}^*$, this entails the partial residues $\widetilde{r}_j^{cc'}$ from (81) are connected to the total residues r_j^c from (82), the reaction residues ${}^{\text{react}}r_j^{cc'}$ from (92), the scattering residues ${}^{\text{scat}}r_j^c$ from (88), and the interference residues ${}^{\text{int}}r_j^c$ from (90), according to

$$\widetilde{r}_j^{cc'} = {}^{\text{react}}r_j^{cc'} + {}^{\text{scat}}r_j^c = {}^{\text{react}}r_j^{cc'} + r_j^c - {}^{\text{int}}r_j^c. \tag{93}$$

Total cross-section decomposition (86) is simpler to interpret physically than expression (82) directly derived from the transmission matrix, because the potential cross section σ_c^{pot} is extracted from the background Laurent expansion: $\sum_{n\geqslant -2} a_n^c z^n$. The same holds for the partial cross section (79), where the residues decomposition (93) untangles the direct expression (81) from the transmission matrix approach. Though mathematically equivalent, some of these approaches may be more numerically stable than others.

Importantly, we do not need the poles of the potential matrix $\boldsymbol{D}$ to express the partial and total cross sections. This is because any such poles (the zeros of $\boldsymbol{H}_+$) cancel out of the scattering matrix (14), and therefore of the cross sections. Before we proved this result in Theorem 3 of [31], Hwang had to explicitly decompose the potential cross section σ_c^{pot} into poles and residues in Eqs. (1) and (2) of [24] [also in Eqs. (3) and (4) of [25]], with severe numerical instability implications which he attempted to remedy by introducing pseudopoles in Ref. [23]. We now known that under proper analytic continuation, these spurious poles have zero residues in the transmission matrix, and thus cancel out of the partial and total cross sections.

3. *Pole expansion: R-matrix construct or rational fit*

So far, we have constructed the transmission matrix Mittag-Leffler expansion (60) by first solving the radioactive states problem (49) and then obtaining the transmission matrix residues from those of the Kapur-Peierls operator, through (59). One could dispense of the intermediary steps and find the radioactive poles $\{p_j\}$ directly through the transmission matrix by solving the generalized eigenvalue problem

$$\boldsymbol{T}^{-1}(z)|_{z=p_j}\boldsymbol{\zeta}_j = \boldsymbol{0} \tag{94}$$

and subjecting the residue widths vectors $\{\boldsymbol{\zeta}_j\}$ to the following normalization:

$$\boldsymbol{\zeta}_j^{\mathsf{T}}\left(\frac{\partial \boldsymbol{T}^{-1}}{\partial z}\bigg|_{z=p_j}\right)\boldsymbol{\zeta}_j = i. \tag{95}$$

Though mathematically equivalent, this all-in-one approach can nonetheless be prone to numerical instabilities. This leads us to the question of how to numerically solve the generalized eigenproblems—either the radioactive ones (49) or directly

(94). On this issue, we direct the reader to the section of Theorem 1 in Ref. [31] for a more detailed discussion, in particular on the multisheeted nature of the Riemann mapping (4), which can complicate the search for solutions. We will here simply state that these are nonlinear eigenvalue problems, and general algorithms to solve them can be found in the *Handbook of Linear Algebra* [54], Chap. 115. One such algorithm is the Rayleigh-quotient method, used by Brune to find alternative parameters in Ref. [55]. Alternatively, it is sometimes more computationally advantageous to first find the radioactive poles $\{p_j\}$ directly by solving the channel determinant problem, $\det(\boldsymbol{R}_L^{-1}(z)|_{z=p_j}) = 0$, or the corresponding level determinant one, $\det(\boldsymbol{A}^{-1}(z)|_{z=p_j}) = 0$, and to second solve the associated eigenvalue problem (which is now linear), or even to directly evaluate the residues at the found poles by contour integrals (83) and (84). Such methods tailored to find all the roots of the radioactive problem were introduced in Ref. [29], in Sec. 5 of [38,39], or in Eqs. (200) and (204) of [56]. Also, solving the Kapur-Peierls radioactive problem (49) will be advantageous over solving the level matrix one (54) when the number of levels N_λ far exceeds the number of channels N_c, and conversely.

Rather than starting from the Wigner-Eisenbud R-matrix resonance parameters $\{E_{T_c}, a_c, B_c, E_\lambda, \gamma_{\lambda,c}\}$ to construct the windowed multipole representation poles p_j and residues $\widetilde{r}_j^{cc'}$ and r_j^c as (81) and (82), an alternative approach is to simply curve fit the pointwise energy dependence of nuclear cross sections $\sigma_{cc}(E)$ with the corresponding windowed multipole representation forms (79) and (80). For instance, this approach was successfully deployed in Ref. [40] and in Ref. [30], where using the black-box rational function approximating algorithm called "vector-fitting" [57,58] led to finding the exact resonant radioactive poles $\{p_j\}$ of ^{16}O, for which no resonance parameters were published [30]. This conversion of pointwise R-matrix cross sections into windowed multipoles representation approach was generalized to most of the nuclides found in the ENDF/B-VII.1 nuclear data library [59,60], and could potentially be facilitated by recent advances in rational approximation algorithms—such as RKFIT [61] or AAA [62].

4. Windowing process: Laurent background fit

Regardless of the method deployed to find the poles $\{p_j\}$ and their corresponding residues, there exists no general way to construct the thresholds Laurent expansions, $\sum_{n\geqslant -2} a_n k_c(z)^n$, from the R-matrix parameters. One must thus select an energy window $\mathcal{W}(E)$ and curve fit the background Laurent expansion $\sum_{n\geqslant -2} a_n k_c(z)^n$ by subtracting the resonances, that is the poles contribution $\sum_{j\in\mathcal{W}(E)} \frac{r_j^c}{z-p_j}$. Nonetheless, there is a difficulty as to which such poles one should include explicitly into the window. It is not necessary to explicitly call all the poles $\{p_j\}$ for each window $\mathcal{W}(E)$, rather the contribution of far-away poles is best curve fitted and included in the Laurent expansion $\sum_{n\geqslant -2} a_n k_c(z)^n$. The criterion used to decide which poles $\{p_j\}$ to include within each window is to select an accuracy bound for the Doppler broadened cross section, and include in window $\mathcal{W}(E)$ all the poles the Doppler broadened resonances of which have a significant impact on the cross section within that window. Thus, the greater the maximum temperature, the more far-away poles have to be included to compute the cross section within window $\mathcal{W}(E)$. Once the contributing poles (after Doppler broadening) have been found, we subtract them from the 0-K cross sections and curve fit the difference with a Laurent expansion $\sum_{n\geqslant -2} a_n k_c(z)^n$. More detailed explanations on this windowing process can be found in Refs. [26–28].

Though the background Laurent expansion must be numerically fitted, and the resonant poles themselves may be accurately found using rational approximation black-box algorithms, it is critical to understand that the windowed multipole representation (79) and (80) is not a curve-fitting approximation: this is a rigorous representation, mathematically and physically equivalent to the exact R-matrix theory cross sections (for real energies in open channels), or the Humblet-Rosenfeld pole expansions in wave-number space. This can be tested by curve fitting in E and k_c space, both the resonances and the background Laurent expansions. One will notice that the E-space Breit-Wigner profiles (74) capture exactly one for one the resonance behavior. However, the threshold behaviors are not well represented by the E variable: while few coefficients suffice to reach high accuracy using Laurent expansions in k_c (usually no more than a_{-2}, a_{-1}, a_0, and a_1), many more expansion coefficients are necessary when fitting the background with Laurent expansions with powers of E.

Finally, remember that for nonmassless particles, wave-number–energy mapping (2) entails that $k_c^2 \propto z^2 - E_{T_c}$. Thus, for zero-threshold reactions ($E_{T_c} = 0$), we have a direct proportionality $k_c \propto z$. In order to achieve closed-form Doppler-broadening expressions, we may be willing to sacrifice the physically accurate Laurent expansion in k_c, and replace it with an approximation in powers of z—that is a Laurent expansion $\sum_{n\geqslant -2} a_n z^n$—plus rational Padé-type approximations with simple poles—that is adding nonphysical pseudopoles—so as to approximate the exact threshold behavior $\sum_{n\geqslant -2} a_n k_c(z)^n$ with powers of z and pseudopoles $\sum_{n\geqslant -2} \widetilde{a}_n z^n + \sum_{n\geqslant 1} \frac{\widetilde{r}_n}{z-\widetilde{p}_n}$. Runge's theorem guarantees such approximation can always be performed to high accuracy, though this is often costly, as many more pseudopoles and Laurent expansion coefficients have to be introduced. Nonetheless, this approximation will have advantages when Doppler-broadening massive (not massless photons) particles (both charged and neutral), and it also provides a unified windowed multipole formalism:

$$\sigma(z) \underset{\mathcal{W}(E)}{=} \sum_{n\geqslant -2} a_n z^n + \frac{1}{z^2}\mathrm{Re}_{\mathrm{cont}}\left[\sum_{j\geqslant 1} \frac{r_j}{z-p_j}\right]. \tag{96}$$

In addition to the residues (83) and (84) of Theorem 1, one can now also obtain the Laurent expansion coefficients by means of contour integrals:

$$\begin{aligned} a_{-2} &= \mathrm{Re}_{\mathrm{cont}}\left[\sum_{j\geqslant 1} \frac{r_j}{p_j}\right] + \frac{1}{2i\pi}\oint_{\mathfrak{C}_0} z\,\sigma(z)dz, \\ a_{-1} &= \mathrm{Re}_{\mathrm{cont}}\left[\sum_{j\geqslant 1} \frac{r_j}{p_j^2}\right] + \frac{1}{2i\pi}\oint_{\mathfrak{C}_0} \sigma(z)dz, \\ a_n &\underset{n\geqslant 0}{=} \frac{1}{2i\pi}\oint_{\mathfrak{C}_0} \frac{\sigma(z)}{z^{n+1}}dz = \frac{1}{2\pi\epsilon^n}\int_{\theta=0}^{2\pi} \sigma(\epsilon e^{i\theta})e^{-in\theta}d\theta \end{aligned} \tag{97}$$

where $\mathfrak{C}_0$ designates a positively oriented simple closed contour containing only pole zero, for instance a circle centered at zero with small radius $\epsilon > 0$. Relations (97) are obtained by performing partial fraction decomposition:

$$\frac{1}{z^2}\frac{r_j/2}{z-p_j} = \frac{r_j/2}{p_j^2}\left[\frac{1}{z-p_j} - \frac{1}{z} - \frac{p_j}{z^2}\right].$$

Therefore, converting R-matrix cross sections to the unified windowed multipole representation formalism (96) is conceptually simple: it suffices to solve for the z-space poles $\{p_j\}$ of the $\boldsymbol{A}$ level matrix (18)—that is radioactive problem (54)—and then perform contour integrals (84), (83), and (97) on the continued conjugate (61) R-matrix cross sections (10) and (5) to find their residues and Laurent expansion coefficients.

Henceforth, we will only treat this unified windowed multipole representation formalism (96): it is physically exact for any R-matrix cross section of zero threshold, and an approximation of the exact windowed multipole representations (79) and (80) only in windows that include nonzero thresholds.

F. Hwang's special case: Zero-threshold neutron cross sections

There is one special case where it is possible to fully and explicitly convert R-matrix parameters into their exact windowed multipole representation (96), without any need of curve fitting or truncating the Laurent expansion: this is the case of neutron cross sections with no thresholds, which Hwang first investigated in Ref. [21]. In this case, because all channels have zero energy threshold ($E_{T_c} = 0$), every channel's wave number is proportional to the square root of energy, $k_c \propto z$, and we can therefore write the dimensionless wave number as

$$\begin{aligned}\rho_c &= \rho_{0c}\, z,\\ \rho_{0c} &\triangleq a_c\sqrt{\frac{2m_{c,1}m_{c,2}}{(m_{c,1}+m_{c,2})\hbar^2}}.\end{aligned} \tag{98}$$

Moreover, there are no branch points to mapping (2) other than zero, so that the windowed multipole representation (96) is exact and valid everywhere for positive energies $E > 0$: the Laurent development $\sum_{n\geqslant -2} a_n z^n$ at zero accurately describes the threshold behavior (as there is no exponential dampening from charges). Because there are no charges, the dimensionless Coulomb field parameter (9) is null, $\eta_c = 0$, so that the difference $\omega_c \triangleq \sigma_{\ell_c}(\eta_c) - \sigma_0(\eta_c)$ in Coulomb phase shift (8) is such that we always have $e^{i\omega_c} = 1$. From this, definitions (12) entail that the incoming and outgoing wave functions are then simply the H_- and H_+ combination of regular and irregular Bessel functions:

$$\begin{aligned}O(\rho) = H_+(\rho) = G(\rho) + iF(\rho) = \rho[-y_\ell(\rho) + ij_\ell(\rho)],\\ I(\rho) = H_-(\rho) = G(\rho) - iF(\rho) = \rho[-y_\ell(\rho) - ij_\ell(\rho)]\end{aligned} \tag{99}$$

where $j_\ell(\rho)$ is the spherical Bessel function of the first kind, and $y_\ell(\rho)$ is the spherical Bessel function of the second kind, respectively, defined in Chap. 10, Eqs. (10.47.3) and (10.47.4) of [41], or in Chap. 10, Eq. (10.1.1) of Abramowitz and Stegun [42]. This in turn entails the remarkable property that the reduced logarithmic derivative (17) of the outgoing-wave function $L(\rho)$ is now a rational function (that is the ratio of polynomials) in ρ, the expressions of which, along with those of $O(\rho)$, are reported in Table I of [32], and we refer to Sec. II.B of [32] for a more detailed description of these functions.

1. *Solving the radioactive states problem: Polynomial rootfinding*

Crucially, in this special case of only neutron channels without threshold, the fact that $L(\rho)$ is now a rational function in z entails that (15), the Kapur-Peierls operator $\boldsymbol{R}_L$, is also a rational function in z space. Therefore, the radioactive problem (49) itself becomes that of finding the roots of a rational function. We solve the radioactive problem through the level matrix approach (54), where the residue width vectors are normalized as (55), which we can calculate through (56) where the partial derivative (53) is now simply $\frac{\partial\rho}{\partial z} = \rho_{0_c}$ from (98). The key is now to find the radioactive poles $\{p_j\}$ in z space. We can do so by solving for the roots of the inverse level matrix (18) determinant: $\det(\boldsymbol{A}^{-1}(z)|_{z=p_j}) = 0$. Since this determinant is a rational function in z, one can find all its zeros by expressing it in irreducible form, and solve for all the roots of the numerator polynomial. This can be accomplished by developing the determinant and applying Lemma 3 of [32] on *diagonal divisibility and capped multiplicities*, in an analogous fashion as in the proof of Theorem 3 in Ref. [32], to which we point for more detailed explanations. More precisely, one can see in Table I of [32] that $L_\ell(\rho) = \frac{u_{\ell+1}(\rho)}{q_\ell(\rho)}$ is a proper rational function with simple poles, with a denominator $q_\ell(\rho)$ of degree ℓ and a numerator $u_{\ell+1}(\rho)$ of degree $\ell+1$. The polynomial factor $Q(z)$ that makes the denominator of the $\det(\boldsymbol{A}^{-1})(z)$ rational function irreducible can then be found by applying Lemma 3 of [32] on diagonal divisibility and capped multiplicities, yielding

$$Q(z) \triangleq \prod_{c=1}^{N_c} q_{\ell_c}(z) \tag{100}$$

so that for only neutron channels without thresholds, finding all the radioactive poles $\{p_j\}$ is akin to solving for all the roots of the following polynomial:

$$Q(z)\,\det(\boldsymbol{e} - z^2\mathbb{I} - \boldsymbol{\gamma}(\boldsymbol{L}(z) - \boldsymbol{B})\boldsymbol{\gamma}^{\mathsf{T}})|_{z=p_j} = 0. \tag{101}$$

The degree of this polynomial, and thus the number of (complex) roots $\{p_j\}$, is

$$N_L = 2N_\lambda + \sum_{c=1}^{N_c}\ell_c \tag{102}$$

which is a particular case of the general number of radioactive poles N_L we stated in Eq. (42) (and proved in Theorem 1 of [31]), but with only one threshold, $E_{T_c} = 0$, so that the number of different thresholds is 1: $N_{E_{T_c}\neq E_{T_{c'}}} = 1$.

In the simple case of multilevel Breit-Wigner approximation (22), the diagonal level matrix $\boldsymbol{A}^{-1}_{\mathbf{MLBW}}$ greatly simplifies the radioactive states eigenproblem (54): it is now diagonal and the poles $\{p_j\}$ are the roots of

$$E_\lambda - p_j^2 - \sum_{c=1}^{N_c}\gamma_{\lambda,c}^2(L_c(p_j) - B_c) = 0. \tag{103}$$

We then have $[\boldsymbol{\kappa}_j\boldsymbol{\kappa}_j^{\mathsf{T}}]_{\text{MLBW}} = \boldsymbol{\gamma}^{\mathsf{T}}[\boldsymbol{\alpha}_j\boldsymbol{\alpha}_j^{\mathsf{T}}]_{\text{MLBW}}\boldsymbol{\gamma}$ where normalization (55) entails

$$[\boldsymbol{\alpha}_j\boldsymbol{\alpha}_j^{\mathsf{T}}]_{\text{MLBW}} = \text{diag}_{N_\lambda}\left(\frac{-1}{2p_j + \sum_{c=1}^{N_c}\gamma_{\lambda,c}^2\frac{\partial L_c}{\partial z}(p_j)}\right). \quad (104)$$

This approach will yield the same results as those in Ref. [63].

Interestingly, besides adding the spurious poles $\{\omega_n\}$ of the potential cross section σ_c^{pot} [Eqs. (1) and (2) of [24] or Eqs. (3) and (4) of [25]], Hwang also accounted for too many $\{p_j\}$ poles, in Eq. (35a) Sec. III.A, p. 197 of [21]. This is for two fundamental reasons: (1) Lemma 3 of [32] on diagonal divisibility and capped multiplicities means Hwang's $q_\ell(\sqrt{E})$ functions can be taken out of his product in Eq. (36) of [21]; (2) Hwang's $q_\ell(\sqrt{E})$ functions are not the same as our $q_\ell(\rho)$ functions, which are the denominator of $L_\ell(\rho)$. Instead, Hwang's $q_\ell(\sqrt{E})$ functions are the denominator of the penetration $P_\ell(\rho)$ and shift $S_\ell(\rho)$ functions—defined as the analytically continued $L_\ell(\rho) = S_\ell(\rho) + iP_\ell(\rho)$ in (29) of [32] where a thorough and in-depth study of these functions is undertaken—and these denominators are different from the denominator of $L_\ell(\rho)$, as we show in Table III of [32]. In essence, this is because by writing $L_\ell(\rho) = S_\ell(\rho) + iP_\ell(\rho)$, the denominator is brought to its squared modulus, $L_\ell(\rho) = \frac{u_{\ell+1}(\rho)\,q_\ell^*(\rho)}{q_\ell(\rho)\,q_\ell^*(\rho)}$, which is no longer its irreducible form, and which therefore doubles the number of $L_\ell(\rho)$ poles by introducing superfluous complex conjugate poles from $q_\ell^*(\rho)$. These superfluous poles have always been overlooked until now; recent examples are Eqs. (9) and (10) of [63], Eq. (I.7.28) of [64], or Eq. (2.29) p. 75 of [65], where they count them to find $N_L = 2N_\lambda + 2\sum_{c=1}^{N_c}\ell_c$, which is actually the number of alternative analytic poles N_S we establish in Eq. (49) Theorem 3 of [32], instead of the correct number (102) of radioactive poles $N_L = 2N_\lambda + \sum_{c=1}^{N_c}\ell_c$ we demonstrated in Theorem 1 of [31].

Because polynomial root finding is no simple endeavor—see [29] or [65] for methods applied to the radioactive problem (101) and see [66–79] for more general methods—searching for the wrong number of poles (in particular too many) can have dire numerical consequences. For instance, Hwang explains in Ref. [21] how he had to go to quadruple precision in his code WHOPPER. He was finding the poles one by one using a Newton-Raphson method, and then removing them to search for the next pole. But once he had eliminated all the true poles, he was still searching for additional ones which did not actually exist. Numerically, though, one can never fully cancel out a pole, and thus will always find fictitious poles in the immediate vicinity of the canceled ones. This is exactly what happened to Hwang, and why he had many spurious poles clustered around the nonresonant N_λ ones. Hence knowing the correct number N_L of poles (102)—and more generally (42)—is crucial in practice.

2. *Exact multipole representations*

Hwang also spent a lot of subsequent work performing a pole expansion of the potential cross section σ_c^{pot} as well as of the energy dependence he found in his scattering residues, in Eqs. (1) and (2) of [24] or Eqs. (3) and (4) of [25]. We recall that though the potential cross section does have poles—roots $\{\omega_n\}$ of the $H_+(\rho)$ function reported in Table I of [32] or expressed by radicals in Table II of [32]—these poles actually have zero residues in the scattering matrix, and thus cancel out of the partial and total cross sections, as we prove in Theorem 3 of [31]. It will thus suffice to write that for the case of neutron cross sections with zero threshold, (25) and (26) entail the potential cross section takes the form

$$\begin{aligned}\sigma_c^{\text{pot}}(z) &= 4\pi a_c^2\frac{g_{J_c^\pi}}{\rho_{0_c}^2}\frac{\sin^2\phi_c(z)}{z^2}\\ &= 4\pi a_c^2\frac{g_{J_c^\pi}}{\rho_{0_c}^2}\frac{1}{z^2}\text{Re}_{\text{cont}}\left[\frac{1-e^{-2i\phi_c(z)}}{2}\right]. \end{aligned}\quad (105)$$

With all this in mind, we can now finish the explicit windowed multipole representation of no-threshold neutral particles cross sections. Upon finding the N_L roots $\{p_j\}$ of the polynomial radioactive problem (101), we can then solve for the nullspace of the inverse level matrix (which we here assume is an eigenline and we refer to [31] for the degenerate cases), and notice that the degree of the level matrix components $\boldsymbol{A}$ is at most -2, which leads to the following, exact, partial fraction decomposition of the level matrix and of the Kapur-Peierls operator:

$$\begin{aligned}\boldsymbol{A}(z) &= \sum_{j=1}^{N_L}\frac{\boldsymbol{\alpha}_j\boldsymbol{\alpha}_j^{\mathsf{T}}}{z-p_j},\\ \boldsymbol{\kappa}_j &\triangleq \boldsymbol{\gamma}^{\mathsf{T}}\boldsymbol{\alpha}_j,\\ \boldsymbol{R}_L(z) &= \sum_{j=1}^{N_L}\frac{\boldsymbol{\kappa}_j\boldsymbol{\kappa}_j^{\mathsf{T}}}{z-p_j}.\end{aligned}\quad (106)$$

We can then build a pole expansion of the resonance matrix $\boldsymbol{Z}$ from (23) by noticing that the $\boldsymbol{\rho}^{1/2}(z) = \sqrt{z}\boldsymbol{\rho_0}^{1/2}$ lead to an additional z term for each residue, and that the degrees of the numerator and denominator of z times the level matrix, $z\boldsymbol{A}(z)$, are still negative (degree of at most -1), guaranteeing the level matrix is a proper rational fraction with simple poles in z space:

$$\boldsymbol{\rho}^{\frac{1}{2}}\boldsymbol{R}_L\boldsymbol{\rho}^{\frac{1}{2}}(z) = \sum_{j=1}^{N_L}\frac{p_j\boldsymbol{\rho_0}^{\frac{1}{2}}\boldsymbol{\kappa}_j\boldsymbol{\kappa}_j^{\mathsf{T}}\boldsymbol{\rho_0}^{\frac{1}{2}}}{z-p_j}. \quad (107)$$

This has as consequence the remarkable property that for zero-threshold neutral cross sections, the z-space radioactive squared widths $\boldsymbol{\kappa}_j\boldsymbol{\kappa}_j^{\mathsf{T}}$ (rank-1 residues of the Kapur-Peierls operator at poles p_j), add up to nullity:

$$\sum_{j=1}^{N_L}\boldsymbol{\kappa}_j\boldsymbol{\kappa}_j^{\mathsf{T}} = \boldsymbol{0}. \quad (108)$$

From (23), we therefore obtain the following expression for the resonance matrix:

$$\boldsymbol{Z}(z) = \boldsymbol{H}_+^{-1}(z)\sum_{j=1}^{N_L}\frac{p_j\boldsymbol{\rho_0}^{\frac{1}{2}}\boldsymbol{\kappa}_j\boldsymbol{\kappa}_j^{\mathsf{T}}\boldsymbol{\rho_0}^{\frac{1}{2}}}{z-p_j}\boldsymbol{H}_+^{-1}(z) \quad (109)$$

where we deliberately left the energy dependence of $\boldsymbol{H}_+^{-1}(z)$, and recall that for neutral particles $H_+(\rho) = O(\rho)$. Polar decomposition (13) entails $H_{+\ell}^{-1}(\rho) = |d_\ell^{-1}(\rho)|e^{-i\phi_\ell(\rho)} = e^{-i\rho}\,d_\ell^{-1}(\rho)$, which is Hwang's notation in Eq. (3) of [25].

A closer look at the last column of Table I of [32] shows that $d_\ell^{-1}(\rho)$ is the rational function of degree zero (that is a proper rational fraction plus a constant) with ℓ poles—the roots $\{\omega_n\}$—that is the square root of that which Hwang identified in Eq. (1) of [24]. Careful analysis of this functions, using Table I of [32] and conjugate continuation definitions (66), yields the following expressions:

$$\begin{aligned} e^{-2i\phi_c(z)} &= e^{-2i\rho_c(z)}\frac{d_{\ell_c}^{-1}(z)}{d_{\ell_c}^{-1*}(z)} = Y_c[\rho_c(z)],\\ d_\ell(\rho) &= e^{i\ell\frac{\pi}{2}}\frac{\rho^\ell}{\prod_{n=1}^{\ell}(\rho-\omega_n)},\\ \frac{d_\ell^{-1}(\rho)}{d_\ell^{-1*}(\rho)} &= (-1)^\ell\prod_{n=1}^{\ell}\left(\frac{\rho-\omega_n^*}{\rho-\omega_n}\right),\\ |d_\ell|^{-2}_{\text{cont}}(\rho) &= \frac{\rho^{2\ell}}{\prod_{n=1}^{\ell}(\rho-\omega_n)(\rho-\omega_n^*)}. \end{aligned} \tag{110}$$

The diagonal elements of (109) are therefore exactly

$$Z_{cc}(z) = \left|d_{\ell_c}\right|^{-2}_{\text{cont}}(z)e^{-2i\phi_c(z)}\sum_{j=1}^{N_L}\frac{\rho_{0c}p_j\left[\boldsymbol{\kappa}_j\boldsymbol{\kappa}_j^{\mathsf{T}}\right]_{cc}}{z-p_j} \tag{111}$$

which, upon partial fraction decomposition, yields the Hwang multipole representation [21]:

$$\begin{aligned} \sigma_c(z) &= \sigma_c^{\text{pot}}(z)+\sigma_c^{\text{Hwang}}(z)\\ &\quad+\frac{1}{z^2}\text{Re}_{\text{cont}}\left[-i\,e^{-2i\phi_c(z)}\sum_{j=1}^{N_L}\frac{{}^{\text{Hwang}}r_j^c}{z-p_j}\right],\\ {}^{\text{Hwang}}r_j^c &\triangleq 4\pi a_c^2\frac{g_{J_c^\pi}}{\rho_{0c}^2}\left|d_{\ell_c}\right|^{-2}_{\text{cont}}(p_j)\;\rho_{0c}p_j\left[\boldsymbol{\kappa}_j\boldsymbol{\kappa}_j^{\mathsf{T}}\right]_{cc},\\ \sigma_c^{\text{Hwang}}(z) &\triangleq 4\pi a_c^2\frac{g_{J_c^\pi}}{\rho_{0c}^2}\frac{1}{z^2}\text{Re}[-i\,e^{-2i\phi_c(z)}\Delta(z)],\\ \Delta(z) &\triangleq \sum_{n=1}^{\ell_c}\left[\frac{\Delta_n\left[\boldsymbol{\rho}^{\frac{1}{2}}\boldsymbol{R}_L\boldsymbol{\rho}^{\frac{1}{2}}\right]_{cc}\left(\frac{\omega_n}{\rho_0}\right)}{\rho-\omega_n}\right.\\ &\quad\left.+\frac{\Delta_n^*\left[\boldsymbol{\rho}^{\frac{1}{2}}\boldsymbol{R}_L\boldsymbol{\rho}^{\frac{1}{2}}\right]_{cc}\left(\frac{\omega_n^*}{\rho_0}\right)}{\rho-\omega_n^*}\right],\\ \Delta_n &\triangleq \frac{\omega_n^{2\ell_c}}{\prod_{k=1}^{\ell_c}(\omega_n-\omega_k^*)\prod_{k\neq n}^{\ell_c}(\omega_n-\omega_k)} \end{aligned} \tag{112}$$

where the Hwang residues in Eq. (112) are identical to Eq. (2) of [25]. This scripture is the conjugate continuation real part of $N_L+\ell_c$ poles, as identified in Ref. [65]: the N_L radioactive poles (102), poles of the Kapur-Peierls operator (49), plus the roots $\{\omega_n\}$ of the outgoing wave function $\boldsymbol{O}(\boldsymbol{\rho})$. However, we have proved the latter cancel out of the transmission matrix, and thus of the cross section (Theorem 3 of [31]). Therefore, there must exist a multipole representation with only the N_L Kapur-Peierls poles. This can be achieved by developing the potential cross section (105) into poles and residues, factoring the $e^{-2i\rho_c}$ component (which has no poles) using expressions (110), and performing a partial fraction decomposition of the rational terms. Upon careful consideration, one will notice that this rational function is of degree zero, that its poles are the radioactive poles (and only those), and that the constant (obtained by evaluating at infinity $|\rho_c|\to\infty$) is $(-1)^{\ell_c}$. This shifts the potential cross section, so that the total cross section (27) can be expressed as the sum of a background cross section (with no poles),

$$\sigma_c^{\text{back}}(z) \triangleq 4\pi a_c^2\frac{g_{J_c^\pi}}{\rho_{0c}^2}\frac{\sin^2\left[\rho_c(z)+\ell_c\frac{\pi}{2}\right]}{z^2}, \tag{113}$$

plus a resonant cross section with the N_L radioactive poles:

$$\begin{aligned} \sigma_c(z) &= \sigma_c^{\text{back}}(z)+\frac{1}{z^2}\text{Re}_{\text{cont}}\left[-i\,e^{-2i\rho_c(z)}\sum_{j=1}^{N_L}\frac{{}^{\text{tot}}r_j^c}{z-p_j}\right],\\ {}^{\text{tot}}r_j^c &\triangleq 4\pi a_c^2\frac{g_{J_c^\pi}}{\rho_{0c}^2}d_{\ell_c}^{-2}(p_j)\;\rho_{0c}p_j\left[\boldsymbol{\kappa}_j\boldsymbol{\kappa}_j^{\mathsf{T}}\right]_{cc}\\ &= 4\pi a_c^2\frac{g_{J_c^\pi}}{\rho_{0c}^2}(-1)^\ell\frac{(\rho_{0c}p_j)^{2\ell+1}\left[\boldsymbol{\kappa}_j\boldsymbol{\kappa}_j^{\mathsf{T}}\right]_{cc}}{\prod_{n=1}^{\ell}(\rho_0p_j-\omega_n)^2}. \end{aligned} \tag{114}$$

To the best of our knowledge, expression (114) is the first time the exact multipole representation of no-threshold neutron cross sections is derived with the proper number of poles. It is exact and complete, in the sense that no window-by-window Laurent expansions are needed. This is only made possible in this specific case of neutron cross sections with zero threshold (no charged particles or thresholds): though quite restrictive, it is still a case of great practical importance for nuclear reactor physics, as most heavy isotopes are evaluated with only two channels (neutron and fission) with all the other channels being eliminated under the Reich-Moore approximation. This significant difference with light isotopes (in which many more channels are explicitly treated) is partly due to the fact that for heavy isotopes the number of photon channels is large enough that one can average their contribution out, and also because the resonance region starts at lower energies for heavy isotopes, with many resonances before the first nonzero threshold.

Note that the advantage of not needing local Laurent developments in Eq. (114) comes at the computational cost of having to sum all the radioactive poles for each energy call, instead of accounting for the contributions of far-away poles in the Laurent expansion of each window—in this sense, the windowing process is a form of local compression algorithm for improved efficiency [23,26].

To compute the partial cross sections (31), we can calculate the reaction cross section (30) and the interference one (29). For the reaction cross section, we use the square modulus conjugate continuation (66), and notice that $|\boldsymbol{H}_+^{-1}|^{-2}_{\text{cont}}(z) = |\boldsymbol{d}|^{-2}_{\text{cont}}(z) \triangleq \text{diag}[d_{\ell_c}(\rho)\;d_{\ell_c}(\rho^*)^*]^{-2}$ is now a rational function (the $e^{-i\rho}$ terms cancel out). Therefore, evaluating at the pole values yields the partial fraction decomposition of the square modulus of the resonance matrix:

$$|\boldsymbol{Z}|^2_{\text{cont}}(z) = \text{Re}_{\text{cont}}\left[\sum_{j=1}^{N_L}\frac{\boldsymbol{\aleph}_j}{z-p_j}\right] \tag{115}$$

TABLE I. Multipole parameters of the two p-wave resonances of ^{134}Xe, spin-parity group $J^\pi = 1/2^{(-)}$, converted from ENDF/B-VIII.0 evaluation (MLBW) to multipole representation using Reich-Moore level matrix (21).

$z = \sqrt{E}$ with E in eV
$A = 132.7600$
$a_c = 5.80$: channel radius (fm)
$\rho_0 = \frac{Aa_c\sqrt{\frac{2m_n}{\hbar}}}{A+1}$ in $(\sqrt{\text{eV}}^{-1})$, so that $\rho(z) \triangleq \rho_0 z$
with $\sqrt{\frac{2m_n}{\hbar}} = 0.002196807122623$ in units $1/(10^{-14}\text{m}\sqrt{\text{eV}})$

Multipole parameters (rounded to five digits): converted from R-matrix parameters using Reich-Moore level matrix (21)

Radioactive poles p_j ($\sqrt{\text{eV}}$) from (101)	Total residues ${}^{\text{tot}}r_j^c$ ($\text{b}\sqrt{\text{eV}}^3$) from (114)	Reaction residues ${}^{\text{react}}r_j^{cc'}$ ($\text{b}\sqrt{\text{eV}}^3$) from (118)	Interference residues ${}^{\text{int}}r_j^c$ ($\text{b}\sqrt{\text{eV}}^3$) from (120)	Hwang residues ${}^{\text{Hwang}}r_j^c$ ($\text{b}\sqrt{\text{eV}}^3$) from (112)
6.4652×10^{-8}	$6.9766 \times 10^{+8}$	2.8519×10^{-2}	-2.8446×10^{-2}	$-4.6048 \times 10^{+5}$
$-i7.9179 \times 10^{+2}$	$-i5.5825 \times 10^{-2}$	$+i4.6048 \times 10^{+5}$	$+i4.6048 \times 10^{+5}$	$-i2.8446 \times 10^{-2}$
$-4.6731 \times 10^{+1}$	$-1.2144 \times 10^{+3}$	-1.5693×10^{-1}	-1.3518×10^{-1}	$-1.2229 \times 10^{+3}$
$-i9.7105 \times 10^{-4}$	$+i1.4390 \times 10^{+2}$	$+i1.7479 \times 10^{+3}$	$+i1.2229 \times 10^{+3}$	$-i1.3518 \times 10^{-1}$
$4.6731 \times 10^{+1}$	$-1.2144 \times 10^{+3}$	1.5693×10^{-1}	1.7868×10^{-1}	$-1.2229 \times 10^{+3}$
$-i1.8048 \times 10^{-3}$	$-i1.4386 \times 10^{+2}$	$+i9.4043 \times 10^{+2}$	$+i1.2229 \times 10^{+3}$	$+i1.7868 \times 10^{-1}$
$-7.9454 \times 10^{+1}$	$-1.0827 \times 10^{+3}$	-4.2538×10^{-1}	-4.1864×10^{-1}	$-1.1047 \times 10^{+3}$
$-i1.0084 \times 10^{-3}$	$+i2.1937 \times 10^{+2}$	$+i1.3735 \times 10^{+3}$	$+i1.1047 \times 10^{+3}$	$-i4.1864 \times 10^{-1}$
$7.9454 \times 10^{+1}$	$-1.0827 \times 10^{+3}$	4.2538×10^{-1}	4.3211×10^{-1}	$-1.1047 \times 10^{+3}$
$-i1.4991 \times 10^{-3}$	$-i2.1936 \times 10^{+2}$	$+i9.2389 \times 10^{+2}$	$+i1.1047 \times 10^{+3}$	$+i4.3211 \times 10^{-1}$

R-matrix parameters: reference ENDF/B-VIII.0 evaluation (MLBW) used with Reich-Moore level matrix (21)

$E_1 = 2186.0$: first resonance energy (eV)
$\Gamma_{1,n} = 0.2600$: neutron width of first resonance
(not reduced width), i.e., $\Gamma_{\lambda,c} = 2P_c(E_\lambda)\gamma_{\lambda,c}^2$
$\Gamma_{1,\gamma} = 0.0780$: eliminated capture width (eV)
$E_2 = 6315.0$: second resonance energy (eV)
$\Gamma_{2,n} = 0.4000$ (eV)
$\Gamma_{2,\gamma} = 0.0780$ (eV)
$g_{J^\pi} = 1/3$: spin statistical factor
$B_c = -1$

where the residues $\boldsymbol{\aleph}_j$ are explicitly constructed as

$$\boldsymbol{\aleph}_j \triangleq 2|\boldsymbol{d}|^{-2}_{\text{cont}}(p_j)\boldsymbol{\rho_0}\left(p_j^2\boldsymbol{\kappa}_j\boldsymbol{\kappa}_j^{\mathsf{T}} \circ [\boldsymbol{R}_L(p_j^*)]^*\right)\boldsymbol{\rho_0}|\boldsymbol{d}|^{-2}_{\text{cont}}(p_j). \tag{116}$$

In summary, the energy dependence of the residues in Eq. (109) cancels out of the reaction residues, hence the reaction cross section (from channel c to c') is exactly

$$\sigma_{cc'}^{\text{react}}(z) = \frac{1}{z^2}\text{Re}_{\text{cont}}\left[\sum_{j\geqslant 1}\frac{{}^{\text{react}}r_j^{cc'}}{z-p_j}\right] \tag{117}$$

where the residues can either simply be evaluated as (92) or constructed as

$${}^{\text{react}}r_j^{cc'} \triangleq \frac{4\pi a_c^2}{\rho_{0_c}^2}g_{J_c^\pi}[\boldsymbol{\aleph}_j]_{cc'}. \tag{118}$$

For the interference cross section (29), we notice using expressions (110) that the phase behavior also cancels out of $\text{Re}[-iZ_{cc}Y_c^*]$, so that plugging the resonance matrix partial fraction decomposition (111) into interference cross-section expression (29) yields rational fraction

$$\sigma_c^{\text{int}}(z) = \frac{1}{z^2}\text{Re}_{\text{cont}}\left[\sum_{j=1}^{N_L}\frac{{}^{\text{int}}r_j^c}{z-p_j}\right] \tag{119}$$

where the interference residues can simply be evaluated as (89), or explicitly constructed as

$$\begin{aligned}{}^{\text{int}}r_j^c &\triangleq -i4\pi a_c^2\frac{g_{J_c^\pi}}{\rho_{0_c}^2}\left|d_{\ell_c}\right|^{-2}_{\text{cont}}(p_j)\ \rho_{0_c}p_j\left[\boldsymbol{\kappa}_j\boldsymbol{\kappa}_j^{\mathsf{T}}\right]_{cc} \\ &= -i4\pi a_c^2\frac{g_{J_c^\pi}}{\rho_{0_c}^2}\frac{(\rho_{0_c}p_j)^{2\ell_c+1}\left[\boldsymbol{\kappa}_j\boldsymbol{\kappa}_j^{\mathsf{T}}\right]_{cc}}{\prod_{n=1}^{\ell}(\rho_{0_c}p_j-\omega_n)(\rho_{0_c}p_j-\omega_n^*)}.\end{aligned} \tag{120}$$

Having explicitly constructed the total, potential, reaction, and interference cross sections, we can thus calculate the partial cross sections explicitly through (31).

3. *Evidence for exact multipole representation in* ^{134}Xe

We discovered shadow alternative poles of ^{134}Xe spin-parity group $J^\pi = 1/2^{(-)}$ two p-wave resonances in Ref. [32], and found the radioactive state poles and residues in Ref. [31]. We now complete this xenon trilogy by here providing the exact multipole representation of the ^{134}Xe spin-parity group

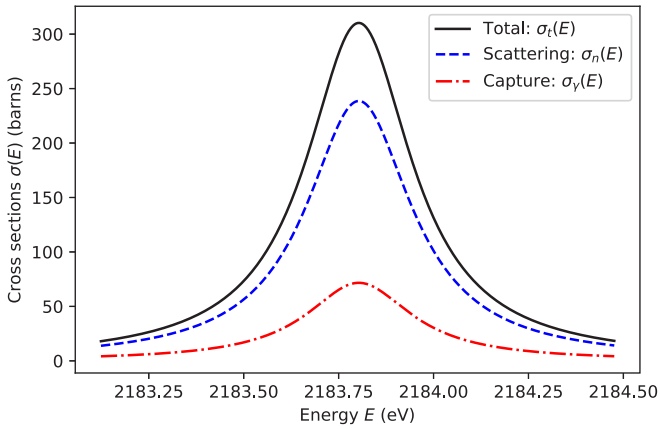

(a)

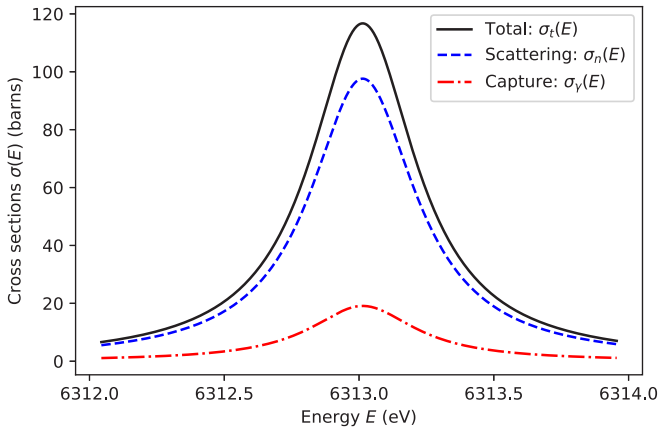

(b)

FIG. 2. Xenon ^{134}Xe Reich-Moore cross sections for spin-parity group $J^\pi = 1/2^{(-)}$ p-wave resonances: the cross sections are generated using the multipole parameters from Table I in the multipole representation total cross section (114), as well as the reaction cross section (117) and interference one (119) to compute the scattering cross section as (31), while the capture cross section is the difference between the total and the scattering. All cross sections are identical to those computed using the Reich-Moore approximation R-matrix equations with the ENDF/B-VIII.0 resonance parameters. (a) First p-wave resonance and (b) Second p-wave resonance.

$J^\pi = 1/2^{(-)}$ cross section. The multipole parameters are documented in Table I, and the corresponding cross sections are plotted in Fig. 2. In ENDF/B-VIII.0, ^{134}Xe is a MLBW evaluation with only one explicit (neutron) channel; all other channels are eliminated using Wigner-Teichmann and Reich-Moore approximations. One can thus compute the total cross section using multipole representation (114), and the scattering cross section as the partial cross section for $\sigma_{nn}(E)$ from (31), using the reaction cross section (117) and interference one (119). The capture cross section is then computed as the difference between the total and the scattering cross section. The p waves ($\ell_c = 1$) entail there are $N_L = 5$ radioactive poles—validating (102)—and the corresponding residues are documented in Table I. As we see in this xenon example, the multipole representation is an exact alternative formalism to compute R-matrix cross sections. Nonetheless, if we want to treat charged particle channels and thresholds, we need to use local Laurent developments in energy windows, which makes the windowed multipole representation cumbersome and somewhat unsuited for standard nuclear data libraries.

4. Exact to windowed multipole representations

Note that we can convert the exact multipole total cross-section expression (114)—which has energy-dependent residues due to $e^{-2i\rho_c(z)}$—into the general windowed multipole representation (96), with energy-independent residues plus a Laurent expansion of order no less than -2. It suffices to evaluate the residues at the pole values, and note that the Laurent expansion part $\underset{\text{tot}}{\text{Laur}}(z)$ is then the difference of the two remaining components, that is,

$$\begin{aligned}\underset{\text{tot}}{\text{Laur}}(z) &= \frac{1}{z^2}\text{Re}_{\text{cont}}\left[\sum_{j=1}^{N_L}\frac{-i\ {}^{\text{tot}}r_j^c}{z-p_j}\left(e^{-2i\rho_{0_c}z}-e^{-2i\rho_{0_c}p_j}\right)\right]\\ &= \text{Re}_{\text{cont}}\left[\sum_{j=1}^{N_L}\frac{{}^{\text{tot}}r_j^c}{iz^2}\left(\sum_{n\geqslant 0}\frac{\left(-2i\rho_{0_c}\right)^n}{n!}\frac{z^n-p_j^n}{z-p_j}\right)\right]\\ &= \sum_{n\geqslant 1}\sum_{m=1}^{n}\frac{z^m}{z^3}\text{Re}_{\text{cont}}\left[\sum_{j=1}^{N_L}\frac{{}^{\text{tot}}r_j^c}{i}p_j^{n-m}\frac{\left(-2i\rho_{0_c}\right)^n}{n!}\right]\\ &= \sum_{n\geqslant -2}a_n z^n \end{aligned} \tag{121}$$

so that the total cross section (112) can be expanded as

$$\begin{aligned}\sigma_c(z) = \sigma_c^{\text{back}}(z) &+ \frac{1}{z^2}\text{Re}_{\text{cont}}\left[\sum_{j=1}^{N_L}\frac{-i\ e^{-2i\rho_{0_c}p_j}\ {}^{\text{tot}}r_j^c}{z-p_j}\right]\\ &+\underset{\text{tot}}{\text{Laur}}(z)\end{aligned} \tag{122}$$

where the residues are now independent of energy. By further performing the analytic expansion of the background cross section (113)

$$\sigma_c^{\text{back}}(z) \triangleq 4\pi a_c^2\frac{g_{J_c^\pi}}{\rho_{0_c}^2}\left[\frac{1-(-1)^\ell}{2\ z^2}+\sum_{n\geqslant 1}\frac{(-1)^n}{2}\frac{\left(2\rho_{0_c}\right)^{2n}}{(2n)!}\frac{z^{2n}}{z^2}\right] \tag{123}$$

one recovers the general windowed multipole representation (96).

As we see, in this special case of neutron channels without threshold, we can explicitly construct the full windowed multipole representation (122) without the need of local expansions for each energy window $\mathcal{W}(E)$. Somewhat ironically, it is also much more cumbersome to explicitly construct both the Laurent expansion and the residues, compared to the more general approaches of Theorem 1. Alternatively, one can solve for the radioactive poles $\{p_j\}$ through polynomial root finding (101), and then revert to the general methods of Theorem 1 to compute the corresponding residues, after which the Laurent expansions can be locally curve fitted.

III. WINDOWED MULTIPOLE COVARIANCES

In Sec. II, we established the windowed multipole representation as a general alternative way to parametrize the energy dependence of R-matrix cross sections (Theorem 1). In this section, we consider how the windowed multipole representation can account for R-matrix cross-section epistemic uncertainties. Such uncertainties exist because nuclear cross sections are known from experiments, and experimental measurements always come with error bars. Therefore, in addition to evaluating R-matrix parameter values, evaluators add resonance parameters covariance matrices to standard nuclear data libraries (File 32 in the ENDF/B-VIII.0 library [14]), aimed at reproducing the empirical uncertainty observed in nuclear cross sections.

A. Converting R-matrix parameters covariances

If it exists, the covariance matrix $\mathbb{V}\mathrm{ar}(X)$ of a random vector X with expectation value $\mathbb{E}[X]$ is a defined as

$$\mathbb{V}\mathrm{ar}(X) \triangleq \mathbb{E}[XX^\dagger] - \mathbb{E}[X]\mathbb{E}[X]^\dagger. \tag{124}$$

We denote $\{\Gamma\}$ the set of R-matrix resonance parameters $\{\Gamma\} \triangleq \{E_\lambda, \gamma_{\lambda,c}\}$, which are implicitly considered to be the expectation value of the underlying distribution, $\{\Gamma\} \triangleq \mathbb{E}[\Gamma]$, and $\mathbb{V}\mathrm{ar}(\Gamma)$ their corresponding covariance matrices. These represent the resonance parameters epistemic uncertainty, which is accounted for by assuming the parameters are drawn from the multivariate normal distribution: $\mathcal{N}(\Gamma, \mathbb{V}\mathrm{ar}(\Gamma))$. Recall that both the channel radii a_c and the boundary conditions B_c are arbitrarily set constants, and therefore have no uncertainty. Also, we here do not explicitly treat the uncertainty on threshold energies E_{T_c}, but our approach could readily be extended to them.

We consider the unified windowed multipole representation of R-matrix cross sections (96), which we proved is an exact representation of R-matrix cross sections everywhere but for windows containing a nonzero threshold $E_{T_c} \in \mathcal{W}(E)$—in these threshold windows, form (96) is only an approximation of exact R-matrix cross sections of Theorem 1, yet this approximation (96) can be made to reach any target accuracy. For each energy window $\mathcal{W}(E)$, we denote $\{\Pi\}$ the windowed multipole parameters—that is the set of poles $\{p_j\}$, residues $\{\widetilde{r}_j^{cc'}, r_j^c\}$, and Laurent expansion coefficients $\{a_n\}$ that parametrize cross section (96) in that energy window: $\{\Pi\} \triangleq \{p_j, \widetilde{r}_j^{cc'}, r_j^c, a_n\}$.

The main result of this section—Theorem 2—establishes a framework to convert R-matrix resonance parameters covariance matrices $\mathbb{V}\mathrm{ar}(\Gamma)$ into *windowed multipole covariances* $\mathbb{V}\mathrm{ar}(\Pi)$. It is based on the following Lemma 1, which derives sensitivities of R-matrix cross sections $\sigma(E)$ to both resonance parameters $\{\Gamma\}$ and multipoles $\{\Pi\}$.

Lemma 1. Cross-Section Parameter Sensitives

Let $z \in \mathbb{C}$ be the complex, analytically continued square root of energy: $z = \sqrt{E}$. Consider windowed multipole cross section (96), i.e., locally of the form

$$\sigma(z) \underset{\mathcal{W}(E)}{=} \sum_{n\geqslant -2} a_n z^n + \frac{1}{z^2}\mathrm{Re}_{\mathrm{cont}}\left[\sum_{j\geqslant 1}\frac{r_j}{z-p_j}\right].$$

We recall the Cauchy-Poincaré-Wirtinger holomorphic complex differential definition for $z = x + iy$, $x, y \in \mathbb{R}$:

$$\partial_z \triangleq \tfrac{1}{2}(\partial_x - i\partial_y) \tag{125}$$

so that $\partial_z z = 1$, and $\partial_z z^* = 0$, where $z^* \triangleq x - iy$.

The cross-section sensitivities to multipoles $\frac{\partial\sigma}{\partial\Pi}(z)$ (i.e., the partial differentials of the cross section with respect to multipoles) are then given, for each window $\mathcal{W}(E)$, by

$$\begin{aligned}
\frac{\partial\sigma}{\partial p_j}(z) &= \frac{1}{z^2}\frac{\frac{r_j}{2}}{(z-p_j)^2},\\
\frac{\partial\sigma}{\partial p_j^*}(z) &= \frac{1}{z^2}\frac{\frac{r_j^*}{2}}{(z-p_j^*)^2},\\
\frac{\partial\sigma(z)}{\partial\mathrm{Re}[p_j]} &= \frac{1}{z^2}\mathrm{Re}_{\mathrm{cont}}\left[\frac{r_j}{(z-p_j)^2}\right],\\
\frac{\partial\sigma(z)}{\partial\mathrm{Im}[p_j]} &= \frac{1}{z^2}\mathrm{Re}_{\mathrm{cont}}\left[\frac{i\,r_j}{(z-p_j)^2}\right],\\
\frac{\partial\sigma}{\partial r_j}(z) &= \frac{1}{z^2}\frac{\frac{1}{2}}{z-p_j},\\
\frac{\partial\sigma}{\partial r_j^*}(z) &= \frac{1}{z^2}\frac{\frac{1}{2}}{z-p_j^*},\\
\frac{\partial\sigma(z)}{\partial\mathrm{Re}[r_j]} &= \frac{1}{z^2}\mathrm{Re}_{\mathrm{cont}}\left[\frac{1}{z-p_j}\right],\\
\frac{\partial\sigma(z)}{\partial\mathrm{Im}[r_j]} &= \frac{1}{z^2}\mathrm{Re}_{\mathrm{cont}}\left[\frac{i}{z-p_j}\right],\\
\frac{\partial\sigma}{\partial a_n}(z) &= z^n.
\end{aligned} \tag{126}$$

Moreover, the cross-section sensitivities to resonance parameters $\frac{\partial\sigma}{\partial\Gamma}(z)$ (i.e., the partial differentials of the cross section with respect to resonance parameters) are subject to the following multipole representation:

$$\begin{aligned}
\frac{\partial\sigma}{\partial\Gamma}(z) \underset{\mathcal{W}(E)}{=} &\frac{1}{z^2}\mathrm{Re}_{\mathrm{cont}}\left[\sum_{j\geqslant 1}\frac{\left(\frac{\partial r_j}{\partial\Gamma}\right)}{z-p_j} + \frac{\left(r_j\,\frac{\partial p_j}{\partial\Gamma}\right)}{(z-p_j)^2}\right]\\
&+ \sum_{n\geqslant -2}\left(\frac{\partial a_n}{\partial\Gamma}\right)z^n.
\end{aligned} \tag{127}$$

We seek to convert R-matrix resonance parameters covariances $\mathbb{V}\mathrm{ar}(\Gamma)$ into windowed multipole covariances $\mathbb{V}\mathrm{ar}(\Pi)$. Yet obtaining multipoles $\{\Pi\}$ from resonance parameters $\{\Gamma\}$ is not a simple transformation: one must solve the radioactive problem (49) for the poles $\{p_j\}$ and then compute the corresponding residues $\{\widehat{r}_j^{cc'}, r_j^c\}$ (Theorem 1). We therefore take an implicit functions approach, and locally invert the $\Gamma \to \Pi$ transformation by means of the Jacobian matrix $(\frac{\partial\Pi}{\partial\Gamma})$, that is the sensitivities of windowed multipole coefficients to the R-matrix resonance parameters (Cauchy-Dini implicit functions theorem). Under the assumption of small deviations from the mean (small relative uncertainties), this yields a first-order linear relation from multipoles $\{\Pi\}$ to resonance parameters $\{\Gamma\}$. In this case, the chain

rule entails the multipoles $\{\Pi\}$ are also subject to a multivariate normal distribution $\mathcal{N}(\Pi, \mathbb{V}\mathrm{ar}(\Pi))$, the covariance of which is given by (129) (sometimes called the "sandwich rule"). Therefore, the key to converting resonance covariances $\mathbb{V}\mathrm{ar}(\Gamma)$ into multipole covariances $\mathbb{V}\mathrm{ar}(\Pi)$ lies in the sensitivities $(\frac{\partial\Pi}{\partial\Gamma})$, illustrated in Fig. 5. Theorem 2 establishes a contour-integrals method to calculate these sensitivities $(\frac{\partial\Pi}{\partial\Gamma})$, provided R-matrix cross-section sensitivities $\frac{\partial\sigma}{\partial\Gamma}(E)$ from Lemma 1.

Theorem 2. WINDOWED MULTIPOLE COVARIANCES

Let us be provided with the sensitivities $\frac{\partial\sigma}{\partial\Gamma}(z)$ of R-matrix cross sections (analytically continued) to resonance parameters (127). Then the multipole sensitivities (Jacobian matrix) with respect to the resonance parameters, $(\frac{\partial\Pi}{\partial\Gamma})$, can be obtained from the following system (128) of contour integrals in the complex plane, where $\mathfrak{C}_{p_j}$ designates any positively oriented simple closed contour containing only pole p_j. For instance, $\mathfrak{C}_{p_j}$ can be a circle of radius $\epsilon > 0$ around pole p_j:

$$
\begin{aligned}
&\frac{1}{2}\frac{r_j}{p_j^2}\left(\frac{\partial p_j}{\partial\Gamma}\right) = \frac{1}{2\pi i}\oint_{\mathfrak{C}_{p_j}}(z-p_j)\frac{\partial\sigma}{\partial\Gamma}(z)dz = \frac{\epsilon^2}{2\pi}\int_{\theta=0}^{2\pi}\frac{\partial\sigma}{\partial\Gamma}(p_j+\epsilon e^{i\theta})e^{2i\theta}d\theta,\\
&\frac{1}{2}\frac{1}{p_j^2}\left(\frac{\partial r_j}{\partial\Gamma}\right) - \frac{r_j}{p_j^3}\left(\frac{\partial p_j}{\partial\Gamma}\right) = \frac{1}{2\pi i}\oint_{\mathfrak{C}_{p_j}}\frac{\partial\sigma}{\partial\Gamma}(z)dz = \frac{\epsilon}{2\pi}\int_{\theta=0}^{2\pi}\frac{\partial\sigma}{\partial\Gamma}(p_j+\epsilon e^{i\theta})e^{i\theta}d\theta,\\
&\left(\frac{\partial a_n}{\partial\Gamma}\right) + \delta_{-1,n}\mathrm{Re}_{\mathrm{cont}}\left[\sum_{j=1}^{N_L}\frac{2\left(r_j\ \frac{\partial p_j}{\partial\Gamma}\right) - p_j\left(\frac{\partial r_j}{\partial\Gamma}\right)}{p_j^3}\right] + \delta_{-2,n}\mathrm{Re}_{\mathrm{cont}}\left[\sum_{j=1}^{N_L}\frac{\left(r_j\ \frac{\partial p_j}{\partial\Gamma}\right) - p_j\left(\frac{\partial r_j}{\partial\Gamma}\right)}{p_j^2}\right]\\
&\quad = \frac{1}{2\pi i}\oint_{\mathfrak{C}_0}\frac{1}{z^{n+1}}\frac{\partial\sigma}{\partial\Gamma}(z)dz = \frac{1}{2\pi\epsilon^n}\int_{\theta=0}^{2\pi}\frac{\partial\sigma}{\partial\Gamma}(\epsilon e^{i\theta})e^{-in\theta}d\theta.
\end{aligned}
\tag{128}
$$

For each energy window $\mathcal{W}(E)$, the multipole sensitivities $(\frac{\partial\Pi}{\partial\Gamma})$ from system (128) can then be converted to first order into windowed multipole covariances $\mathbb{V}\mathrm{ar}(\Pi)$ as

$$
\mathbb{V}\mathrm{ar}(\Pi) = \left(\frac{\partial\Pi}{\partial\Gamma}\right)\mathbb{V}\mathrm{ar}(\Gamma)\left(\frac{\partial\Pi}{\partial\Gamma}\right)^{\dagger} \tag{129}
$$

where $[\,\cdot\,]^{\dagger}$ designates the Hermitian conjugate (adjoint).

Proof. Partial fraction expansion of (127) Lemma 1 yields

$$
\begin{aligned}
\frac{\partial\sigma}{\partial\Gamma}(z) \underset{\mathcal{W}(E)}{=} \mathrm{Re}_{\mathrm{cont}}\Bigg[&\sum_{j=1}^{N_L}\frac{\left(r_j\ \frac{\partial p_j}{\partial\Gamma}\right) - p_j\left(\frac{\partial r_j}{\partial\Gamma}\right)}{p_j^2 z^2}\\
&+\frac{\left(r_j\ \frac{\partial p_j}{\partial\Gamma}\right)}{p_j^2(z-p_j)^2} + \frac{2\left(r_j\ \frac{\partial p_j}{\partial\Gamma}\right) - p_j\left(\frac{\partial r_j}{\partial\Gamma}\right)}{p_j^3 z}\\
&+\frac{p_j\left(\frac{\partial r_j}{\partial\Gamma}\right) - 2\left(r_j\ \frac{\partial p_j}{\partial\Gamma}\right)}{p_j^3(z-p_j)}\Bigg]\\
&+\sum_{n\geqslant -2}\left(\frac{\partial a_n}{\partial\Gamma}\right)z^n.
\end{aligned}
$$

The different residues associated with poles zero or p_j are then obtained by invoking Cauchy's residue theorem and multiplying correspondingly by z^n or $(z-p_j)$, yielding (128). Importantly, these contour integrals cannot be performed without having an analytic representation of the partial derivatives of the cross section at complex energies, $\frac{\partial\sigma}{\partial\Gamma}(z)$, which is made possible for open channels by Hwang's conjugate continuations (66) and (62). Finally, (129) is a direct application of the well-known chain-rule first-order perturbation covariance formula. ■

B. Cross-section uncertainties and parameter covariances

By introducing resonance covariances $\mathbb{V}\mathrm{ar}(\Gamma)$, present standard nuclear data libraries are built with the implicit assumption that sampling resonance parameters from a multivariate normal distribution $\mathcal{N}(\Gamma, \mathbb{V}\mathrm{ar}(\Gamma))$ and computing the corresponding cross sections $\sigma_\Gamma(E)$ generates outcome distributions commensurate to our experimental uncertainty. Note that this parameter uncertainty representation is not obvious *per se*, because cross sections are measured at specific energies, and the measured cross-section uncertainty is usually described with a given exogenous distribution (say normal, log-normal, or exponential), dictated by the experiment. Therefore, no parameter distribution [be it resonance parameters multivariate normal $\mathcal{N}(\Gamma, \mathbb{V}\mathrm{ar}(\Gamma))$ or any other] can exactly reproduce the cross-section uncertainty for each measurement energy. And yet, these parameters distributions are our best way of balancing all the different uncertainties from disjointed experiments with the underlying R-matrix theory which unifies our understanding of nuclear interactions physics.

Significant work has been carried out to infer parameter distributions that accurately reproduce our uncertainty of nuclear cross sections [56,80–87]. Assuming R-matrix cross section uncertainty is well represented by the resonance parameters multivariate normal distribution $\mathcal{N}(\Gamma, \mathbb{V}\mathrm{ar}(\Gamma))$ documented in standard nuclear data libraries (file 32 in ENDF/B-VIII.0 [14]), there are two ways of translating this into cross-section distributions: (1) first-order sensitivity propagation or (2) stochastic cross sections.

(1) For any given energy E, first-order sensitivity propagation simply considers the R-matrix cross-section sensitivities to resonance parameters $\frac{\partial\sigma}{\partial\Gamma}(E)$ and linearly converts the resonance parameter covariance

$\mathbb{V}\mathrm{ar}(\Gamma)$ into a cross-section covariance $\mathbb{V}\mathrm{ar}(\sigma(E))$ at each energy E, using the chain rule:

$$\mathbb{V}\mathrm{ar}(\sigma_\Gamma(E)) = \left(\frac{\partial\sigma(E)}{\partial\Gamma}\right)\mathbb{V}\mathrm{ar}(\Gamma)\left(\frac{\partial\sigma(E)}{\partial\Gamma}\right)^\dagger \quad (130)$$

The same approach can be undertaken using R-matrix cross-section sensitivities to windowed multipoles $\frac{\partial\sigma}{\partial\Pi}(E)$, established in Eqs. (126) of Lemma 1, and then propagating the windowed multipole covariances $\mathbb{V}\mathrm{ar}(\Pi)$ to first order, yielding cross-section covariances:

$$\mathbb{V}\mathrm{ar}[\sigma_\Pi(E)] = \left(\frac{\partial\sigma(E)}{\partial\Pi}\right)\mathbb{V}\mathrm{ar}(\Pi)\left(\frac{\partial\sigma(E)}{\partial\Pi}\right)^\dagger. \quad (131)$$

(2) Stochastic cross sections consist of sampling resonance parameters $\{\Gamma\}$ from their uncertainty distribution—say multivariate normal $\mathcal{N}(\Gamma, \mathbb{V}\mathrm{ar}(\Gamma))$—and computing the corresponding cross section $\sigma_\Gamma(E)$ as a function of energy:

$$d\mathbb{P}[\sigma_\Gamma(E)] = \sigma_{d\mathbb{P}(\Gamma)}(E) \quad (132)$$

Alternatively, one could sample multipoles $\{\Pi\}$ from a windowed multipole distribution—say multivariate normal $\mathcal{N}(\Pi, \mathbb{V}\mathrm{ar}(\Pi))$—and correspondingly generate windowed multipole stochastic cross sections:

$$d\mathbb{P}[\sigma_\Pi(E)] = \sigma_{d\mathbb{P}(\Pi)}(E). \quad (133)$$

Stochastic cross-section uncertainties only match first-order sensitivity approaches (130) and (131) for very small covariances. This is because normally distributed resonance parameters do not translate into normally distributed cross sections (132): sampling resonance parameters from $\mathcal{N}(\Gamma, \mathbb{V}\mathrm{ar}(\Gamma))$ and then computing the corresponding cross sections (5) and (10) through R-matrix equations (7) and (14)–(17), cannot in general lead to normally distributed cross sections $\sigma_\Gamma(E)$ at all energies. However, they do in the linear case, which is a good first-order approximation for small covariances.

Stochastic cross sections (132) are at the core of the TENDL library [19,20], and being able to sample them is a necessary prerequisite to the total Monte Carlo uncertainty propagation method [88–90]. In practice, this has been a major computational challenge, requiring one to sample resonance parameters from standard nuclear data libraries, reconstruct the corresponding nuclear cross sections at 0 K, and then process each one (with codes such as NJOY [91]) to compute the corresponding cross sections at temperature T (see discussion of Doppler broadening and thermal scattering in Sec. IV). All this is costly, and storing the preprocessed cross sections consumes a vast amount of memory. Because one can directly compute Doppler-broadened nuclear cross sections from windowed multipole parameters $\{\Pi\}$ (see Theorem 3 Sec. IV), the Windowed Multipole Library can generate stochastic cross sections (133) on the fly, without any preprocessing or storage, a true physics-enabled computational breakthrough.

Regardless of the method employed to represent nuclear cross-section uncertainty, it would be desirable that the uncertainties stemming from a windowed multipole representation

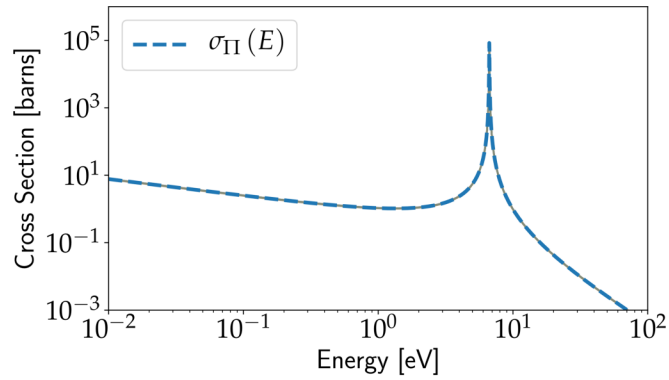

(a)

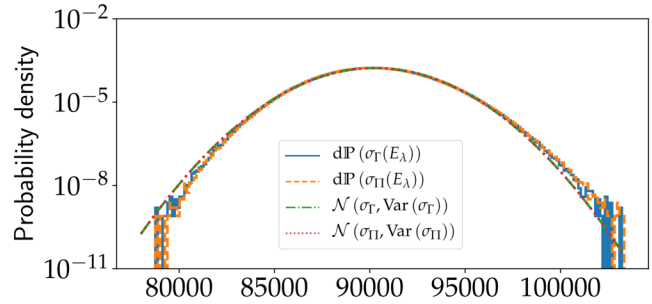

(b)

FIG. 3. R-matrix cross-section uncertainty, computed either from the ENDF/B-VIII resonance parameters covariance $\mathbb{V}\mathrm{ar}(\Gamma)$ (Table II in the Appendix), or from the multipoles covariance $\mathbb{V}\mathrm{ar}(\Pi)$, as converted through (129), for both the stochastic cross sections (132) and (133) and the sensitivities approach (130) and (131). (a) ^{238}U first capture resonance, parameters sampled from ENDF/B-VIII uncertainty. 30 samples shown here and (b) Cross section histogram at resonance energy $E_\lambda = 6.67428$ eV.

$\{\Pi\}$ are consistent with those stemming from resonance parameters $\{\Gamma\}$ upon converting their covariances as indicated in Eq. (129) of Theorem 2. We undertook numerical experiments to measure the cross-section uncertainty distributions generated by either covariances $\mathbb{V}\mathrm{ar}(\Gamma)$ or $\mathbb{V}\mathrm{ar}(\Pi)$, for both sensitivity method (130) and (131), or stochastic cross sections (132) and (133). We treated the simple case of the first single-level Breit-Wigner capture resonance of uranium isotope ^{238}U, which admits closed-form explicit expressions for the multipoles, the cross sections, and the sensitivities, all documented in the Appendix. We compared the methods for both the ENDF/B-VIII.0 resonance parameters covariance (which is small as this is a very well-known resonance), and an enlarged covariance matrix which conserves the same correlations but brings the cross-section dependency past the linear regime. Both covariances are documented in Table II (the Appendix), and Figs. 3 and 4 show the following trends.

(1) For the sensitivity method (130) or (131), the cross-section uncertainty is identical for either the resonance parameter covariance $\mathbb{V}\mathrm{ar}(\Gamma)$ or the windowed multipole covariance $\mathbb{V}\mathrm{ar}(\Pi)$, which is the immediate consequence of conversion (129).

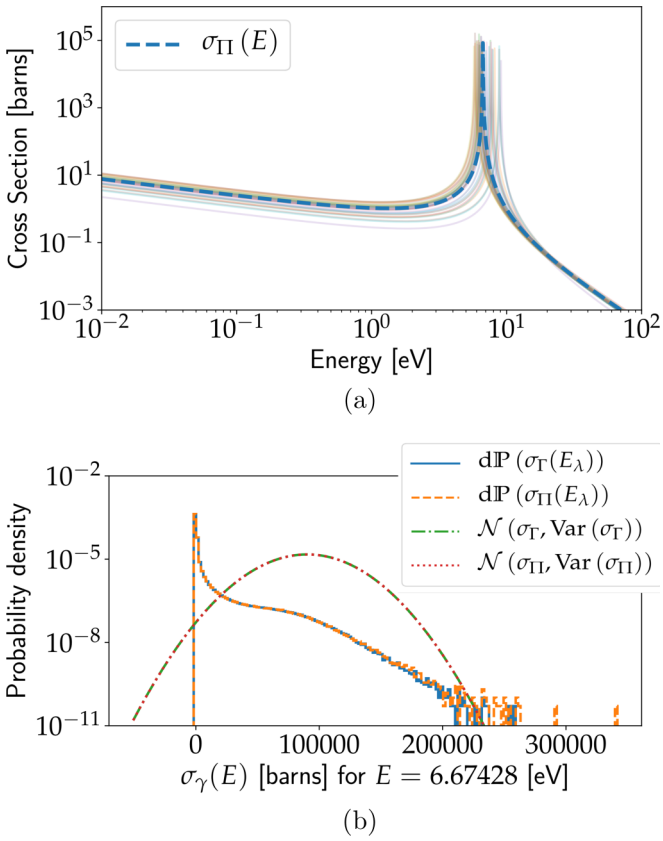

FIG. 4. *R*-matrix cross-section uncertainty, computed either from the enlarged ENDF/B-VIII resonance parameters covariance $\mathbb{V}\mathrm{ar}(\Gamma)$ (Table II in the Appendix), or from the multipoles covariance $\mathbb{V}\mathrm{ar}(\Pi)$, as converted through (129), for both the stochastic cross sections (132) and (133) and the sensitivities approach (130) and (131). (a) ^{238}U first capture resonance, parameters sampled from an enlarged ENDF/B-VIII uncertainty, 30 samples shown here and (b) Cross section histogram at resonance energy $E_\lambda = 6.67428$ eV.

(2) For the stochastic cross-section method (132) or (133), sampling parameters from $\mathcal{N}(\Gamma, \mathbb{V}\mathrm{ar}(\Gamma))$ or $\mathcal{N}(\Pi, \mathbb{V}\mathrm{ar}(\Pi))$ generates similar cross-section distributions.

In the small covariance case of Fig. 3, the stochastic cross-section distributions (132) and (133) are very close to the normal distributions from the sensitivity approach (131), though at the tails they start differing. In the large covariance case of Fig. 4, the stochastic cross-section distributions are radically different from the normal distribution of the sensitivity method. This discrepancy is made more blatant because the cross-section distribution is recorded at resonance peak energy $E_\lambda = 6.674\,28$ eV, hence a small shift in resonance energy E_λ can dramatically lower the cross-section value. This illustrates the fact that in Theorem 2, when converting the resonance parameters covariances $\mathbb{V}\mathrm{ar}(\Gamma)$ into windowed multipoles covariances $\mathbb{V}\mathrm{ar}(\Pi)$ through (129), the linear assumption used for the local inversion using Jacobians $(\frac{\partial\Pi}{\partial\Gamma})$ from (128) holds for a wider range of resonance parameters than the liner assumption for the cross-section sensitivity method (131). This can be seen in Fig. 5, where the tangent

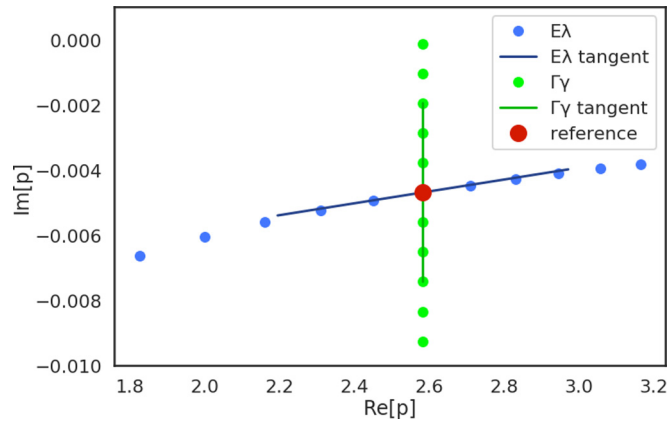

FIG. 5. Multipole sensitivities to *R*-matrix parameters $(\frac{\partial\Pi}{\partial\Gamma})$. Trajectories of pole p as resonance parameters $\{\Gamma\}$ vary, using the SLBW approximation of the first resonance of ^{238}U (the Appendix). The blue points show how the pole changes as E_λ is varied with equal spacing within three standard deviations of the enlarged covariance matrix, while the green points result from equally spaced variations of Γ_γ within their uncertainty range (three standard deviations of enlarged covariance matrix). The Jacobians $(\frac{\partial\Pi}{\partial\Gamma})$ from system (128) are the tangents of these trajectories from the mean pole p (red reference point) and are shown in solid lines. Complex pole p units are $\sqrt{\mathrm{eV}}$.

lines from Jacobians $(\frac{\partial\Pi}{\partial\Gamma})$ are close to the conversion surface, trajectories of $\Pi(\Gamma)$, even after three standard deviations of the large covariance matrix, something clearly not true of the cross-section linear behavior at peak energy from Fig. 4.

Therefore, whichever method is chosen to represent the nuclear cross-section uncertainty, the windowed multipoles covariances $\mathbb{V}\mathrm{ar}(\Pi)$ from Theorem 2 faithfully reproduce the uncertainty from the resonance parameters covariances $\mathbb{V}\mathrm{ar}(\Gamma)$.

IV. DOPPLER BROADENING OF WINDOWED MULTIPOLE CROSS SECTIONS

Hitherto, we have established that the 0-K windowed multipole representation of cross sections is equivalent to the traditional Wigner-Eisenbud *R*-matrix parametrization, in both cross-section values and their uncertainties. We henceforth study how temperature affects *R*-matrix cross sections at the nuclear level through *Doppler broadening* (we do not address thermal neutron scattering at the crystalline level), and derive how the windowed multipole representation exhibits a major advantage: in its form (96)—exact for zero-threshold channels or windows without thresholds, and otherwise an accurate approximation—the window multipole representation of *R*-matrix cross sections can be Doppler broadened precisely by means of closed-form formulas (Theorem 3). This enables the long sought-after computational capability of on-the-fly Doppler broadening of nuclear cross sections [21,26,92–98].

A. Doppler broadening of nuclear cross sections: Solbrig's kernel

As temperature rises, nuclei vibrate, so that the effective cross section for a beam of particles sent upon a target

at a given energy and wave number is the statistical result of the 0-K cross sections averaged out on all the possible relative energies at which the target and the beam interact. For nonrelativistic, nonmassless particles (not photons) in the semiclassical representation, Doppler broadening of nuclear cross sections is the process of integration over the target velocity distribution, assuming the latter is an isotropic Maxwellian (that is a Boltzmann distribution of energies). Solbrig derived this Doppler broadening integral in Eq. (3) p. 259 of [92], where the cross section $\sigma_T(E)$ at temperature T and energy E (in the laboratory coordinates) is related to the cross section $\sigma(E)$ at temperature T_0 as

$$E\sigma_T(E) = \int_0^\infty \frac{\sigma(E')E'^{\frac{1}{2}}}{2\beta\sqrt{\pi}}\left[e^{-(\frac{\sqrt{E'}-\sqrt{E}}{\beta})^2} - e^{-(\frac{\sqrt{E'}+\sqrt{E}}{\beta})^2}\right]dE' \tag{134}$$

where β is the square-root temperature energy parameter:

$$\beta \triangleq \sqrt{\frac{k_{\mathbb{B}}(T-T_0)}{A}} \tag{135}$$

where A designates the atomic mass number, and $k_{\mathbb{B}}$ the universal Boltzmann constant.

Upon change of variable to $z = \sqrt{E}$, the Doppler broadening operation (134) becomes Solbrig's kernel:

$$z^2\sigma_T(z) = \int_0^\infty x^2\sigma_{T_0}(x)\ \mathcal{K}_\beta^{\mathbb{D}}(z,x)dx$$

$$\text{where}\quad \mathcal{K}_\beta^{\mathbb{D}}(z,x) \triangleq \frac{1}{\beta\sqrt{\pi}}\left[e^{-(\frac{z-x}{\beta})^2} - e^{-(\frac{z+x}{\beta})^2}\right]. \tag{136}$$

Note that for zero-threshold channels, where $z \propto k_c(E)$, Solbrig's kernel (136) is an integral operator acting on $k_c^2(E)\ \sigma_c(E)$, which is the transmission matrix square amplitudes from cross-section definition (5). The Solbrig kernel (136) thus acts directly on the interaction probabilities, rather than the actual cross section, just as the channel reversibility equivalence (11).

Solbrig kernel integral (136) has presented major computational challenges in nuclear reactor physics. When no information is provided as to the functional form of the 0-K cross section $\sigma(E)$—i.e., it is considered a pointwise input—the traditional way of computing the Doppler broadened cross section at any temperature $\sigma_T(E)$ has been to pretabulate exact cross sections $\sigma_{T_i}(E)$ (usually using the SIGMA1 algorithm of [94]) for a grid of reference temperatures $\{T_i\}$, and then interpolate between these points to obtain $\sigma_T(E)$ [95,99,100]. However, storing all these precomputed cross sections at reference temperatures $\{T_i\}$ represents a considerable memory burden, which is why methods to minimize the memory footprint and perform Doppler broadening (136) on the fly have been actively sought after [96]. The most state-of-the-art approaches are either optimal temperature Doppler kernel reconstruction quadratures [98] (which only require ten reference temperatures $\{T_i\}$ for standard nuclear reactor codes), new Fourier-transform methods [97], or Monte Carlo target motion sampling rejection schemes [101–103].

To do better, one must look at the functional form of the cross section. When the reference temperature is $T_0 = 0$ K, we have shown in Sec. II that R-matrix cross sections are the sum of threshold behavior and resonances. Resonances have traditionally been Doppler broadened approximately, using Voigt profiles [92], as we here recall in Sec. IV B.

B. Approximate Doppler broadening of Breit-Wigner resonances: Voigt profiles

The traditional approach to Doppler broadening nuclear cross sections has been to consider individual single-level Breit-Wigner resonances (74) at 0 K, with both symmetric (Cauchy-Lorentz distributions) and antisymmetric components, assuming it has a zero energy threshold where it behaves as an s-wave neutron channel (angular momentum $\ell = 0$), so that we can multiply the resonance (74) by the threshold behavior $\frac{1}{\sqrt{E}}$, as described by Wigner in III.A.2 [53]:

$$\begin{aligned}\sigma_0^{\text{SLBW}}(E) &\triangleq \frac{1}{\sqrt{E}}\text{Re}\left[\frac{a+ib}{E-\mathcal{E}_j}\right]\\ &= \frac{1}{\sqrt{E}}\left[\left(\frac{a}{\Gamma_j/2}\right)\chi_0(x) + \left(\frac{b}{\Gamma_j/2}\right)\psi_0(x)\right]\end{aligned} \tag{137}$$

where $x \triangleq (\frac{E-E_j}{\Gamma_j/2})$ with $\mathcal{E}_j \triangleq E_j - i\frac{\Gamma_j}{2}$ from (40), and

$$\begin{aligned}\psi_0(x) &\triangleq \frac{1}{x^2+1} = \frac{\Gamma_j^2/4}{(E-E_j)^2+\frac{\Gamma_j^2}{4}},\\ \chi_0(x) &\triangleq \frac{x}{x^2+1} = \frac{(E-E_j)\frac{\Gamma_j}{2}}{(E-E_j)^2+\frac{\Gamma_j^2}{4}}.\end{aligned} \tag{138}$$

Upon Doppler broadening (134), single-level Breit-Wigner resonance (137) becomes

$$\sigma_T^{\text{SLBW}}(E) = \frac{1}{\sqrt{E}}\left[\left(\frac{a}{\Gamma_j/2}\right)\chi_T(E) + \left(\frac{b}{\Gamma_j/2}\right)\psi_T(E)\right] \tag{139}$$

where χ_T and ψ_T are defined using $x' \triangleq (\frac{E'-E_j}{\Gamma_j/2})$ as

$$\begin{aligned}\chi_T(E) &\triangleq \frac{E^{-\frac{1}{2}}}{2\beta\sqrt{\pi}}\int_0^\infty \chi_0(x')\left[e^{-(\frac{\sqrt{E'}-\sqrt{E}}{\beta})^2} - e^{-(\frac{\sqrt{E'}+\sqrt{E}}{\beta})^2}\right]dE',\\ \psi_T(E) &\triangleq \frac{E^{-\frac{1}{2}}}{2\beta\sqrt{\pi}}\int_0^\infty \psi_0(x')\left[e^{-(\frac{\sqrt{E'}-\sqrt{E}}{\beta})^2} - e^{-(\frac{\sqrt{E'}+\sqrt{E}}{\beta})^2}\right]dE'.\end{aligned} \tag{140}$$

To compute these functions, the following approximations are then traditionally introduced (see [92], or Sec. 3.3.3 Chap. 4, Vol. 1 of [104]).

(1) The Maxwell approximation, whereby we assume the second exponential term is vanishingly small: $e^{-(\frac{\sqrt{E'}+\sqrt{E}}{\beta})^2} \ll 1$. This is valid for $E \gg \beta^2$, but fails at low energies or high temperatures,
(2) A Taylor expansion around the energy of Doppler broadening: $E' = E + \epsilon$, with $\epsilon \ll 1$. This leads to $\sqrt{E'} - \sqrt{E} = \frac{\epsilon}{2\sqrt{E}} + \mathcal{O}(\epsilon^2)$, so that we approximate $e^{-(\frac{\sqrt{E'}-\sqrt{E}}{\beta})^2} \approx e^{-(\frac{E'-E}{2\sqrt{E}\beta})^2}$ in the integrals, which under

change of variable $E' \to x'$ become

$$\psi_T(x) \simeq \frac{1}{2\beta\sqrt{\pi E}} \frac{\Gamma_j}{2} \int_{-2E_j/\Gamma_j}^{\infty} \psi_0(x') e^{-\frac{(x'-x)^2}{4\tau}} dx',$$
$$\chi_T(x) \simeq \frac{1}{2\beta\sqrt{\pi E}} \frac{\Gamma_j}{2} \int_{-2E_j/\Gamma_j}^{\infty} \chi_0(x') e^{-\frac{(x'-x)^2}{4\tau}} dx'$$

where we defined

$$\tau \triangleq 4E\left(\frac{\beta}{\Gamma_j}\right)^2 = 4E\frac{k_{\mathbb{B}}(T-T_0)}{A\Gamma_j^2}. \tag{141}$$

(3) We furthermore assume $2E_j \gg \Gamma_j$, so that we approximate the integral lower limit to $-\infty$, yielding

$$\psi_T(x) \simeq \frac{1}{\sqrt{4\pi\tau}} \int_{-\infty}^{+\infty} \frac{1}{1+x'^2} e^{-\frac{(x'-x)^2}{4\tau}} dx',$$
$$\chi_T(x) \simeq \frac{1}{\sqrt{4\pi\tau}} \int_{-\infty}^{+\infty} \frac{x'}{1+x'^2} e^{-\frac{(x'-x)^2}{4\tau}} dx'. \tag{142}$$

The latter are the standard Voigt functions, $U(x,\tau)$ and $V(x,\tau)$, defined in Sec. 7.19 of [41], which are related to the Faddeyeva function (150) defined in 7.2.3 [41], by

$$\sqrt{\frac{\pi}{4\tau}} w\left(\frac{x+i}{2\sqrt{\tau}}\right) = U(x,\tau) + iV(x,\tau)$$

for $\mathrm{Im}[\frac{x+i}{2\sqrt{\tau}}] > 0$. In the case $\mathrm{Im}[\frac{x+i}{2\sqrt{\tau}}] < 0$, we use $-[w(z^*)]^*$ to calculate the integral, so that the $\psi_T(E)$ and $\chi_T(E)$ functions can approximately be related to the Faddeyeva function as

$$\psi_T(E) \simeq \sqrt{\frac{\pi}{4\tau}} \mathrm{Re}\left[w\left(\frac{x+i}{2\sqrt{\tau}}\right)\right],$$
$$\chi_T(E) \simeq \sqrt{\frac{\pi}{4\tau}} \mathrm{Im}\left[w\left(\frac{x+i}{2\sqrt{\tau}}\right)\right]. \tag{143}$$

Thus the Doppler broadened Breit-Wigner resonance, under these approximations, can be expressed as

$$\sigma_T^{\mathrm{SLBW}}(E) \simeq \frac{1}{\sqrt{E}} \mathrm{Re}\left[\frac{a+ib}{i\Gamma_j/2}\sqrt{\frac{\pi}{4\tau}} w\left(\frac{x+i}{2\sqrt{\tau}}\right)\right]$$
$$= \frac{1}{E}\mathrm{Re}\left[\sqrt{\pi}\frac{a+ib}{i2\beta} w\left(\frac{E-\mathcal{E}_j}{2\beta\sqrt{E}}\right)\right]. \tag{144}$$

This has been the traditional "psi-chi" method to perform approximate Doppler broadening of nuclear resonances, though some improvements have been proposed [see Eq. (57) in Ref. [21]].

Note that the single-level Breit-Wigner profile (137) does not represent higher-order angular momenta for neutron channels, nor does it represent charged particles or photon channels (of any angular momenta), neither does it consider non-zero-threshold behaviors.

C. Analytic Doppler broadening of windowed multipole cross sections

Theorem 1 establishes the windowed multipole representation as an equivalent formalism to parametrize R-matrix cross sections. Windowed multipole cross sections take the form (96) for zero-threshold cross sections of any kind (photons, charged, higher angular momenta), and other thresholds can be approximated with this form (96), though not exactly. Theorem 3 shows how these windowed multipole cross sections (96) can be Doppler broadened analytically to high accuracy, without having to assume an energy dependence of the single-level Breit-Wigner cross-section form $\sigma_0^{\mathrm{SLBW}}(E)$ as in Eq. (137).

Theorem 3. DOPPLER BROADENING OF WINDOWED MULTIPOLE CROSS SECTIONS

Consider the windowed multipole representation of R-matrix cross sections (96), i.e., locally of the form

$$\sigma(z) \underset{\mathcal{W}(E)}{=} \frac{1}{z^2}\mathrm{Re}_{\mathrm{cont}}\left[\sum_{j\geqslant 1}\frac{r_j}{z-p_j}\right] + \sum_{n\geqslant -2} a_n z^n.$$

Upon integration against the Solbrig kernel (136), the Doppler broadened cross section at temperature T takes the following analytic expression:

$$\sigma_T(z) \underset{\mathcal{W}(E)}{=} \sum_{n\geqslant -2} a_n D_\beta^n(z)$$
$$+\frac{1}{z^2}\mathrm{Re}\left[i\sqrt{\pi}\sum_{j\geqslant 1}\frac{r_j}{\beta}\, w\left(\frac{z-p_j}{\beta}\right)\right]$$
$$-\frac{1}{z^2}\mathrm{Re}\left[i\sqrt{\pi}\sum_{j\geqslant 1}\frac{r_j}{\beta}\, C\left(\frac{z}{\beta},\frac{p_j}{\beta}\right)\right] \tag{145}$$

where $C(\frac{z}{\beta},\frac{p_j}{\beta})$ is a correction term defined as

$$C\left(\frac{z}{\beta},\frac{p_j}{\beta}\right) \triangleq \frac{2\,p_j}{i\pi\beta}\int_0^\infty \frac{e^{-(\frac{z}{\beta}+t)^2}}{t^2-\left(\frac{p_j}{\beta}\right)^2} dt \tag{146}$$

which is negligible in most physical ranges of temperatures and energies, so that Doppler broadened windowed multipole cross sections can be well approximated as

$$\sigma_T(z) \underset{\mathcal{W}(E)}{\simeq} \frac{1}{z^2}\mathrm{Re}\left[\sqrt{\pi}\sum_{j\geqslant 1}\frac{r_j}{i\beta}\, w\left(\frac{z-p_j}{\beta}\right)\right]$$
$$+\sum_{n\geqslant -2} a_n D_\beta^n(z) \tag{147}$$

where $D_\beta^n(z)$ are the Doppler broadened monomials:

$$D_\beta^n(z) \triangleq \int_0^\infty \frac{x^{n+2}}{z^2}\mathcal{K}_\beta^{\mathbb{D}}(z,x)dx \tag{148}$$

which are subject to the following recurrence formulas from elemental Gaussian and error functions [defined in Eq. (7.2.1) of [41]] [28],

$$D_\beta^{n+2}(z) \underset{\forall n\geqslant 1}{=} \left[\frac{\beta^2}{2}(2n+1)+z^2\right]D_\beta^n(z)$$
$$-\left(\frac{\beta^2}{2}\right)^2 n(n-1)D_\beta^{n-2}(z),$$

$$\begin{aligned} D^0_\beta(z) &= \left[\frac{\beta^2}{2}+z^2\right]D^{-2}_\beta(z)+\frac{\beta}{z\sqrt{\pi}}e^{-(\frac{z}{\beta})^2}, \\ D^{-1}_\beta(z) &= \frac{1}{z}, \\ D^{-2}_\beta(z) &= \frac{1}{z^2}\text{erf}\left(\frac{z}{\beta}\right) \end{aligned} \tag{149}$$

and where $w(z)$ is the Faddeyeva function [defined in Eq. (7.2.3) of [41]],

$$w(z) \triangleq e^{-z^2}[1-\text{erf}(-iz)] = e^{-z^2}\left(1+\frac{2i}{\sqrt{\pi}}\int_0^z e^{t^2}dt\right) \tag{150}$$

called at poles in the complex lower semiplane, i.e., $\text{Im}[\frac{z-p_j}{\beta}] > 0$. For all other poles, which satisfy $\text{Im}[\frac{z-p_j}{\beta}] \leqslant 0$, we use the fact that the windowed multipole representation has complex conjugate poles to call the Faddeyeva function at $-[w(z^*)]^* = -w(-z)$.

Proof. This analytic Doppler broadening comes from

$$\sigma_T(z) \underset{\mathcal{W}(E)}{=} \frac{1}{z^2}\text{Re}\left[\sum_{j\geqslant 1} r_j \int_0^\infty \frac{\mathcal{K}^{\mathbb{D}}_\beta(z,x)}{x-p_j}dx\right] + \sum_{n\geqslant -2} a_n D^n_\beta(z).$$

Doppler broadening of the Laurent expansion part (148), which describes the threshold behavior, was established in Ref. [98] [Eqs. (14)–(16)], and the recurrence formulas (149) are obtained through integration by parts.

The resonances Doppler broadening was established in Ref. [21] [Eqs. (60)–(75)], which we here recall:

$$\begin{aligned} &\beta\sqrt{\pi}\int_0^\infty \frac{\mathcal{K}^{\mathbb{D}}_\beta(z,x)}{x-p_j}dx \\ &\triangleq \int_0^\infty \frac{dx}{x-p_j}\left[e^{-(\frac{z-x}{\beta})^2}-e^{-(\frac{z+x}{\beta})^2}\right] \\ &= \int_{-\infty}^\infty \frac{e^{-(\frac{z-x}{\beta})^2}}{x-p_j}dx - \int_{-\infty}^0 \frac{e^{-(\frac{z-x}{\beta})^2}}{x-p_j}dx - \int_0^\infty \frac{e^{-(\frac{z+x}{\beta})^2}}{x-p_j}dx \\ &= \int_{-\infty}^\infty \frac{e^{-t^2}}{t-(\frac{z-p_j}{\beta})}dt + \int_0^\infty e^{-(\frac{z+x}{\beta})^2}\left[\frac{1}{x+p_j}-\frac{1}{x-p_j}\right]dx \\ &= i\pi\, w\left(\frac{z-p_j}{\beta}\right) - 2p_j\int_0^\infty \frac{e^{-(\frac{z+x}{\beta})^2}}{x^2-p_j^2}dx \end{aligned}$$

where in the last line we introduced the Faddeyeva function (150), defined in Eq. (7.2.3) of [41], which admits the following integral representation for $\text{Im}[z] > 0$:

$$w(z) \underset{\text{Im}[z]>0}{=} \frac{1}{i\pi}\int_{-\infty}^\infty \frac{e^{-t^2}}{t-z}dt = \frac{2z}{i\pi}\int_0^\infty \frac{e^{-t^2}}{t^2-z^2}dt. \tag{151}$$

In the case $\text{Im}[z] < 0$, we then use the following integral representation:

$$-[w(z^*)]^* = -w(-z) \underset{\text{Im}[z]<0}{=} \frac{1}{i\pi}\int_{-\infty}^\infty \frac{e^{-t^2}}{t-z}dt. \tag{152}$$

Thus, calling the Faddeyeva function directly for the poles in the complex lower semiplane, $\text{Im}[\frac{z-p_j}{\beta}] > 0$, while for the others we use $-[w(z^*)]^* = -w(-z)$ to calculate the integral representation (the pole representation has complex conjugate poles), the Solbrig kernel Doppler broadening operation yields (145). Hwang undertook an in-depth study of the correction term $C(\frac{z}{\beta}, \frac{p_j}{\beta})$ in Sec. IV.D of [21], showing it is negligible in most physical applications. Therefore, approximation (147) is effectively faithful, in particular at high energies-to-temperature ratios $z/\beta \gg 1$. ■

Compared to the traditional psi-chi method (144), Theorem 3 gives a much more general way to Doppler broaden nuclear cross sections, applicable to charged or uncharged particles of any angular momentum. Theorem 3 also motivates why we decomposed the resonances in $z = \sqrt{E}$ space: it enables more accurate analytic Doppler broadening, since the latter happens in wave-number space as Hwang showed in Eq. (65) of [21].

Note that Hwang derived equations to analytically Doppler broaden his pole representation (112), with energy-dependent residues, showing that the $e^{-2i\rho}$ component shifts the Faddeyeva function evaluation, adding a purely imaginary offset in Eq. (6) of [25]. Nonetheless, this approach is not generalizable to Coulomb channels or to thresholds, while Theorem 3 is.

To compare these different Doppler broadening methods, we conducted numerical calculations on the first capture resonance of ^{238}U, in the simple single-level Breit-Wigner resonance case of the Appendix, reporting the results in Fig. 6. They show the analytic windowed multipole Doppler broadening exactly matches the direct piecewise integration of Solbrig's kernel (136) to 10^{-6} relative error, significantly outperforming the SIGMA1 method [94] of NJOY [91], while the traditional ψ_T/χ_T approximation (144) breaks down at high temperatures. Note than in this particular SLBW case of the Appendix, the poles are exact opposites of one another, while the residues are the same, so that they cancel out of the C-function correction (146), hence the analytic Doppler broadening of the windowed multipole representation (147) is exact. This canceling out of C-function correction (146) is also true in general of zero-threshold neutral particles s-wave cross sections, which behave as $1/z$ at low energies, thereby yielding identical residues $r_j^+ = r_j^-$ for opposite z-poles pairs $p_j^+ = -p_j^-$.

D. Temperature derivatives of Doppler broadened windowed multipole cross sections

The analytic Doppler broadening of windowed multipole cross sections (Theorem 3) has the additional advantage that one can compute all its temperature derivatives by means of simple recurrence formulas, as we here establish in Theorem 4.

Theorem 4. TEMPERATURE DERIVATIVES OF WINDOWED MULTIPOLE CROSS SECTIONS

Consider the approximate Doppler broadened windowed multipole representation of R-matrix cross sections (147)

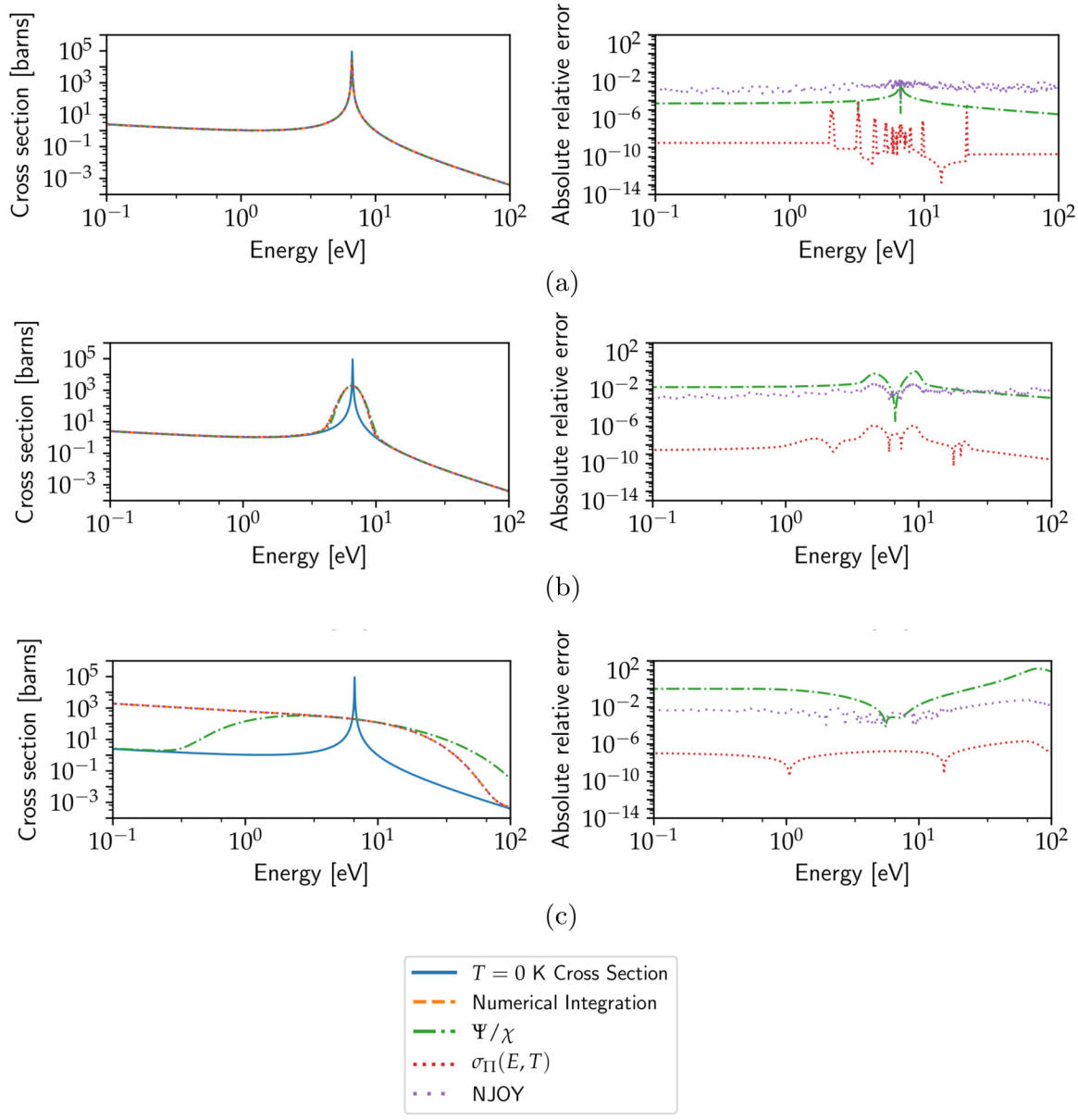

FIG. 6. Accuracy of different Doppler-broadening methods. Using the SLBW resonance description given in the Appendix, the cross section (A1) is reconstructed at $T = 0$ K. For each temperature $\{300, 10^5, 10^7\}$ K, the cross section is broadened using four different methods: (i) numerical integration of the Solbrig kernel (136); (ii) using the ψ_T/χ_T approximation (143) for SLBW Doppler broadening (144); (iii) conversion (A5) of the resonance parameters $\{\Gamma\}$ to multipoles $\{\Pi\}$ and analytic Doppler broadening of windowed multipole representation (A4) from Theorem 3 Eq. (147); and (iv) formulation of the parameters in ENDF format and processing using NJOY [91]. For each temperature, the right column shows the absolute relative error for methods (ii), (iii), and (iv) to the direct integration of the Solbrig kernel (i). Note: NJOY was run with a tolerance parameter of 10^{-2} as higher accuracy required a prohibitively long computation time. (a) T = 300 K, (b) T = 10^5 K, and (c) T = 10^7 K.

from Theorem 3, upon change of variables $\theta \triangleq \frac{1}{\beta}$:

$$\sigma_T(z) \underset{\mathcal{W}(E)}{\simeq} \frac{1}{z^2}\mathrm{Re}\left\{i\sqrt{\pi}\sum_{j\geqslant 1} r_j\ \theta\ w[\theta(z-p_j)]\right\} + \sum_{n\geqslant -2} a_n D_\beta^n(z).$$

Then its kth temperature derivative can be computed as

$$\partial_T^{(k)}\sigma_T(z) \underset{\mathcal{W}(E)}{\simeq} \frac{1}{z^2}\mathrm{Re}\left[i\sqrt{\pi}\sum_{j\geqslant 1} r_j\ X_\beta^{(k)}(z-p_j)\right] + \sum_{n\geqslant -2} a_n\ \partial_T^{(k)} D_\beta^n(z). \quad (153)$$

$X_\beta^{(k)}(z-p_j)$ are the kth temperature derivatives of the Doppler broadened resonances:

$$\begin{aligned} X_\beta^{(k)}(z-p_j) &\triangleq \partial_T^{(k)}\{\theta\ w[\theta(z-p_j)]\} \\ &= \sum_{n=1}^{k}\Big(\big\{\partial_\theta^{(n)}\theta\ w[\theta(z-p_j)]\big\} \\ &\quad \times B_{k,n}(\theta^{(1)},\theta^{(2)},\ldots,\theta^{(k-n+1)})\Big) \end{aligned} \tag{154}$$

where the sum is the Arbogast composite derivatives (Faà di Bruno) formula [105], linking the θ derivatives

$$\partial_\theta^{(n)}\theta\ w[\theta(z-p_j)] \underset{\forall n\geqslant 1}{=} -\frac{(z-p_j)^{n-1}}{2}w^{(n+1)}[\theta(z-p_j)] \tag{155}$$

to the $\theta^{(n)}$ temperature derivatives of θ

$$\theta^{(n)} \triangleq \partial_T^{(n)}\theta = \frac{1}{\beta}\left(\frac{-1}{2}\right)^n\frac{(2n-1)!!}{(T-T_0)^n} \tag{156}$$

by means of the partial exponential Bell polynomials $B_{k,n}(\theta^{(1)},\theta^{(2)},\ldots,\theta^{(k-n+1)})$ [106–108].

The derivatives of the Faddeyeva function can be computed using recurrence formulas [see Eq. (7.10) in Ref. [41]]:

$$\begin{aligned} w^{(1)}(z) &= -2zw(z)+\frac{2i}{\sqrt{\pi}}, \\ w^{(n+2)}(z) &= -2zw^{(n+1)}(z)-2(n+1)w^{(n)}(z). \end{aligned} \tag{157}$$

$\partial_T^{(k)}D_\beta^n(z)$ are the temperature derivatives of the Doppler broadened monomials, which are subject to the following recurrence formulas, defining $a \triangleq \frac{k_{\mathbb{B}}}{A}$:

$$\begin{aligned} \partial_T^{(k)}D_\beta^{n+2}(z) &\underset{\forall n\geqslant 1}{=} \left[\frac{\beta^2}{2}(2n+1)+z^2\right]\partial_T^{(k)}D_\beta^n(z) \\ &\quad +\frac{a}{2}(2n+1)k\ \partial_T^{(k-1)}D_\beta^n(z) \\ &\quad -\frac{n(n-1)}{4}\big[\beta^4\partial_T^{(k)}D_\beta^{n-2}(z) \\ &\quad +2a\beta k\ \partial_T^{(k-1)}D_\beta^{n-2}(z) \\ &\quad +a^2k(k-1)\partial_T^{(k-2)}D_\beta^{n-2}(z)\big], \\ \partial_T^{(k)}D_\beta^0(z) &= \left[\frac{\beta^2}{2}+z^2\right]\partial_T^{(k)}D_\beta^{-2}(z)+\frac{a}{2}k\ \partial_T^{(k-1)}D_\beta^{-2}(z) \\ &\quad +\frac{1}{z\sqrt{\pi}}\big[\beta^2\partial_T^{(k)}\theta e^{-(z\theta)^2}+ak\ \partial_T^{(k-1)}\theta e^{-(z\theta)^2}\big], \\ \partial_T^{(k)}D_\beta^{-1}(z) &= \frac{1}{z}\delta_{k,0}, \\ \partial_T^{(k)}D_\beta^{-2}(z) &= \frac{1}{z^2}\partial_T^{(k)}\mathrm{erf}(z\theta). \end{aligned} \tag{158}$$

In recurrence relations (158), the terms $\partial_T^{(k)}\theta e^{-(z\theta)^2}$ can themselves be computed using Arbogast's formula:

$$\partial_T^{(k)}\theta e^{-(z\theta)^2} = e^{-(z\theta)^2}\sum_{n=1}^{k}\big[F_z^{(n)}(\theta)B_{k,n}(\theta^{(1)},\theta^{(2)},\ldots,\theta^{(k-n+1)})\big] \tag{159}$$

where $F_z^{(n)}(\theta)$ are polynomials of degree $n+1$ defined as

$$F_z^{(n)}(\theta) \triangleq e^{(z\theta)^2}\partial_\theta^{(n)}\theta e^{-(z\theta)^2} = \sum_{i=0}^{n+1}\alpha_i^{(n)}\theta^i \tag{160}$$

which are recursively constructed from $F_z^{(0)}(\theta)=\theta$ as

$$F_z^{(n+1)}(\theta) = \partial_\theta F_z^{(n)}(\theta) - 2z^2\theta F_z^{(n)}(\theta) \tag{161}$$

entailing these recurrence formulas on their coefficients:

$$\begin{aligned} &\alpha_0^{(0)}=0, \quad \alpha_1^{(0)}=1, \\ &\alpha_{n+1}^{(n+1)} = -2z^2\alpha_n^{(n)}, \quad \alpha_{n+2}^{(n+1)} = -2z^2\alpha_{n+1}^{(n)}, \\ &\alpha_i^{(n+1)} \underset{1\leqslant i\leqslant n}{=} (i+1)\alpha_{i+1}^{(n)} - 2z^2\alpha_{i-1}^{(n)}. \end{aligned} \tag{162}$$

Finally, the terms $\partial_T^{(k)}\mathrm{erf}(z\theta)$ in recurrence relations (158) can also be computed using Arbogast's formula:

$$\partial_T^{(k)}\mathrm{erf}(z\theta) = \sum_{n=1}^{k}\big[\partial_\theta^{(n)}\mathrm{erf}(z\theta)\big]\ B_{k,n}(\theta^{(1)},\ldots,\theta^{(k-n+1)}) \tag{163}$$

in which the θ derivatives can be expressed as

$$\partial_\theta^{(n)}\mathrm{erf}(z\theta) \underset{n\geqslant 1}{=} z^n(-1)^{n-1}\frac{2}{\sqrt{\pi}}H_{n-1}(z\theta)e^{-(z\theta)^2} \tag{164}$$

where the Hermite polynomials $H_n(z)$ are recursively calculable from $H_0=1$ and $H_1=2z$ as

$$H_{n+1} \underset{n\geqslant 1}{=} 2zH_n - 2nH_{n-1}. \tag{165}$$

Proof. The underlying assumption of the proof is that one can neglect the derivatives of the correction term (146). The proof consists of a series of derivatives expanded using the general Leibniz rule and the Arbogast formula for composite derivatives (Faà di Bruno) (see p. 43 of [105]), in which the Bell polynomials can be computed as referenced in Refs. [106–108]. Direct differentiation yields the temperature derivatives of θ (156). Expression (155) is obtained using the Faddeyeva function recurrence formula (157), documented in Eq. (7.10) of [41]. The $F_z^{(n)}(\theta)$ polynomials (160) are defined from $\partial_\theta^{(n)}\theta e^{-(z\theta)^2} = F_z^{(n)}(\theta)e^{-(z\theta)^2}$ and their degree $n+1$ stems from the recursive derivatives (161) initialized at $F_z^{(0)}(\theta)=\theta$, entailing the recurrence formula for the coefficients (162). Similarly, expression (164) is derived from change of variable $z\to\theta z$, and using the derivative formula for the error function (see Abramowitz and Stegun, p. 298, Eq. (7.1.19) [42], or Eq. (7.10.1) in Ref. [41]):

$$\mathrm{erf}^{(n+1)}(z) = (-1)^n\frac{2}{\sqrt{\pi}}H_n(z)e^{-z^2}$$

while the Hermite polynomials recurrence relation (165) is well known and documented [see Eq. (18.9) of [41]]. ■

Underpinning this direct differentiation approach is the assumption that the C-function correction term (146), itself negligible, also has negligible temperature derivatives. It is nonetheless possible to extend this method to explicitly include thermal derivatives of the correction term (146), by noticing that these derivatives follow a similar polynomial

structure as (160) and are subject to a recurrence relation similar to (161).

E. Fourier-transform approach to temperature treatment

Ferran developed a more general approach, based on Fourier transforms, to Doppler broaden nuclear cross sections (we here only discussed Doppler broadening of angle-integrated cross sections) [97]. In Theorem 5, we generalize Ferran's method, begetting arbitrary-order temperature derivatives of Doppler broadened cross sections, while setting a more general framework for temperature treatments such as low-energy thermal neutrons scattering with the phonons of the target's crystalline structure. Moreover, when applied to the windowed multipole representation of *R*-matrix cross sections, this Fourier-transform approach exactly accounts for the entire nuclear cross section, without neglecting the *C*-function correction term (146). This generality comes at the additional cost of having to compute Fourier transforms on the fly. Also, Fourier transforms can be numerically sensitive to the tails of distributions, meaning one has to be careful as to how the cross sections are extended beyond the treated windows (see Ferran's discussion in Sec. IV.B.2 of [97]).

We here recall Ferran's general Fourier-transform method from [97]. The function $f \star g$ designates the convolution product between functions f and g, defined as

$$f \star g\,(x) \underset{\forall x\in\mathbb{R}}{\triangleq} \int_{\mathbb{R}} f(t)g(x-t)dt. \tag{166}$$

Ferran expressed Solbrig's kernel (136) Doppler broadening operation as a convolution product by introducing the *Ferran representation* odd-parity function [97]:

$$s_T : z \in \mathbb{R} \mapsto \begin{cases} z^2\sigma_T(z) & \forall z \in \mathbb{R}_+^* \\ 0 & \text{if } z = 0 \\ -z^2\sigma_T(-z) & \forall z \in \mathbb{R}_-^* \end{cases}. \tag{167}$$

Applying Solbrig's kernel to s_T yields a linear convolution product operator that transforms the Ferran representation s_0 of the cross section at temperature T_0, to s_T at temperature $T > T_0$ as follows [97]:

$$s_T = s_0 \star \mathcal{K}_T^{\mathbb{B}} \tag{168}$$

where $\mathcal{K}_T^{\mathbb{B}}$ is the Maxwell-Boltzmann distribution of energies of the target:

$$\mathcal{K}_T^{\mathbb{B}}(z) \underset{\forall z\in\mathbb{R}}{\triangleq} \frac{1}{\beta\sqrt{\pi}} e^{-\left(\frac{z}{\beta}\right)^2}. \tag{169}$$

The Fourier transform of a function f is defined as (unitary, ordinary frequency convention) [109]

$$\widehat{f}(\nu) \triangleq \int_{\mathbb{R}} f(t)\; e^{-i2\pi\nu t} dt \tag{170}$$

for which the inverse Fourier transform is

$$f(x) = \int_{\mathbb{R}} \widehat{f}(\nu)\; e^{i2\pi\nu x} d\nu. \tag{171}$$

The Fourier transform of any odd-parity function g can be expressed as

$$\widehat{g}(\nu) = -2i \int_{\mathbb{R}_+} g(t) \sin(2\pi\nu t) dt. \tag{172}$$

Fourier transforms satisfy the convolution property:

$$\widehat{f \star g} = \widehat{f}\,\widehat{g}. \tag{173}$$

The Doppler broadening operation can therefore be performed by calculating the inverse Fourier transform of

$$\widehat{s_T} = \widehat{s_0 \star \mathcal{K}_T^{\mathbb{B}}} = \widehat{s_0}\;\widehat{\mathcal{K}_T^{\mathbb{B}}}. \tag{174}$$

Since the Fourier transform of Boltzmann kernel $\mathcal{K}_T^{\mathbb{B}}$ is well known,

$$\widehat{\mathcal{K}_T^{\mathbb{B}}}(\nu) = e^{-(\pi\beta\nu)^2} \tag{175}$$

given $\widehat{s_0}$, Doppler broadening can therefore be performed as the inverse Fourier transform of $\widehat{s_0}\; e^{-(\pi\beta\nu)^2}$.

In Theorem 5, we derive the Fourier transform of windowed multipole cross sections, and generalize Ferran's method to account for arbitrary-order temperature derivatives, as an alternative to Theorem 4.

Theorem 5. Fourier-Transform Doppler Broadening of Windowed Multipole Cross Sections

Consider the 0-K Ferran representation of windowed multipole *R*-matrix cross sections (96), i.e., the odd-parity function $s_0(z) = -s_0(-z)$ locally of the form

$$s_0(z) \underset{z>0}{\triangleq} z^2\;\sigma_0(z) \underset{\mathcal{W}(E)}{=} \mathrm{Re}_{\mathrm{cont}}\left[\sum_{j\geqslant 1} \frac{r_j}{z-p_j}\right] + \sum_{n\geqslant 0} a_{n-2} z^n. \tag{176}$$

Then its Fourier transform (170) can be expressed as

$$\widehat{s_0}(\nu) \underset{\mathcal{W}(E)}{=} \mathrm{Re}_{\mathrm{cont}}\left[\sum_{j\geqslant 1} r_j \widehat{V}_{p_j}(\nu)\right] + \sum_{n\geqslant 0} a_{n-2}\widehat{\mathrm{F}}_n(\nu) \tag{177}$$

where the Fourier transforms of the Laurent expansions $\widehat{\mathrm{F}}_n(\nu)$ can be expressed for either even or odd positive integers $n \geqslant 0$ as [$\delta^{(n)}(\nu)$ designates the nth derivative of Dirac's delta distribution]

$$\begin{aligned} \widehat{\mathrm{F}}_{2n}(\nu) &\triangleq (-1)^{n+1} \frac{2i(2n)!}{(2\pi\nu)^{2n+1}}, \\ \widehat{\mathrm{F}}_{2n+1}(\nu) &\triangleq \frac{(-1)^n i}{(2\pi)^{2n+1}} \delta^{(n)}(\nu) \end{aligned} \tag{178}$$

and the Fourier transforms of the resonances at pole p_j $\widehat{V}_{p_j}(\nu)$ can be expressed as

$$\widehat{V}_{p_j}(\nu) \underset{|\mathrm{ph}(p_j)|<\pi}{\triangleq} -2i\;\mathrm{sgn}(\nu)\; f(-2\pi|\nu|p_j) \tag{179}$$

where $\mathrm{sgn}(z)$ designates the sign function, and f is the auxiliary function defined in Eq. (6.2.17) of [41].

The kth-order temperature derivative of windowed multipole *R*-matrix cross sections is the convolution:

$$\partial_T^{(k)} s_T = s_0 \star \partial_T^{(k)} \mathcal{K}_T^{\mathbb{B}} \tag{180}$$

which is the inverse Fourier transform (171) of product

$$\widehat{\partial_T^{(k)} s_T} = \widehat{s_0}\ \partial_T^{(k)} \widehat{\mathcal{K}_T^{\mathbb{B}}} \tag{181}$$

the expressions of which are (177) for $\widehat{s_0}$ and, defining $a \triangleq \frac{k_{\mathbb{B}}}{A}$,

$$\partial_T^{(k)} \widehat{\mathcal{K}_T^{\mathbb{B}}} = a^k (i\pi\nu)^{2k} \widehat{\mathcal{K}_T^{\mathbb{B}}} = a^k (i\pi\nu)^{2k} e^{-(\pi\beta\nu)^2}. \tag{182}$$

Proof. The proof consists of directly calculating the corresponding Fourier transforms by developing the linear operators. Equation (181) stems from the Fourier-transform linear property $\widehat{\partial_T^{(k)} \mathcal{K}_T^{\mathbb{B}}} = \partial_T^{(k)} \widehat{\mathcal{K}_T^{\mathbb{B}}}$ applied to (180). Expression (182) is obtained by direct differentiation of (175). In key expression (177), the Fourier transforms of the Laurent development part (178) are obtained by noticing that odd-parity polynomials are already odd functions, while the even-parity ones must be written as the difference of (176) multiplied by the Heaviside function for domains $\mathbb{R}_-$ and $\mathbb{R}_+$, and then applying standard Fourier-transform properties. The Fourier transforms of resonance terms (179) are obtained by identifying the integral representation (6.7.13) in Ref. [41], and using identity $f(ze^{\pm i\pi}) = \pi e^{\mp iz} - f(z)$ [see Eq. (6.4.6) [41]] if the phase of the pole p_j does not respect $|\mathrm{ph}(p_j)| < \pi$. ■

The Fourier-transform approach of Theorem 5 to arbitrary-order temperature derivatives is conceptually more elegant than the direct differentiations of Theorem 4: there is no need for Arbogast–Faà di Bruno composition expansions nor recurrences. It is also more general, as the correction C-function term (146) is not neglected in the Doppler broadening, and the Fourier-transform approach could potentially be expanded to treat thermal scattering with the phonon distributions of targets: one would then need to replace the Boltzmann distributions $\widehat{\mathcal{K}_T^{\mathbb{B}}}$ (175) with the corresponding phonon Fourier spectra (see the "Neutron Slowing Down and Thermalization" chapter in Refs. [104] or [110,111]). In practice, Theorem 5 also runs into its own hurdles: nothing guarantees that numerically performing the on-the-fly Fourier transforms of Theorem 5—using the fast Fourier-transform and subsequent algorithms [112–114]—is more computationally efficient than calling the Faddeyeva functions—which also have benefited from great algorithmic and computational performance gains [115–119]—and the recursive formulas of Theorem 4. This is all the more true as Theorem 5 requires the computation of the f auxiliary function (179), which could be more costly than calling the Faddeyeva function. Also, Fourier transforms are global integrals, so the windowing process complicates this approach, and the windows have now to be selected according to the method Ferran discussed in Sec. IV.B.2 of [97], considering that the Doppler broadening only affects the cross section $\sigma(E)$ at a given energy E for a convolution over an interval commensurate to the temperature energy β^2, say four times $E \pm 4\beta^2$ [21,92,94,97]. Note that this locality problem already exists in the direct Doppler broadening of Theorem 3 and by extension Theorem 4, and even in the windowing process itself, when selecting which poles p_j to include in window $\mathcal{W}(E)$ as discussed in Sec. II E 4 and established in Refs. [26,28]. Though in theory the Mittag-Leffler expansion converges on the entire energy domain between two thresholds $[E_{T_c}, E_{T_c+1}]$, in practice it is too costly to compute the Faddeyeva functions for all poles, and the essence of the windowing process is therefore to only account for the poles which affect the cross section in window $\mathcal{W}(E)$ upon Doppler broadening, in practice extending the domain ("external window" in Refs. [26,28]) for a couple of temperature energy variances in the Boltzmann distribution—$[\mathcal{W}(E_{\min} - 4\beta^2_{\max(T)}), \mathcal{W}(E_{\max} + 4\beta^2_{\max(T)})]$: this is a very similar process to Ferran's continuation of the function for the Fourier transform, discussed in Sec. IV.B.2 of [97]. Therefore, if the windowing process is well performed, the expression of Theorem 5 will be valid within each window. Otherwise, one would need to truncate the Fourier transforms at the boundary of each energy window, and laboriously concatenate the Ferran representation window by window in the Fourier transforms.

Finally, note that Ferran's Doppler broadening method presents similarities with the optimal temperature kernel reconstruction quadratures developed in Ref. [98]: both are kernel methods operating on the cross sections, in particular the Boltzmann kernel Eq. (6) of [98]. Appendix D of [98] studies the consequences of the windowed multipole representation of R-matrix cross sections on the Fourier transforms involved in Theorem 5. In particular are discussed the general shapes of the Fourier transforms of the nuclear resonances, compared to the $\mathcal{K}_T^{\mathbb{B}}$ Boltzmann kernel (175), and how this can entail properties of interest, such as frequency separation in the L_2 norm [see Eq. (D.9) and Secs. D.2 and D.3 of Appendix D in Ref. [98]].

V. CONCLUSION

This paper establishes the theoretical foundations for the Windowed Multipole Library.

We derive how the windowed multipole representation of R-matrix cross sections can be constructed by finding the poles of the Kapur-Peierls operator (radioactive states) and performing Hwang's conjugate continuation (Theorem 1). In the process, we connect the windowed multipole representation to both the Bloch and Wigner-Eisenbud R-matrix theory and to the Humblet-Rosenfeld pole expansions in wave-number space.

We establish a method to convert R-matrix resonance parameters covariance matrices into windowed multipole covariances (Theorem 2), and show they generate the same uncertainty distribution on nuclear cross sections, either through the sensitivity approach or by sampling stochastic cross sections.

We recall windowed multipole cross sections can be Doppler broadened analytically to high accuracy (Theorem 3), and expand this on-the-fly capability to arbitrary-order temperature derivatives (Theorem 4), while deriving new capabilities for temperature treatment by means of Fourier transforms of windowed multipole cross sections (Theorem 5).

The windowed multipole representation of R-matrix cross sections has already proved its efficacy on a vast range of nuclear physics applications. We hope the foundational results of this paper will allow for the widespread adoption of the Windowed Multipole Library, and underpin new research efforts to expand its capabilities.

ACKNOWLEDGMENTS

This work was partly funded by the Consortium for Advanced Simulation of Light Water Reactors, an Energy Innovation Hub for Modeling and Simulation of Nuclear Reactors under US Department of Energy Contract No. DE-AC05-00OR22725. The first author was also partly funded by the 2019-2020 AXA Fellowship of the Schwarzman Scholars Program at Tsinghua University. We would like to thank Mark Paris and Gerald Hale from Los Alamos National Laboratory for their help on *R*-matrix theory and the *R*-matrix 2016 summer workshop in Santa Fe; Grégoire Allaire from École Polytechnique for his help on Fredholm's alternative and Perron-Frobenius theory; Semyon Dyatlov from Massachusetts Institute of Technology and University of California Berkeley for his help on Gohberg-Sigal theory; Javier Sesma from Universidad de Zaragoza for his help on properties of the Hankel functions; Yoann Desmouceaux for his help in proving the diagonal divisibility and capped multiplicities Lemma 3 of [32]; Andrew Holcomb for his help in testing Theorem 1 of [32]; and Haile Owusu for his help on Hamiltonian degeneracy.

APPENDIX: SINGLE LEVEL BREIT-WIGNER CAPTURE RESONANCE

In order to derive a simple reference case that is tractable analytically, we here study the multipole representation of the first radiative capture s-wave resonance of uranium ^{238}U. We neglect the energy dependence of the widths in the resonance (this constitutes the $B = S$ approximation), and denote $\Gamma_\lambda \triangleq \Gamma_\gamma + \Gamma_n$, so that the γ-channel cross section takes the form

$$\sigma_\gamma(E) = \pi g_{J^\pi} a_c^2 \frac{\Gamma_\gamma \Gamma_n}{\rho_0^2 \sqrt{E_\lambda}} \frac{1}{\sqrt{E}} \frac{1}{(E_\lambda - E)^2 + \Gamma_\lambda^2/4} \tag{A1}$$

which is a single-level Breit-Wigner resonance (137) with $\mathcal{E}_\lambda \triangleq E_\lambda - i\frac{\Gamma_\lambda}{2}$, $a = 0$, and $b \triangleq 2\pi \frac{\Gamma_\gamma \Gamma_n}{\rho_0^2 \sqrt{E_\lambda} \Gamma_\lambda}$, i.e.,

$$\sigma_\gamma(E) = \frac{1}{\sqrt{E}} \mathrm{Re}\left[\frac{ib}{E - \mathcal{E}_\lambda}\right]. \tag{A2}$$

Let us now cast (A1) into the multipole representation (96). We perform this by change of variables $z^2 = E$, and $p^2 = \mathcal{E}_\lambda$, and partial fraction decomposition:

$$\frac{1}{\sqrt{E}} \mathrm{Re}\left[\frac{ib}{E - \mathcal{E}_\lambda}\right] = \frac{1}{z^2} \mathrm{Re}\left[\frac{ib/2}{z - p} + \frac{ib/2}{z + p}\right]. \tag{A3}$$

Thus the multipole cross section in z space is then

$$\sigma_\gamma(z) = \frac{1}{z^2} \mathrm{Re}_{\mathrm{cont}}\left[\frac{r}{z - p} + \frac{r}{z + p}\right] \tag{A4}$$

with

$$r \triangleq i\pi \frac{\Gamma_\gamma \Gamma_n}{\rho_0^2 \sqrt{E_\lambda}\, \Gamma_\lambda},$$
$$p \triangleq \sqrt{E_\lambda - i\frac{\Gamma_\lambda}{2}}. \tag{A5}$$

TABLE II. Resonance parameters of the first s-wave radiative γ-capture resonance of ^{238}U used for generating temperature tolerance plot (Fig. 6) and sensitivities demonstration (Figs. 3 and 4). The resonance energies and widths, as well as their covariance matrix, are those of ENDF/B-VIII.0 evaluation [14]. The enlarged covariance matrix, as well as the channel radius a_c, the atomic weight A, and ρ_0, are those of the analytic neutron slowdown benchmark [38,39].

$z = \sqrt{E}$ with E in eV
$A = 238$
$a_c = 0.000948$: channel radius (fm)
$\rho_0/a_c = 0.002196807122623/2$ ($\sqrt{\mathrm{eV}}^{-1}$)
$E_\lambda = 6.674280$: first resonance energy (eV)
$\Gamma_n = 0.00149230$: neutron width of first resonance
$\Gamma_\gamma = 0.0227110$: eliminated capture width (eV)
$g_{J^\pi} = 1$: spin statistical factor
ENDF/B-VIII.0 covariance matrix:
$\mathbb{V}\mathrm{ar}([E_0, \Gamma_n, \Gamma_\gamma]) =$

$$\begin{bmatrix} 1.1637690 \times 10^{-7} & -2.7442070 \times 10^{-10} & 1.8617500 \times 10^{-8} \\ -2.7442070 \times 10^{-10} & 3.9366000 \times 10^{-10} & -6.5102670 \times 10^{-9} \\ 1.8617500 \times 10^{-8} & -6.5102670 \times 10^{-9} & 1.6255630 \times 10^{-7} \end{bmatrix}$$

Enlarged covariance matrix (same correlation):
$\mathbb{V}\mathrm{ar}([E_0, \Gamma_n, \Gamma_\gamma])=$

$$\begin{bmatrix} 1.2373892 & -1.1217107 \times 10^{-5} & 5.6993358 \times 10^{-4} \\ -1.1217107 \times 10^{-5} & 6.1859980 \times 10^{-8} & -7.6617177 \times 10^{-7} \\ 5.6993358 \times 10^{-4} & -7.6617177 \times 10^{-7} & 1.4327486 \times 10^{-5} \end{bmatrix}$$

One can then verify the results of Theorem 1 with these explicit formulas.

In Theorem 2, we develop a method to compute the Jacobian matrix $(\frac{\partial \Pi}{\partial \Gamma})$, using the sensitivities $\frac{\partial \sigma}{\partial \Gamma}(E)$ of the cross section $\sigma(E)$ to resonance parameters $\{\Gamma\}$. These can here be derived by direct differentiation of (A1), yielding the relative sensitivities (derivatives):

$$\begin{aligned} \frac{1}{\sigma_\gamma}\frac{\partial \sigma_\gamma}{\partial E_\lambda} &= \frac{-1}{2E_\lambda} + 2(E - E_\lambda)\sigma_\gamma \frac{\rho_0^2 \sqrt{E}\sqrt{E_\lambda}}{\pi \Gamma_n \Gamma_\gamma}, \\ \frac{1}{\sigma_\gamma}\frac{\partial \sigma_\gamma}{\partial \Gamma_n} &= \frac{1}{\Gamma_n} - \frac{\Gamma_\lambda}{2}\sigma_\gamma \frac{\rho_0^2 \sqrt{E}\sqrt{E_\lambda}}{\pi \Gamma_n \Gamma_\gamma}, \\ \frac{1}{\sigma_\gamma}\frac{\partial \sigma_\gamma}{\partial \Gamma_\gamma} &= \frac{1}{\Gamma_\gamma} - \frac{\Gamma_\lambda}{2}\sigma_\gamma \frac{\rho_0^2 \sqrt{E}\sqrt{E_\lambda}}{\pi \Gamma_n \Gamma_\gamma}. \end{aligned} \tag{A6}$$

Alternatively, these same cross-section sensitivities $\frac{\partial \sigma}{\partial \Gamma}(E)$ can be computed using (A2). For real $b \in \mathbb{R}$, the partial derivatives to any real coefficient $\Lambda \in \mathbb{R}$ follow:

$$\frac{1}{\sigma_\gamma}\frac{\partial \sigma_\gamma}{\partial \Lambda} = \frac{1}{b}\frac{\partial b}{\partial \Lambda} + \frac{\mathrm{Re}\left[\frac{i}{(E - \mathcal{E}_\lambda)^2}\frac{\partial \mathcal{E}_\lambda}{\partial \Lambda}\right]}{\mathrm{Re}\left[\frac{i}{E - \mathcal{E}_\lambda}\right]}.$$

Since we have

$$\begin{aligned} \frac{\partial \mathcal{E}_\lambda}{\partial E_\lambda} &= 1, & \frac{1}{b}\frac{\partial b}{\partial E_\lambda} &= -\frac{1}{2E_\lambda}, \\ \frac{\partial \mathcal{E}_\lambda}{\partial \Gamma_n} &= \frac{\partial \mathcal{E}_\lambda}{\partial \Gamma_\gamma} = -\frac{i}{2}, & \frac{1}{b}\frac{\partial b}{\partial \Gamma_n} &= \frac{1}{\Gamma_n} - \frac{1}{\Gamma_\lambda}, \\ & & \frac{1}{b}\frac{\partial b}{\partial \Gamma_\gamma} &= \frac{1}{\Gamma_\gamma} - \frac{1}{\Gamma_\lambda} \end{aligned} \tag{A7}$$

the cross-section sensitivities $\frac{\partial\sigma}{\partial\Gamma}(E)$ to resonance energy E_λ, neutron-scattering width Γ_n, and radiative capture width Γ_γ are thus, respectively,

$$\begin{aligned}\frac{1}{\sigma_\gamma}\frac{\partial\sigma_\gamma}{\partial E_\lambda} &= \frac{-1}{2E_\lambda} + \frac{\mathrm{Re}\left[\frac{i}{(E-\mathcal{E}_\lambda)^2}\right]}{\mathrm{Re}\left[\frac{i}{E-\mathcal{E}_\lambda}\right]},\\ \frac{1}{\sigma_\gamma}\frac{\partial\sigma_\gamma}{\partial\Gamma_n} &= \frac{1}{\Gamma_n} - \frac{1}{\Gamma_\lambda} + \frac{1}{2}\frac{\mathrm{Re}\left[\frac{1}{(E-\mathcal{E}_\lambda)^2}\right]}{\mathrm{Re}\left[\frac{i}{E-\mathcal{E}_\lambda}\right]},\\ \frac{1}{\sigma_\gamma}\frac{\partial\sigma_\gamma}{\partial\Gamma_\gamma} &= \frac{1}{\Gamma_\gamma} - \frac{1}{\Gamma_\lambda} + \frac{1}{2}\frac{\mathrm{Re}\left[\frac{1}{(E-\mathcal{E}_\lambda)^2}\right]}{\mathrm{Re}\left[\frac{i}{E-\mathcal{E}_\lambda}\right]}\end{aligned} \tag{A8}$$

where the derivatives could be taken within the real part because all the parameters were real. Using the cross-section sensitivities $\frac{\partial\sigma}{\partial\Gamma}(E)$—either from (A6) or (A8)—and performing the corresponding Hwang's conjugate continuation (Sec. II D), one can therefore compute the multipole sensitivities ($\frac{\partial\Pi}{\partial\Gamma}$) of Theorem 2 using the contour integrals system (128).

In this simple case of a single-level Breit-Wigner resonance in multipole representation (A4), we are also able to explicitly calculate the multipole sensitivities to resonance parameters—i.e., Jacobian ($\frac{\partial\Pi}{\partial\Gamma}$)—by direct differentiation of the explicit formulas (A5), yielding

$$\frac{\partial p_+}{\partial E_\lambda} = -\frac{\partial p_-}{\partial E_\lambda} = \frac{1}{2p_+}, \quad \frac{\partial r_+}{\partial E_\lambda} = \frac{\partial r_-}{\partial E_\lambda} = -\frac{r_+}{2E_\lambda}$$

and

$$\begin{aligned}\frac{\partial p_+}{\partial\Gamma_n} &= -\frac{\partial p_-}{\partial\Gamma_n} = \frac{-i}{4p_+},\\ \frac{\partial r_+}{\partial\Gamma_n} &= \frac{\partial r_-}{\partial\Gamma_n} = r_+\left(\frac{1}{\Gamma_n} - \frac{1}{\Gamma_\lambda}\right)\end{aligned}$$

and

$$\begin{aligned}\frac{\partial p_+}{\partial\Gamma_\gamma} &= -\frac{\partial p_-}{\partial\Gamma_\gamma} = \frac{-i}{4p_+},\\ \frac{\partial r_+}{\partial\Gamma_\gamma} &= \frac{\partial r_-}{\partial\Gamma_\gamma} = r_+\left(\frac{1}{\Gamma_\gamma} - \frac{1}{\Gamma_\lambda}\right).\end{aligned} \tag{A9}$$

The latter multipole sensitivities (A9) can then be used to validate Theorem 2.

For verification and reproducibility purposes, we generated Figs. 3, 4, and 6 using cross section (A1) with the parameters from the neutron slowdown analytic benchmark [38,39], which we here report in Table II. These parameters are similar (but not identical) to those of ENDF/B-VIII.0 evaluations, yielding the same cross section to a multiplicative constant. The resonance energies and widths are those of ENDF/B-VIII.0, as well as their covariance matrix. The enlarged covariance matrix in Table II is that of the analytic benchmark [38,39], and was designed to bring the neutron slowdown problem past the linear regime in resonance sensitivity.

[1] P. L. Kapur and R. Peierls, Proc. R. Soc. A **166**, 277 (1938).
[2] E. P. Wigner and L. Eisenbud, Phys. Rev. **72**, 29 (1947).
[3] C. Bloch, Nucl. Phys. **4**, 503 (1957).
[4] A. M. Lane and R. G. Thomas, Rev. Mod. Phys. **30**, 257 (1958).
[5] J. Humblet and L. Rosenfeld, Nucl. Phys. **26**, 529 (1961).
[6] L. Rosenfeld, Nucl. Phys. **26**, 597 (1961).
[7] J. Humblet, Nucl. Phys. **31**, 544 (1962).
[8] J. Humblet, Nucl. Phys. **50**, 1 (1964).
[9] J. P. Jeukenne, Nucl. Phys. **58**, 1 (1965).
[10] J. Humblet, Nucl. Phys. **57**, 386 (1964).
[11] C. Mahaux, Nucl. Phys. **68**, 481 (1965).
[12] L. Rosenfeld, Nucl. Phys. **70**, 1 (1965).
[13] C. Mahaux, Nucl. Phys. **71**, 241 (1965).
[14] D. A. Brown, M. B. Chadwick, R. Capote, A. C. Kahler, A. Trkov, M. W. Herman, A. A. Sonzogni, Y. Danon, A. D. Carlson, M. Dunn, D. L. Smith, G. M. Hale, G. Arbanas, R. Arcilla, C. R. Bates, B. Beck, B. Becker, F. Brown, R. J. Casperson, J. Conlin, D. E. Cullen, M. A. Descalle, R. Firestone, T. Gaines, K. H. Guber, A. I. Hawari, J. Holmes, T. D. Johnson, T. Kawano, B. C. Kiedrowski, A. J. Koning, S. Kopecky, L. Leal, J. P. Lestone, C. Lubitz, J. I. Márquez Damián, C. M. Mattoon, E. A. McCutchan, S. Mughabghab, P. Navratil, D. Neudecker, G. P. A. Nobre, G. Noguere, M. Paris, M. T. Pigni, A. J. Plompen, B. Pritychenko, V. G. Pronyaev, D. Roubtsov, D. Rochman, P. Romano, P. Schillebeeckx, S. Simakov, M. Sin, I. Sirakov, B. Sleaford, V. Sobes, E. S. Soukhovitskii, I. Stetcu, P. Talou, I. Thompson, S. van der Marck, L. Welser-Sherrill, D. Wiarda, M. White, J. L. Wormald, R. Q. Wright, M. Zerkle, G. Žerovnik, and Y. Zhu, Nucl. Data Sheets Special Issue Nuclear Reaction Data **148**, 1 (2018).
[15] A. J. M. Plompen, O. Cabellos, C. De Saint Jean, M. Fleming, A. Algora, M. Angelone, P. Archier, E. Bauge, O. Bersillon, A. Blokhin, F. Cantargi, A. Chebboubi, C. Diez, H. Duarte, E. Dupont, J. Dyrda, B. Erasmus, L. Fiorito, U. Fischer, D. Flammini, D. Foligno, M. R. Gilbert, J. R. Granada, W. Haeck, F.-J. Hambsch, P. Helgesson, S. Hilaire, I. Hill, M. Hursin, R. Ichou, R. Jacqmin, B. Jansky, C. Jouanne, M. A. Kellett, D. H. Kim, H. I. Kim, I. Kodeli, A. J. Koning, A. Y. Konobeyev, S. Kopecky, B. Kos, A. Krása, L. C. Leal, N. Leclaire, P. Leconte, Y. O. Lee, H. Leeb, O. Litaize, M. Majerle, J. I. Márquez Damián, F. Michel-Sendis, R. W. Mills, B. Morillon, G. Noguère, M. Pecchia, S. Pelloni, P. Pereslavtsev, R. J. Perry, D. Rochman, A. Röhrmoser, P. Romain, P. Romojaro, D. Roubtsov, P. Sauvan, P. Schillebeeckx, K. H. Schmidt, O. Serot, S. Simakov, I. Sirakov, H. Sjöstrand, A. Stankovskiy, J. C. Sublet, P. Tamagno, A. Trkov, S. van der Marck, F. Álvarez-Velarde, R. Villari, T. C. Ware, K. Yokoyama, and G. Žerovnik, Eur. Phys. J. A **56**, 181 (2020).
[16] A. Blokhin, E. Gai, A. Ignatyuk, I. Koba, V. Manokhin, and V. Pronyaev, 2016, https://www.vant.ippe.ru/en/year2016/2/neutron-constants/1150-5.html.
[17] K. Shibata, O. Iwamoto, T. Nakagawa, N. Iwamoto, A. Ichihara, S. Kunieda, S. Chiba, K. Furutaka, N. Otuka, T. Ohsawa, T. Murata, H. Matsunobu, A. Zukeran, S.

Kamada, and J.-i. Katakura, J. Nucl. Sci. Technol. **48**, 1 (2011).
[18] Z. Ge, H. Wu, G. Chen, and R. Xu, EPJ Web Conf. **146**, 02002 (2017).
[19] A. J. Koning and D. Rochman, Nucl. Data Sheets Special Issue Nuclear Reaction Data **113**, 2841 (2012).
[20] A. J. Koning, D. Rochman, J. C. Sublet, N. Dzysiuk, M. Fleming, and S. van der Marck, Nucl. Data Sheets Special Issue Nuclear Reaction Data **155**, 1 (2019).
[21] R. N. Hwang, Nucl. Sci. Eng. **96**, 192 (1987).
[22] R. N. Hwang, Argonne National Laboratory Report No. ANL/CP–71459 (1991).
[23] R. N. Hwang, Nucl. Sci. Eng. **111**, 113 (1992).
[24] R. N. Hwang, in *Proceedings of the International Conference on the Physics of Nuclear Science and Technology*, (1998).
[25] R. N. Hwang, Trans. Am. Nucl. Soc. **88**, 491 (2003).
[26] B. Forget, S. Xu, and K. Smith, Ann. Nucl. Energy **64**, 78 (2014).
[27] C. Josey, B. Forget, and K. Smith, J. Nucl. Sci. Technol. **52**, 987 (2015).
[28] C. Josey, P. Ducru, B. Forget, and K. Smith, J. Comput. Phys. **307**, 715 (2016).
[29] P. Ducru, V. Sobes, B. Forget, and K. Smith, in *Proceedings of PHYSOR 2016* (American Nuclear Society, La Grange Park, IL, 2016), pp. 2138–2150.
[30] X. Peng, P. Ducru, S. Liu, B. Forget, and J. Liang, Comput. Phys. Commun. **224**, 52 (2018).
[31] P. Ducru, B. Forget, V. Sobes, G. Hale, and M. Paris, Phys. Rev. C **103**, 064608 (2021).
[32] P. Ducru, B. Forget, V. Sobes, G. Hale, and M. Paris, Phys. Rev. C **103**, 064609 (2021).
[33] MIT NSE CRPG, Windowed multipole library, 2019, https://github.com/mit-crpg/WMP_Library
[34] P. Ducru, J. Liang, V. Sobes, A. Alhajri, I. Meyer, B. Forget, and K. Smith, in *Proceedings of the International Conference on Mathematics and Computational Methods Applied to Nuclear Science and Engineering*, (2019).
[35] A. Alhajri and B. Forget, in *Proceedings of the International Conference on Mathematics and Computational Methods Applied to Nuclear Science and Engineering*, (2019).
[36] S. S. M. Harper, Ph.D. thesis, Massachusetts Institute of Technology, 2016.
[37] S. Harper, K. Smith, and B. Forget, *in Proceedings of the PHYSOR Conference*, (2018).
[38] V. Sobes, P. Ducru, A. Alhajri, B. D. Ganapol, and B. Forget, Nucl. Sci. Eng. (2021), doi: 10.1080/00295639.2021.1874777.
[39] A. Alhajri, V. Sobes, P. Ducru, B. D. Ganapol, and B. Forget, Nucl. Sci. Eng. (2021), doi: 10.1080/00295639.2021.1898923.
[40] J. Liang, P. Ducru, and B. Forget, Trans. Am. Nucl. Soc. **119**, 1163 (2018).
[41] F. W. J. Olver, A. B. Olde Daalhuis, D. W. Lozier, B. I. Schneider, R. F. Boisvert, C. W. Clark, B. R. Miller, B. V. Saunders, and editors, *NIST Digital Library of Mathematical Functions*, National Institute of Standards and Technology, US Department of Commerce, 2020, https://dlmf.nist.gov
[42] M. Abramowitz and I. A. Stegun, in *Handbook of Mathematical Functions with Formulas, Graphs, and Mathematical Tables*, United States Department of Commerce (National Bureau of Standards, Applied Mathematics Series, 1964).
[43] T. Teichmann and E. P. Wigner, Phys. Rev. **87**, 123 (1952).
[44] C. W. Reich and M. S. Moore, Phys. Rev. **111**, 929 (1958).
[45] G. Arbanas, V. Sobes, A. Holcomb, P. Ducru, M. Pigni, and D. Wiarda, EPJ Web Conf. **146**, 12006 (2017).
[46] A. J. F. Siegert, Phys. Rev. **56**, 750 (1939).
[47] G. Breit, Phys. Rev. **58**, 1068 (1940).
[48] A. Lejeune and C. Mahaux, Nucl. Phys. A **145**, 613 (1970).
[49] J.-M. Li, L. V. Ky, Y.-Z. Qu, J. Yan, P.-H. Zhang, H.-L. Zhou, and P. Faucher, Phys. Rev. A **55**, 3239 (1997).
[50] H. Comisel, C. Hategan, and R. A. Ionescu, Romanian J. Phys. **57**, 138 (2012).
[51] G. Mittag-Leffler, Acta Mathematica **4**, 1 (1884).
[52] A. E. Taylor, Pacific J. Mathematics **10**, 1049 (1960).
[53] E. P. Wigner, Phys. Rev. **73**, 1002 (1948).
[54] H. Voss, in *Handbook of Linear Algebra*, 2nd ed., Nonlinear Eigenvalue Problems, edited by L. Hogben (Chapman and Hall, London, 2014), Chap. 115, pp. 1–24, https://www.mat.tuhh.de/forschung/rep/rep164.pdf
[55] C. R. Brune, Phys. Rev. C **66**, 044611 (2002).
[56] F. H. Frohner, Evaluation and analysis of nuclear resonance data, Technical Report No. 18, IAEA, 2000.
[57] B. Gustavsen and A. Semlyen, IEEE Transactions Power Delivery **14**, 1052 (1999).
[58] B. Gustavsen, IEEE Transactions Power Delivery **21**, 1587 (2006).
[59] S. Liu, X. Peng, C. Josey, J. Liang, B. Forget, K. Smith, and K. Wang, Ann. Nucl. Energy **112**, 30 (2018).
[60] J. Liang, X. Peng, S. Liu, C. Josey, B. Forget, and K. Smith, *in Proceedings of the PHYSOR Conference*, (2018).
[61] M. Berljafa and S. Güttel, SIAM J. Sci. Comput. **39**, A2049 (2017).
[62] Y. Nakatsukasa, O. Sète, and L. N. Trefethen, SIAM J. Sci. Comput. **40**, A1494 (2018).
[63] C. Jammes and R. N. Hwang, Nucl. Sci. Eng. **134**, 37 (2000).
[64] R. N. Hwang, R. N. Blomquist, L. C. Leal, and W. S. Yang, Neutron resonance theory for nuclear reactor applications: Modern theory and practices, Technical Report No. ANL/NE-16/34, Argonne National Laboratory, Argonne, IL, 2016.
[65] T. Freiman, Ph.D. thesis, Université Paris-Saclay, 2020, https://tel.archives-ouvertes.fr/tel-02906474
[66] J. H. Wilkinson, Numer. Math. **1**, 150 (1959).
[67] E. Durand, in *Equations du Type F(x) = 0: Racines d'un Polynome* (Mason, Paris, 1960).
[68] O. Aberth, Mathematics Computation **27**, 339 (1973).
[69] M. Petkovic, *Iterative Methods for Simultaneous Inclusion of Polynomial Zeros*, 1st ed., Vol. 1387 (Springer-Verlag, Berlin, 1989).
[70] A. Schönhage, The fundamental theorem of algebra in terms of computational complexity, Technical Report, Mathematisches Institut der Universität Tübingen, 1982.
[71] X. Gourdon, Ph.D. thesis, École Polytechnique, 1996.
[72] V. Y. Pan, Comput. Math. Appl. **31**, 97 (1996).
[73] V. Y. Pan, SIAM Rev. **39**, 187 (1997).
[74] G. Malajovich and J. P. Zubelli, Comput. Math. Appl. **33**, 1 (1997).
[75] V. Y. Pan, J. Complexity **16**, 213 (2000).
[76] I. Z. Emiris and V. Y. Pan, Journal of Complexity **21**, 43 (2005).
[77] V. Y. Pan and A.-L. Zheng, Comput. Math. Appl. **61**, 1305 (2011).

[78] J. M. McNamee and V. Y. Pan, Comput. Math. Appl. **63**, 239 (2012).
[79] V. Y. Pan and E. Tsigaridas, Theor. Comput. Sci. Symbolic Numeric Computation, **681**, 138 (2017).
[80] E. Bauge, S. Hilaire, and P. Dossantos-Uzarralde, in *International Conference on Nuclear Data for Science and Technology* (EDP Sciences, 2007), pp. 259–264.
[81] R. Capote, D. L. Smith, A. Trkov, and M. Meghzifene, J. ASTM International **9**, 1 (2012).
[82] A. J. Koning, Eur. Phys. J. A **51**, 184 (2015).
[83] A. J. Koning, Nucl. Data Sheets **123**, 207 (2015).
[84] P. Helgesson, H. Sjöstrand, A. J. Koning, J. Rydén, D. Rochman, E. Alhassan, and S. Pomp, Prog. Nucl. Energy **96**, 76 (2017).
[85] D. Rochman, E. Bauge, A. Vasiliev, H. Ferroukhi, S. Pelloni, A. J. Koning, and J. C. Sublet, Eur. Phys. J. Plus **133**, 537 (2018).
[86] E. Alhassan, D. Rochman, H. Sjöstrand, A. Vasiliev, A. J. Koning, and H. Ferroukhi, Ann. Nucl. Energy **139**, 107239 (2020).
[87] D. Rochman, A. J. Koning, and J. C. Sublet, Nucl. Data Sheets **163**, 163 (2020).
[88] D. Rochman, A. Koning *et al.*, Ann. Nucl. Energy **38**, 942 (2011).
[89] D. Rochman, W. Zwermann, A. Koning *et al.*, Nucl. Sci. Eng. **177**, 337 (2014).
[90] E. Alhassan, H. Sjöstrand, P. Helgesson, A. Koning, M. Österlund, S. Pomp, and D. Rochman, Ann. Nucl. Energy **75**, 26 (2015).
[91] R. E. MacFarlane and A. C. Kahler, Nucl. Data Sheets Nuclear Reaction Data, **111**, 2739 (2010).
[92] A. Solbrig Jr., Am. J. Phys. **29**, 257 (1961).
[93] G. L. Blackshaw and R. L. Murray, Nucl. Sci. Eng. **27**, 520 (1967).
[94] D. E. Cullen and C. R. Weisbin, Nucl. Sci. Eng. **60**, 199 (1976).
[95] T. H. Trumbull, Nucl. Tech. **156**, 75 (2006).
[96] G. Yesilyurt, W. R. Martin, and F. B. Brown, Nucl. Sci. Eng. **171**, 239 (2012).
[97] G. Ferran, W. Haeck, and M. Gonin, Nucl. Sci. Eng. **179**, 285 (2015).
[98] P. Ducru, C. Josey, K. Dibert, V. Sobes, B. Forget, and K. Smith, J. Comput. Phys. **335**, 535 (2017).
[99] J. Conlin, W. Ji, J. Lee, and W. Martin, Trans. Am. Nucl. Soc. **92**, 225 (2005).
[100] S. Peng, A. B. S. Zhang, and X. Jiang, Ann. Nucl. Energy **45**, 155 (2012).
[101] T. Viitanen and J. Leppnen, Nucl. Sci. Eng. **171**, 165 (2012).
[102] T. Viitanen and J. Leppänen, Nucl. Sci. Eng. **177**, 77 (2014).
[103] P. K. Romano and J. A. Walsh, Ann. Nucl. Energy **114**, 318 (2018).
[104] *Handbook of Nuclear Engineering*, edited by D. G. Cacuci (Springer, New York, 2010), Vols. 1–5.
[105] L.-F.-A. Arbogast, in *Du calcul des dérivations* (A Strasbourg, de l'Imprimerie de Levrault, Frères, An VIII (1800)) https://docnum.unistra.fr/digital/collection/coll7/id/39933
[106] E. T. Bell, Ann. Math. **35**, 258 (1934).
[107] M. Abbas and S. Bouroubi, Discrete Mathematics 19th British Combinatorial Conference **293**, 5 (2005).
[108] K. N. Boyadzhiev, Abstract Applied Analysis **2009**, 168672 (2009).
[109] J.-B.-J. Fourier, *Théorie analytique de la chaleur* (Firmin Didot, Imprimeur du Roi, 1822) https://gallica.bnf.fr/ark:/12148/bpt6k1045508v
[110] C. T. Ballinger, in *Proceedings of the international conference on mathematics and computations, reactor physics, and environmental analyses*, (1995).
[111] G. H. Vineyard, Phys. Rev. **110**, 999 (1958).
[112] J. W. Cooley and J. W. Tukey, Mathematics Computation **19**, 297 (1965).
[113] D. H. Bailey and P. N. Swarztrauber, SIAM J. Sci. Comput. **15**, 1105 (1994).
[114] G. W. Inverarity, SIAM J. Sci. Comput. **24**, 645 (2002).
[115] J. a. C. Weideman, SIAM J. Numer. Anal. **31**, 1497 (1994).
[116] G. P. M. Poppe and C. M. J. Wijers, ACM Transactions Mathematical Software **16**, 38 (1990).
[117] M. R. Zaghloul and A. N. Ali, ACM Transactions Mathematical Software **38**, 1 (2012).
[118] M. R. Zaghloul, ACM Transactions Mathematical Software **44**, 1 (2017).
[119] S. G. Johnson, Faddeeva package, *Ab initio*, MIT License, 2013, http://ab-initio.mit.edu/wiki/index.php/Faddeeva_Package